MnO$_2$/CARBON MATERIAL CATHODE FOR RECHARGEABLE AQUEOUS ELECTROLYTE-BASED ZINC-ION BATTERIES

Mr. Sonti Khamsanga

จุฬาลงกรณ์มหาวิทยาลัย
CHULALONGKORN UNIVERSITY

A Dissertation Submitted in Partial Fulfillment of the Requirements

for the Degree of Doctor of Engineering in Chemical Engineering

Department of Chemical Engineering

FACULTY OF ENGINEERING

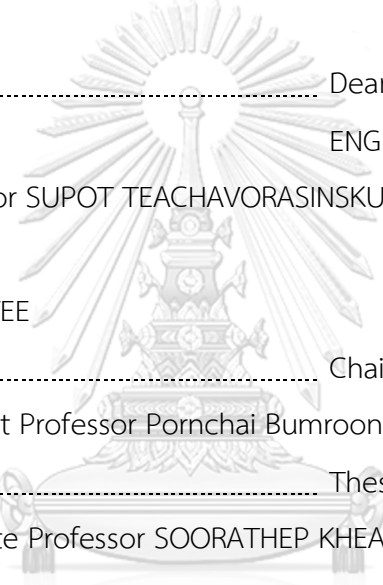Chulalongkorn University

Academic Year 2020

คาโทดแมงกานีสออกไซด์/วัสดุคาร์บอนสำหรับแบตเตอรี่ไอออนสังกะสีชนิดอิเล็กโตรไลต์ฐานน้ำแบบอัดประจุซ้ำได้

นายสนธิ ขำสง่า

วิทยานิพนธ์นี้เป็นส่วนหนึ่งของการศึกษาตามหลักสูตรปริญญาวิศวกรรมศาสตรดุษฎีบัณฑิต
สาขาวิชาวิศวกรรมเคมี ภาควิชาวิศวกรรมเคมี
คณะวิศวกรรมศาสตร์ จุฬาลงกรณ์มหาวิทยาลัย
ปีการศึกษา 2563
ลิขสิทธิ์ของจุฬาลงกรณ์มหาวิทยาลัย

Thesis Title MnO_2/CARBON MATERIAL CATHODE FOR RECHARGEABLE
                    AQUEOUS ELECTROLYTE-BASED ZINC-ION BATTERIES
By   Mr. Sonti Khamsanga
Field of Study   Chemical Engineering
Thesis Advisor   Associate Professor SOORATHEP KHEAWHOM, Ph.D.

Accepted by the FACULTY OF ENGINEERING, Chulalongkorn University in Partial Fulfillment of the Requirement for the Doctor of Engineering

.... Dean of the FACULTY OF
                                             ENGINEERING
(Professor SUPOT TEACHAVORASINSKUN, D.Eng.)

DISSERTATION COMMITTEE

.... Chairman
(Assistant Professor Pornchai Bumroongsri, D.Eng.)

.... Thesis Advisor
(Associate Professor SOORATHEP KHEAWHOM, Ph.D.)

.... Examiner
(VARUN TAEPAISITPHONGSE, Ph.D.)

.... Examiner
(Assistant Professor Palang Bumroongsakulsawat, Ph.D.)

.... Examiner
(Assistant Professor Pattaraporn Kim, Ph.D.)

.... Examiner
(Associate Professor ROJANA PORNPRASERTSUK, Ph.D.)

สนธิ ขำสง่า : คาโทดแมงกานีสออกไซด์/วัสดุคาร์บอนสำหรับแบตเตอรี่ไอออนสังกะสีชนิดอิเล็กโตรไลต์ฐานน้ำแบบอัดประจุซ้ำได้. (MnO$_2$/CARBON MATERIAL CATHODE FOR RECHARGEABLE AQUEOUS ELECTROLYTE-BASED ZINC-ION BATTERIES) อ.ที่ปรึกษาหลัก : รศ. ดร.สุรเทพ เขียวหอม

งานวิจัยนี้มุ่งเน้นการปรับปรุงการนำไฟฟ้าของวัสดุขั้วคาโทดโดยการสังเคราะห์แมงกานีสออกไซด์สำหรับใช้ในแบตเตอรี่ไอออนสังกะสีชนิดอิเล็กโตรไลต์ฐานน้ำแบบอัดประจุซ้ำได้ งานวิจัยได้แบ่งออกเป็น 2 ส่วน ส่วนแรกการสังเคราะห์แมงกานีสออกไซด์ชนิดเดลต้าที่มีโครงสร้างแบบนาโนฟลาวเออร์ลงบนตัวรองรับเกร็ดกราไฟต์(MNG) เพื่อใช้เป็นขั้วคาโทด ผลทดสอบพบว่า MNG มีพฤติกรรมการเคลื่อนที่เข้าและออกของไอออนสังกะสีที่รวดเร็วทั้งแบบแพร่ผ่านและแบบpseudocapacitive เมื่อมีการอัดประจุที่อัตรา 200 mA/g แบตเตอรี่ที่ใช้ขั้วคาโทดMNGให้ค่าความจุทางไฟฟ้าของการปล่อยประจุเริ่มต้นที่ 235 mA h/g เมื่อเปรียบเทียบกับแมงกานีสออกไซด์ชนิดเดลต้าแบบดั้งเดิมซึ่งให้ค่าความจุทางไฟฟ้าของการปล่อยประจุเริ่มต้นเพียง 130 mA h/g เท่านั้น จากค่าความจุไฟฟ้าดังกล่าวแสดงให้เห็นว่าขั้วคาโทดจMNGมีความสามารถในการนำไฟฟ้าที่เหนือกว่าแมงกานีสออกไซด์ชนิดเดลต้าแบบดั้งเดิม จากผลดังกล่าวสามารถสรุปได้ว่าค่าการนำไฟฟ้าสามารถปรับปรุงให้มากขึ้นโดยใช้MNG ในงานวิจัยส่วนที่สองเป็นการสังเคราะห์โครงสร้างผสมของแมงกานีสออกไซด์ลงบนคาร์บอนนาโนทิวป์ชนิดผนังหลายชั้นหรือMN-CNT เพื่อใช้ทำวัสดุขั้วคาโทด นอกจากการสังเคราะห์ดังกล่าวพบว่าแมงกานีสออกไซด์ที่ได้มีการเกิดผสมกันระหว่างแมงกานีสออกไซด์ชนิดเดลต้าและชนิกแกมม่าอยู่ด้วยกัน แบตเตอรี่ไอออนสังกะสีที่ใช้ขั้วคาโทดMN-CNTให้ค่าความจุทางไฟฟ้าของการปล่อยประจุเริ่มต้นที่ 236 mA h/g เมื่อมีการอัดประจุที่อัตรา 400 mA/g และให้ค่าความจุทางไฟฟ้าของการปล่อยประจุเริ่มต้นที่ 108 mA h/g เมื่อมีการอัดประจุที่อัตรา 1600 mA/g นอกจากนี้แบตเตอรี่ยังมีความเสถียรของรอบในการอัดประจุที่ดีอีกด้วย เมื่อกล่าวโดยรวมแล้วจะเห็นได้ว่าขั้วคาโทดจากMNG และMN-CNT นั้นมีประสิทธิภาพทางไฟฟ้าเคมีที่ดี ดังนั้นงานวิจัยนี้จึงเป็นการนำเสนอทางเลือกหนึ่งในการปรับปรุงค่าความจุทางไฟฟ้าและความเสถียรของรอบการอัดประจุของแบตเตอรี่ไอออนสังกะสีชนิดอิเล็กโตรไลต์ฐานน้ำแบบอัดประจุซ้ำได้

สาขาวิชา	วิศวกรรมเคมี	ลายมือชื่อนิสิต ....
ปีการศึกษา	2563	ลายมือชื่อ อ.ที่ปรึกษาหลัก ....

6071443721 : MAJOR CHEMICAL ENGINEERING

KEYWORD: zinc-ion battery, graphite, CNTs, manganese oxide

Sonti Khamsanga : MnO_2/CARBON MATERIAL CATHODE FOR RECHARGEABLE AQUEOUS ELECTROLYTE-BASED ZINC-ION BATTERIES. Advisor: Assoc. Prof. SOORATHEP KHEAWHOM, Ph.D.

This research focused on improvement of the electrical conductivity of cathode material by using the MnO_2 on carbon material for the rechargeable aqueous electrolyte-based zinc-ion batteries (ZIBs). This study has been divided into two sections. delta-MnO_2 with nanoflower structure supported on graphite flake (MNG) was synthesized for cathode material in first section. MNG exhibits a fast insertion/extraction of Zn^{2+} ions with diffusion scheme and pseudocapacitive behavior. The battery using MNG cathode exhibited a high initial discharge capacity of 235 mA h/g at 200 mA/g specific current density compared to 130 mA h/g which is displayed by the pristine delta-MnO_2 cathode at the same specific current density. MNG demonstrated superior electrical conductivity compared to the pristine delta-MnO_2. The results obtained pave the way for improving the electrical conductivity of MnO_2 by using graphite flake support. In second section, MnO_2 heterostructure on multi-walled carbon nanotubes (MNH-CNT) was synthesized for cathode material. Besides, the synthesized MNH-CNT is composed of delta-MnO_2 and gamma-MnO_2. ZIB using the MNH-CNT cathode delivers a high initial discharge capacity of 236 mA h/g at 400 mA/g, 108 mA h/g at 1600 mA/g and excellent cycling stability. Overall, MNG and MNH-CNT cathode were seen to exhibit superior electrochemical performance. This work presents new opportunities for improving the discharge capacity and cycling stability of aqueous ZIBs.

Field of Study: Chemical Engineering   Student's Signature ....

Academic Year: 2020   Advisor's Signature ....

ACKNOWLEDGEMENTS

TABLE OF CONTENTS

LIST OF TABLES

LIST OF FIGURES

CHAPTER 1

INTRODUCTION

1.1 General introduction

Nowadays, development of energy conversion and energy storage systems, such as solar photovoltaics, photo-electrochemical cells and batteries, is of utmost concern for sustainable civilization and environmental balance because of the rapid depletion of fossil fuels [1]. Thus, lithium-ion batteries (LIBs) have been intensively studied to meet the growing need for high energy-density portable electronic devices and large-scale energy storage systems [2]. However, choosing newer materials beyond Li are essential for replacing environmentally harmful and inherently volatile Li-chemistries [3]. Zinc-ion batteries (ZIBs) have been studied to replace Li-ion batteries due to the superior properties of zinc metal such as low cost, abundance low toxicity and reasonable stability in aqueous electrolytes [4].

Misnon et al. [5] reported that manganese oxide (MnO_2) is widely used as a cathode material in battery technologies because of its several advantageous properties. Manganese dioxide (MnO_2) cathodes are inexpensive and have a high theoretical capacity. These cathodes were previously studied for a variety of metal-ion batteries including Li-ion battery [6], Mg-ion battery (MIB) [7] and Zn-ion battery (ZIB) [8]. Recently, aqueous Zn/MnO_2 batteries have been considered as promising alternative energy devices owing to their high safety and abundance of Zn, MnO_2 and the electrolyte [9].

However, MnO_2 suffers from its poor conductivity that often results in high internal resistance of the electrode and, hence, results in poor performance of the battery. Therefore, in order to improve the performance of MnO_2 based zinc-ion battery, it was found necessary to increase the specific surface area of MnO_2 as well

as the ion diffusion rate [9]. Thus, this led to a significant increase in the power density of the Zn-ion battery. Another approach undertaken was to support MnO_2 nanostructures by a matrix material with a high surface area. It was observed that these nanostructures can accelerate charge transport during the electrochemical redox process [10]. The incorporation of nanostructured MnO_2 into carbonaceous materials could provide a large electroactive surface. In this respect, various carbonaceous materials, including activated carbon, carbon nanotubes (CNTs), carbon nanofibers (CNFs), graphene and graphite, have been integrated with MnO_2. Alfaruqi et al. [8] produced the tunneled-type nanorod MnO_2 cathodes with a high surface area for ZIB applications. Another interesting form proved to be the combination of MnO_2 with graphene. The incorporation of MnO_2 with a high conducting material, such as graphene or carbon, showed a significant improvement in capacitive performance [5]. Further, carbon-coated manganese dioxide nanoparticles were prepared to enhance the electrochemical properties in ZIBs [11].

The MnO_2/graphene nanoflowers were synthesized in the form of sandwich-structured nanoflowers which exhibited excellent super capacitive properties, making them very conductive electrode materials for high-performance super capacitors [12]. However, MnO_2 supported on graphite and allotropes of carbon have not been reported previously for ZIB applications. Therefore, it is clear that MnO_2 supported on graphite and allotropes of carbon are considered as the candidate due to an improvement in conductivity and an increase in the stability of electrode material for ZIBs.

In this study, the electrical conductivity of cathode material was improved. The effects of MnO_2 supported on different allotropes of carbon as a cathode host material on the electrochemical properties and performances of the rechargeable aqueous electrolyte-based ZIB were investigated.

Graphite was used as MnO_2 supporter in the first research article and multiwalled carbon nanotubes (MWCNTs) were used as MnO_2 supporter in the second one. These are allotropes of carbon material.

1.2 Research objectives

1) To improve the electrical conductivity of cathode material by using the MnO_2/carbon material

2) To investigate the effect of the MnO_2 supported on different allotropes of carbon as cathode material on the electrochemical properties and performances of the rechargeable aqueous electrolyte-based ZIB.

3) To compare the effect of the MnO_2 supported on different allotropes of carbon as cathode material on the capacity and cyclic ability of the rechargeable aqueous electrolyte-based ZIB.

1.3 Research scopes

<u>Part I</u> δ-MnO_2 nanoflowers/graphite cathode for rechargeable aqueous zinc-ion batteries

- Synthesis of MnO_2 nanoflowers/graphite (MNG) from modified method of Liu et al.[12]

- Characterization of δ-MnO_2 nanoflowers/graphite (MNG)

  a) Crystalline structure by X-Ray Diffraction (XRD)

  b) Morphology by Field Emission Scanning Electron Microscope (FESEM)

- Preparation of cathode by mixing MNG, carbon black and cellulose acetate with a weight ratio of 70:20:10, respectively, and coating on

carbon foil current collector. The pristine MnO_2 was also used for comparison.

- Preparation of anode from Zn electroplated on Ni foam and electrolyte from aqeuous $ZnSO_4$.

- Assembling cathode, anode, and elecrolyte into CR2032 coin cell battery.

- Measurement of electrochemical properties and performance of battery:

  a) Ion insertion/extraction with Cyclic Voltammograms (CVs) by Potentiostat

  b) Charge transfer resistance with Nyquist plots by Potentiostat

  c) Electrochemical behavior with CVs by Potentiostat

  d) Charge/discharge profile by Battery Testing System

  e) Cyclic performance by Battery Testing System

  f) Rate capability by Battery Testing System

Part II MnO_2 heterostructure on multiwalled carbon nanotubes (MWCNTs) as cathode material for rechargeable aqueous zinc-ion batteries

- Synthesis of MnO_2 Heterostructure/Multiwalled Carbon Nanotubes (MN-CNT) with different weight ratios of MnO_2 and MWCNTs at 60:40 (MN-CNT6040), 75:25 (MN-CNT7525), and 90:10 (MN-CNT9010).

- Characterization of MN-CNT

  a) Crystalline structure by X-Ray Diffraction (XRD)

  b) Morphology by Field Emission Scanning Electron Microscope (FESEM)

c) Presence of MWCNTs in MN-CNT by Transmission Electron Microscope with Energy Dispersive Spectroscopy (TEM-EDS)

- Preparation of cathode by mixing MN-CNT, carbon black, and carboxymethylcellulose sodium salt with a weight ratio of 70:20:10, respectively, and coating on carbon foil current collector. The pristine MnO_2 was also used for comparison.

- Preparation of anode from Zn electroplated on Ni foam and electrolyte from aqeuous $ZnSO_4$.

- Assembling cathode, anode and elecrolyte into cup cell battery.

- Measurement of electrochemical properties and performance of battery:

  a) Ion insertion/extraction with Cyclic Voltammograms (CVs) by electrochemical measurement system

  b) Electrochemical behavior with CVs by electrochemical measurement system

  c) Charge/discharge profile by Battery Testing System

  d) Cyclic performance by Battery Testing System

  e) Rate capability by Battery Testing System

1.4 Research methodology

Research methodology was shown as following:

Part I: δ-MnO_2 nanoflower/graphite cathode for rechargeable aqueous zinc-ion batteries
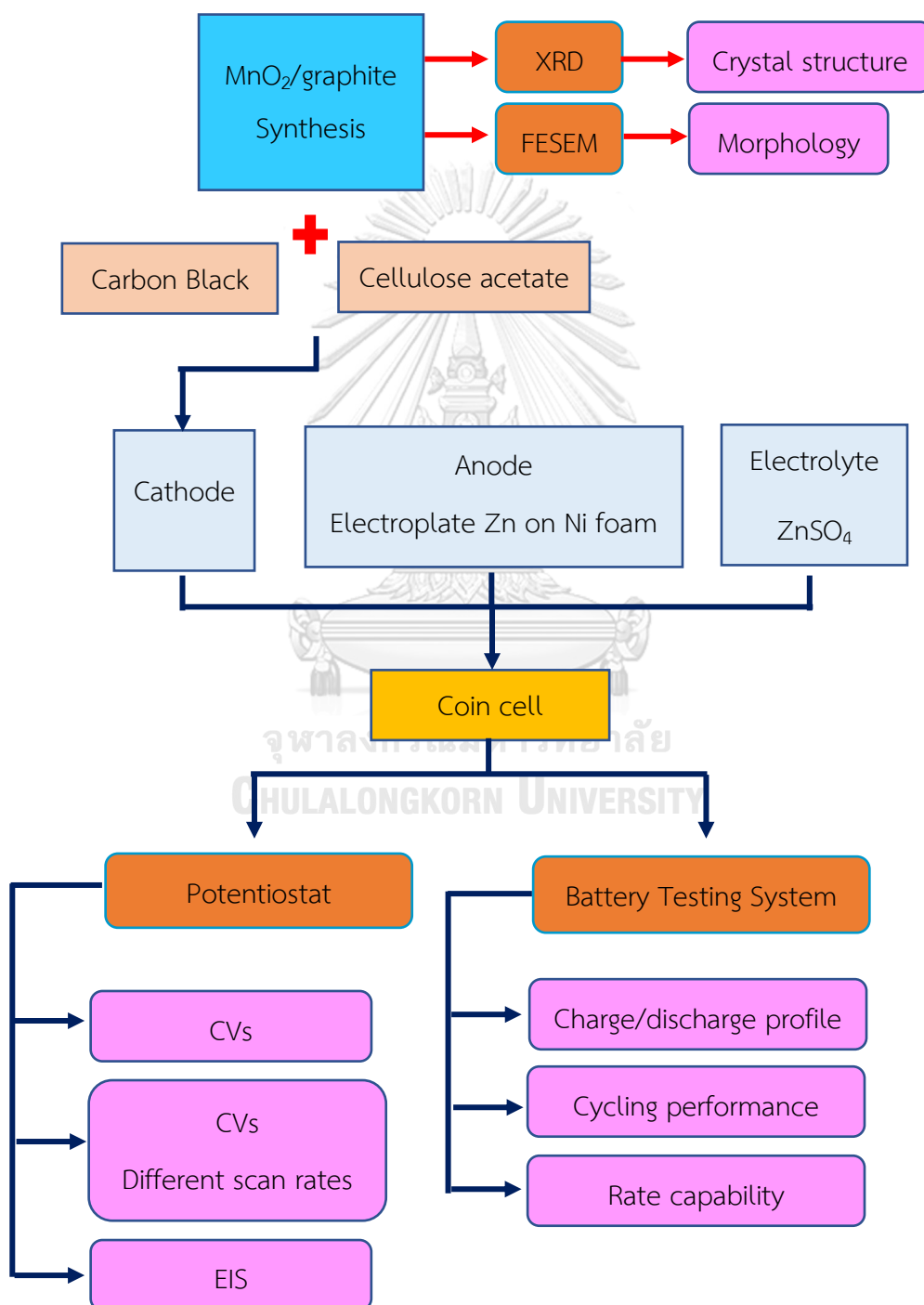
Part II: MnO$_2$ heterostructure on multiwalled carbon nanotubes (MWCNTs) as cathode material for aqueous zinc-ion batteries
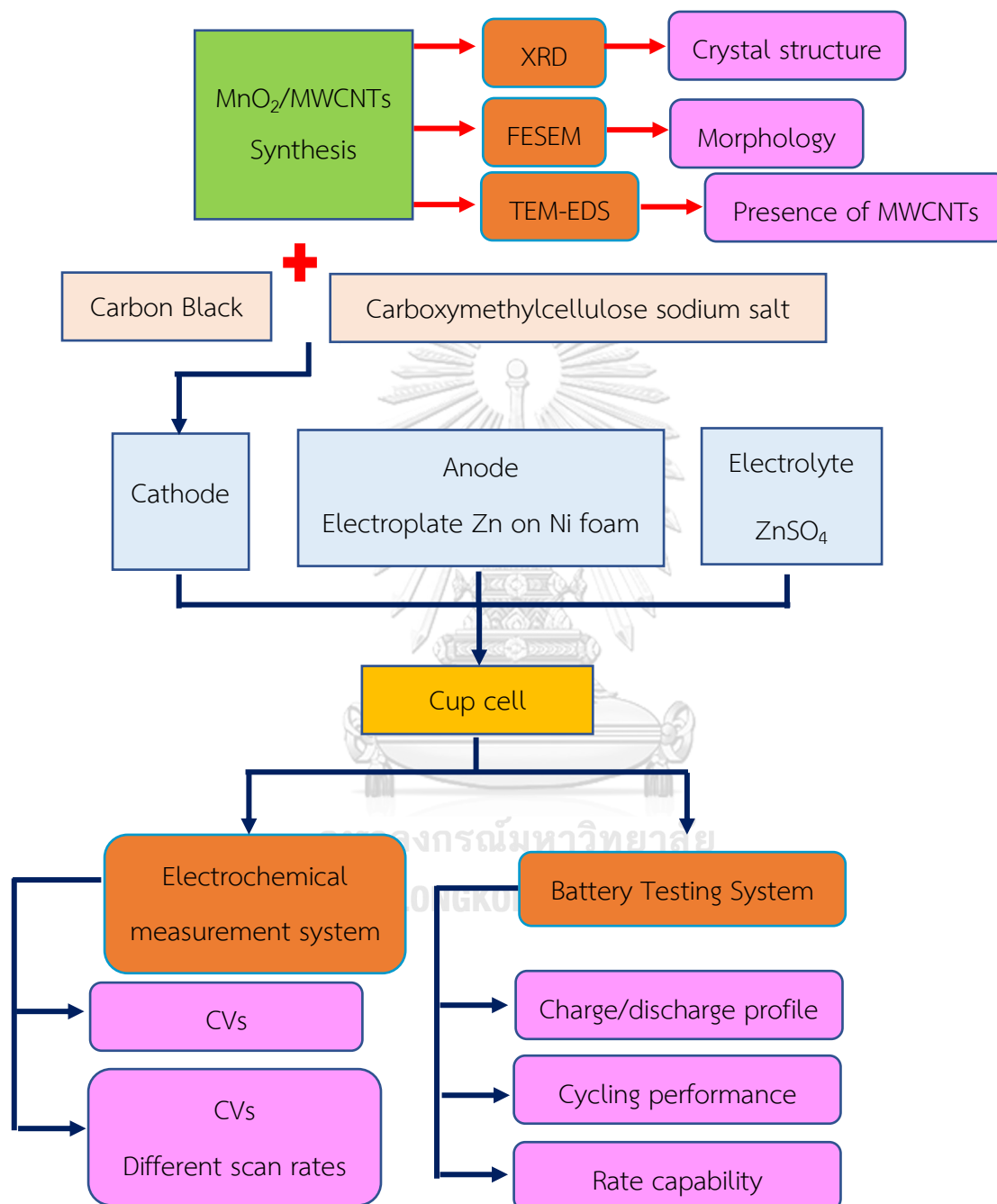
1.5 Research benefits

1.5.1 New cathode candidate for using in zinc-ion batteries

1.5.2 Electrode optimization for battery operation

1.5.3 Deep knowledge in battery chemistry

1.5.4 Development a new type of battery for energy storage technology

1.6 Research plan

Table 1.1 Research plan

Research Plan	2017		2018		2019		2020
	1	2	1	2	1	2	1
1. Literature reviews			←———————————————————→				
2. MnO_2/Graphite synthesis and characterization		←————→					
3. Battery fabrication and test for Part I			←————→				
4. MnO_2/MWCNTs synthesis and characterization					←————→		
5. Battery fabrication and test Part II					←————————→		
6. Discussion			←————————————————→				

CHAPTER 2

THEORY

2.1 Energy storage

Energy is an abstract scalar quantity that must be transferred to an object in order to perform work on or to heat the object. Common forms of energy include the kinetic energy of a moving object, the potential energy stored by an object's position in a force field (gravitation, electricity or magnet), the elastic energy stored by stretching solid objects, the chemical energy released when a fuel burns, the radiant energy carried by light, and the thermal energy due to an object's temperature [13]. When it is produced, it is stored at one time for use at a later time.

Energy can be stored in several ways. It is generally stored in five forms including mechanical, electro-chemical, thermal, capacitor, and chemical [14].
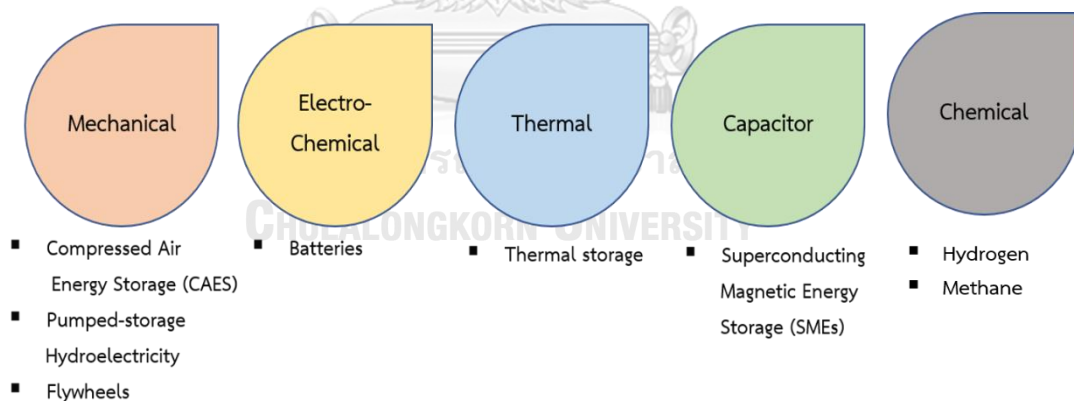
Figure 1.1 Energy storage technology [14]

2.2 Batteries

The environmental concerns regarding global warming and climate change lead to the development of renewable energy technologies. Many forms of renewable energy, e.g., solar energy, wind energy, and biomass, are used to produce electricity

with the will of being green energy. A battery, which is used to store the produced electricity, is a collection of one or more cells that undergo chemical reactions to create the flow of electrons within a circuit. Batteries generally can be classified into different categories and types, ranging from chemical composition, size, form factor, and use cases; but all of these are divided into two major battery types [15]:

1. Primary batteries

2. Secondary batteries

2.2.1 Primary batteries

A primary battery is a battery (a galvanic cell) that is designed to be used once and discarded, and not to be recharged with electricity and reused. Primary batteries are made of electrochemical cells whose electrochemical reaction cannot be reversed. The most popular type of primary batteries are alkaline batteries. They have a high specific energy, are environmental friendly, are cost effective, and do not self-discharge even when fully discharged . The only disadvantage of the alkaline batteries is the low load current, which limits its use to devices with low current requirements like remote controls, flashlights, and portable entertainment devices.

2.2.2 Secondary batteries

Secondary batteries are batteries with electrochemical cells whose chemical reactions can be reversed by applying a certain voltage to the battery in the reversed direction. It can be referred to as "rechargeable battery." Secondary batteries can be further classified into several other types based on their chemistries. There are basically four major chemistries for rechargeable batteries:

1. Lithium-ion (Li-ion)

Lithium-ion battery is a type of rechargeable battery in which lithium ions from the negative electrode migrate to the positive electrode during discharge and migrate

back to the negative electrode when the battery is being charged. Lithium-ion batteries generally possess high energy density and low self-discharge compared to other battery types [16]. However, limited lithium resources, high cost and safety issue strongly limit their development for industrial scale applications.

2. Nickel Cadmium (Ni-Cd)

The nickel–cadmium battery (Ni-Cd battery or Ni-Cad battery) is a type of rechargeable battery which is produced using nickel oxide hydroxide and metallic cadmium as electrodes. The advantages of this battery system are its high resilience, fast recharge time and low-temperature durability to minus 15 °C. High Cd content in Ni–Cd battery is classified as hazardous waste [17].

3. Nickel-Metal Hydride (Ni-MH)

The chemical reaction at the positive electrode of battery is similar to that of the nickel–cadmium cell (Ni-Cd). However, the negative electrode in Nickel-Metal Hydride uses a hydrogen-absorbing alloy instead of cadmium which is used in Ni-Cd battery. Its application is further limited because of its low discharge capacity of about 320 mA h/g [18].

4. Lead-Acid

Lead-Acid battery (LAB) is usually very large and, because of their weight, they are always used in non-portable applications such as solar-panel energy storage, vehicle ignition, lights and backup power. The irreversible sulfation in negative plates leads to the quick failure of lead-acid batteries [19].

Even many batteries are at commercially successful, namely lithium-ion, nickel-cadmium, nickel-metal hydride and lead-acid but they possess some limitations for application in large-scale systems such as their high cost, potential safety issue, and eco-unfriendliness [20]. Thus, the battery development aims to find a new system that meets the demand for economy, safety, eco-friendliness, and efficiency. Among various types of battery, the batteries that employ zinc anode are very promising as

zinc is abundant, non-toxic, inflammable, and relatively cheap compared with other materials [21]. Also, they provide large theoretical gravimetric and volumetric capacities (820 mA h/g and 5,845 mA h/cm^3, respectively) [22]. Nowadays, there are several types of zinc-based battery, e.g., zinc-nickel, zinc-air, and alkaline batteries, which have been developed so far for better performance compared to those in the past. However, these batteries are non-rechargeable as zinc exhibits poor reversibility in aqueous electrolyte [23].

2.3 Zinc-ion battery

The new framework of zinc battery is a system which composes of the zinc anode and intercalated cathode in near-neutral electrolytes. This system is called zinc-ion battery (ZIB). A zinc-ion battery is a second battery of energy storage device. Its performance is unique having a fast charge–discharge capability, high power and energy density. It is also safe and environmentally friendly [21]. A ZIB uses zinc ions (Zn^{2+}) as the charge carriers. The reduction potential of Zn is -0.76 V vs. standard hydrogen electrode (SHE). Metal Zn is usually used as the anode part of the ZIB. Fig. 2.1 shows the schematic of the chemistry of the zinc-ion battery which consists of a cathode of MnO_2, Zn anode and mild electrolyte.
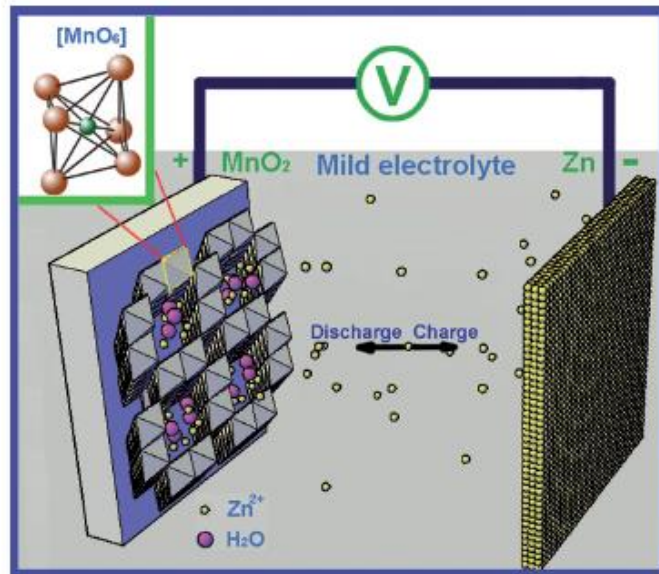
Figure 2.1 Schematic of the chemistry of the zinc-ion battery [21]

According to recent studies [24], ZIBs based on MnO_2 cathode have the same charge-storage mechanism as the other metal-ion batteries (MIBs), which the reactions can be written as

Cathode Reaction: $xZn^{2+} + 2xe^- + MnO_2 \leftrightarrow Zn_xMnO_2$ (2.1)

Anode Reaction: $xZn \leftrightarrow xZn^{2+} + 2xe^-$ (2.2)

Total Reaction: $xZn + MnO_2 \leftrightarrow Zn_xMnO_2$ (2.3)

During discharging, anodic zinc is dissolved in the form of Zn^{2+} ions, which rapidly diffuse and intercalate into a MnO_2 cathode to generate an electron current flow in the electrical loop.

During charging, the MnO_2 cathode will receive electrons in the electrical loop. Then, Zn^{2+} ions suddenly extract from the cathode since the charge storage mechanism is based on the migration of Zn^{2+} ions between the cathode and anode. Both of these processes involve the participation of Zn^{2+} ions in the mild electrolyte.

2.4 Cathode

The positive electrode or cathode is a composite material which comprises of an active material and other ingredients, namely, conductive carbon and binders. A composite material is coated on a conductive substrate, which is called current collector. The cathode components are shown in Fig. 2.2. The electron must be able to transfer from the current collector to the active material when the redox reaction takes place. Hence, the electronic conductivity is an important factor on the design of the cathode. The low electronic conductivity of the active material, which normally being transition metal oxide, can be compensated by the addition of conductive carbon black. Furthermore, the mechanical properties, namely, strength and elasticity, are critical also. Because of a volume change of the active material during the intercalation reaction, the type and amount of binder are a very crucial factors that affect the long term stability of the cathode. However, the addition of the mentioned ingredients would increase the weight of the cathode and, especially, the cost of the raw materials which may limit the commercial viability and its application. Thus, in order to obtain the high-performance and commercializable cathode, the composition of these components must be optimized [25].
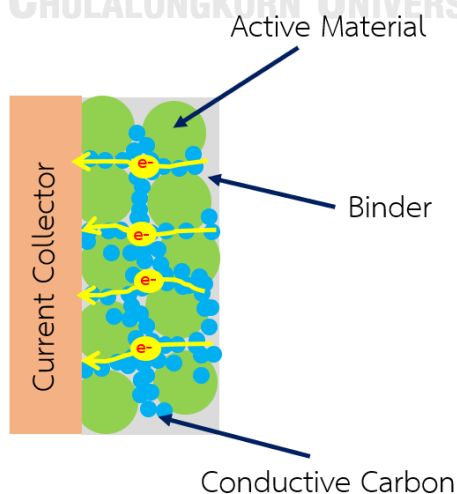
Figure 2.2 Schematic of the cathode components

Most of recent studies on ZIBs were on the development of new intercalation cathodes. Several cathodes for ZIBs have been reported, i.e., manganese oxide (MnO_2), vanadium oxide (V_2O_5), Prussian blue analog (PBAs) and others [26]. The typical cathode materials for ZIBs reported in the literatures are listed in Table 2.1. A Zn/MnO_2 battery is the most intensively investigated ZIB device. It stores energy via conversion reactions attributed to the existence of a variety of oxidation states of MnO_2 [27].

Table 2.1 Typical cathode materials for ZIBs

Cathode material	Reversible Capacity (mA h/g)	Current density (mA/g or C-rate)	Reference
α-MnO_2	210	0.5C	[21]
γ-MnO_2	285	0.05 mA/cm^2	[28]
Todorokite-type MnO_2	108	0.5C	[29]
α-MnO_2	195	0.5C	[30]
Copper hexacyanoferrate	56	20	[31]
Carbon coated MnO_2	272	66	[11]
Mn_2O_3	135	100	[32]
Potassium nickel hexacyanoferrate	55.6	0.2C	[33]
α-MnO_2 nanorod	233	83	[8]
Ni foam-supported polyaniline	183.28	2.5 mA/cm^2	[34]

Nonetheless, MnO_2 is one of the most promising cathodes for ZIBs, as it exhibits a high theoretical specific capacity of 308 mA h/g for divalent cation intercalation [35]. However, in practice, the specific capacity of MnO_2 is lower than that of theoretical value. It depends on its crystal structure [26].

2.4.1 Manganese Oxide (MnO_2)

Manganese (IV) oxide is an inorganic compound with the formula MnO_2. This blackish or brown solid occurs naturally as the mineral pyrolusite, which is the main ore of manganese and a component of manganese nodules. Due to low-cost, non-toxicity, and environmental safety, as well as its high theoretical specific capacity (308 mA h/g), MnO_2 is generally considered to be the most promising transition metal oxide for the next generation of supercapacitors [36]. It is important to notice that the maximum capacity of the host MnO_2 is strongly dependent on the crystal structures of MnO_2, which exist in many forms, namely, **β**-, **γ**, **α**-, **R**-, **λ**-, and **δ**-type. MnO_2 can exist as different polymorphs, depending on the linkage of fundamental MnO_6 octahedron units [37]:
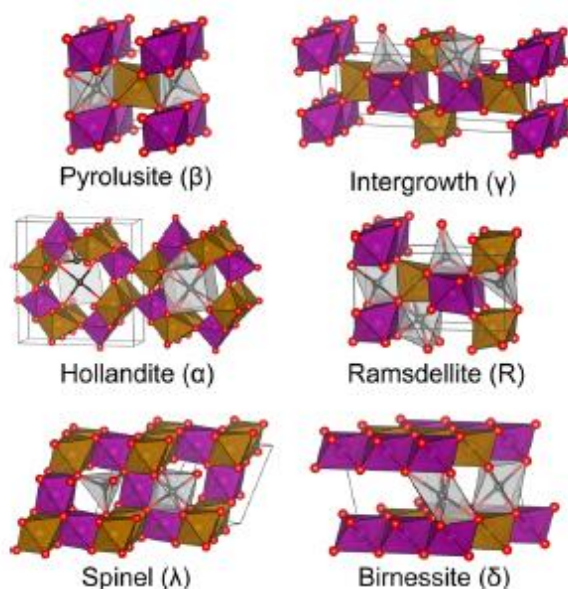
Figure 2.3 Common polymorphs of MnO_2 [38]

There are many nanostructures of MnO_2 including nanosheets, nanotubes, nanorods, nanowires, nanoflakes, nanoneedles, nanoflowers, nanourchins and nanospheres. Fig. 2.4 shows SEM images of the various nanostructured MnO_2 materials; the size and morphology of particles depend on the nature of the oxidant and the pH of the mixture.
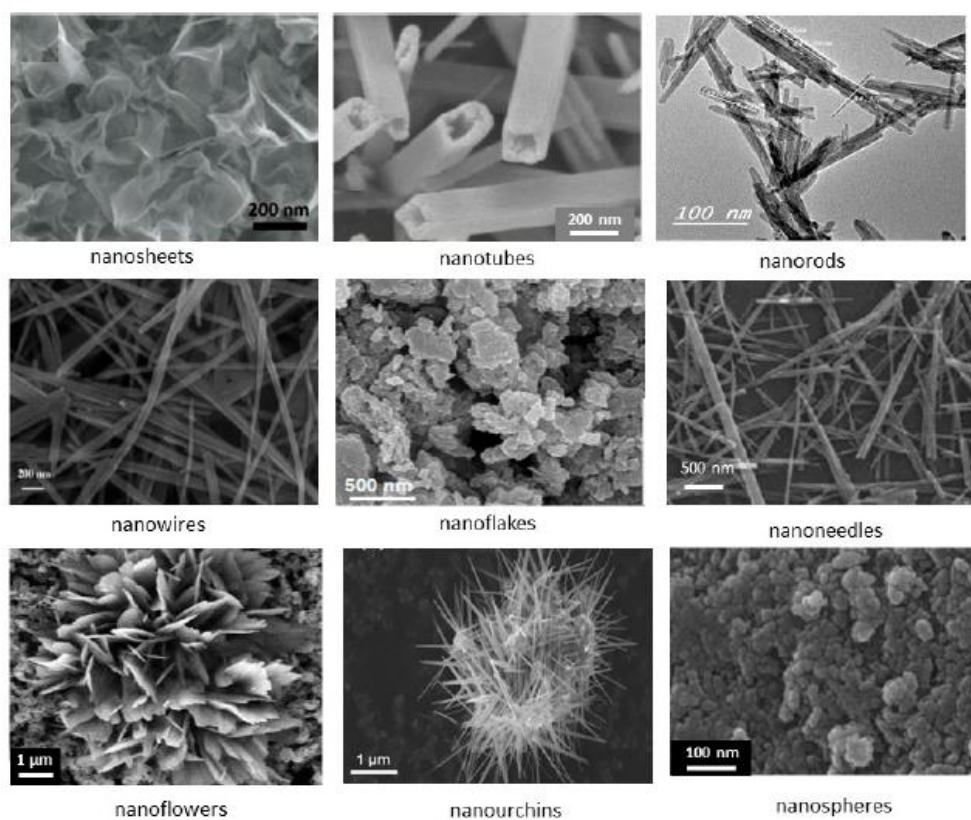
Figure 2.4 SEM images of the various nanostructured MnO_2 materials [39]

Ali et al. [40] studied the electrochemical performance of MnO_2 nanoflowers which were recovered from a spent household zinc–carbon battery. The MnO_2 was recovered as 3D nanostructure with nanoflower morphology and it delivered high specific capacitance with stable electrochemical cycling. Alfaruqi et al. [8] showed a nanorod-type α-MnO_2 cathode which was prepared by a facile hydrothermal method. This cathode exhibited an initial discharge capacity of 233 mA h/g at a

current density of 83 mA/g with nearly 100% coulombic efficiency for ZIBs. Xu et al. [41] prepared rod-like manganese oxide (MnO_2)/acid-treated carbon nanotube (a-CNT) nanocomposites for ZIBs. The ZIBs displayed both excellent storage properties with zinc ions (~400 mA h/g at 1 A/g) and reversibility at various current rates. The electron transfer efficiency of the MnO_2/a-CNT nanocomposites greatly increased and resulted in high electrical conductivity. Wang et al. [42] synthesized a nanoflower-like **δ**-MnO_2 via a microwave-assisted hydrothermal method as an electrode material for application in supercapacitors. The supercapacitors showed a specific capacitance of 328 F/g at 5 mV/s which could be used as high-performance electrode material. Lee et al. [29] prepared a todorokite-type MnO_2 for use as a new cathode material for zinc-ion cells. A discharge capacity of 108 mA h/g at 0.5C and a good rate performance were observed in the potential range of 0.7–2.0 V.

2.4.2 Carbon material

Carbon is a chemical element, like hydrogen, oxygen, lead or any of the others in the periodic table. It is a very abundant element. Carbon is capable of forming many allotropes (meaning having the same chemical formula but different physical properties) due to its valency as shown in Fig.2.5. Allotropes of carbon include:

1. Graphite: a sheet of hexagonal carbon structure

2. Graphene: essentially single-atom-thick sheets of graphite

3. Carbon Nanotubes: graphene sheets rolled into a tube shape (really a spiral)

4. Buckyball: a graphene sheet rolled into a sphere forming a buckyball
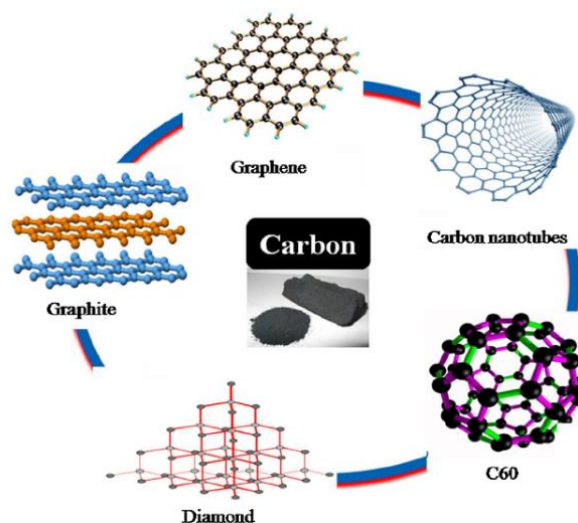
Figure 2.5 Various allotropes of carbon [43]

Graphite is a crystalline allotrope or polymorph of carbon element, a semimetal, a native element mineral, and a form of coal. It is one of three allotropic forms of carbon which exist in nature.

2.5 Anode

Zinc is the fourth most common metal in use. Worldwide, 95% of new zinc is mined from sulfidic ore deposits, in which sphalerite (ZnS) is nearly always mixed with the sulfides of copper, lead and iron. Zinc has an electron configuration of $3d^{10}4s^2$ and is a member of group 12 in the periodic table. It is a moderately reactive metal and strong reducing agent [44]. In the literature, zinc metal is used as anode material, typically, in the form of foil plate and electrodeposition on other metals, for example Nickel foam [8, 32]. The anode for ZIB is the zinc in metal form, which has a role in supplying the electron and the zinc cation for the intercalation reaction. A zinc foil is the most widely used form of the anode among the ZIB researches due to its simplicity and low cost. However, it is interesting to note that those works had avoided some important issues when choosing the anode material, for instance, the

morphology and the amount of zinc that should be necessary for the intercalation reaction, and the corrosion of the zinc in the electrolyte.

2.6 Electrolyte

An electrolyte is a charge conducting medium of battery, which contains at least two species of ion. In ZIB, the electrolyte is the polar solvent with the addition of zinc salts, for instance, zinc sulphate ($ZnSO_4$), zinc trifluoromethanesulfonate ($Zn(OTf)_2$), zinc nitrate ($Zn(NO_3)_2$), zinc bis(trifluoromethanesulfonyl)imide ($Zn(TFSI)_2$), zinc chloride ($ZnCl_2$) and zinc perchlorate ($Zn(ClO_4)_2$), and some of the supporting electrolytes in order to enhance its ionic conductivity [26]. Electrolyte is a zinc-ion source for the zinc intercalation reaction at cathode and the zinc deposition at the anode. Many aspects are considered in order to choose the electrolyte for the ZIB, including the solubility of zinc salts, the electrical stability, the compatibility with the electrode and the tendency of some parasitic reactions that may harm the battery [26].

Zinc sulfate ($ZnSO_4$) is an inorganic compound and can be formed in three hydrates: monohydrate, hexahydrate and heptahydrate. It is easily soluble in water; its aqueous solution is acidic. It is slightly soluble in ethanol and glycerol. It is mainly used as an electrolyte in an electrolytic media for a zinc-ion battery [31, 45].

2.7 Intercalation principle of ion batteries

Batteries are the electrochemical cells, which include at least two electroactive materials. One is some kind of reducing agents (negative electrode or anode), while another is some kind of oxidizing agents (positive electrode or cathode). In other word, there is the difference in the electron energy between them, which is the driving force for moving electron to produce the electricity. In general case, negative electrode or anode is an electron source in batteries, which usually are monovalent

or multivalent metals, for instance, Li, Na, Mg, Ca, Zn, Ni and Al. These materials have negative potential compared with the standard hydrogen electrode (SHE), as shown in Table 2.2.

Table 2.2 Standard reduction potential at 25°C (298 K) of common metals [46]

Half-Reaction	Potential, $^{\circ}E$ (V)
$2H^+ + 2e^- \leftrightarrow H_2$	0.00
$Ni^{2+} + 2e^- \leftrightarrow Ni$	-0.23
$Zn^{2+} + 2e^- \leftrightarrow Zn$	-0.76
$Al^{3+} + 3e^- \leftrightarrow Al$	-1.66
$Mg^{2+} + 2e^- \leftrightarrow Mg$	-2.37
$Ca^{2+} + 2e^- \leftrightarrow Ca$	-2.76
$Li^+ + e^- \leftrightarrow Li$	-3.05

The positive electrode is the electron sink. For the purpose of being an electron sink, for rechargeable batteries, the positive electrode or cathode should have the ability to store electron when the battery is utilized and release the electron when recharging with good reversibility. The difference between these two processes is the change in the chemical structure of the cathode. The conversion reaction has changed most of the chemical structure of the cathode materials, whilst the intercalation reaction is the insertion/extraction of the guest metal cation into/from the cathode materials without significantly changing their chemical structure. Such materials are called host materials and batteries based on this mechanism are called metal-ion batteries (MIBs). The intercalation reaction can be illustrated as shown in Fig. 2.6.
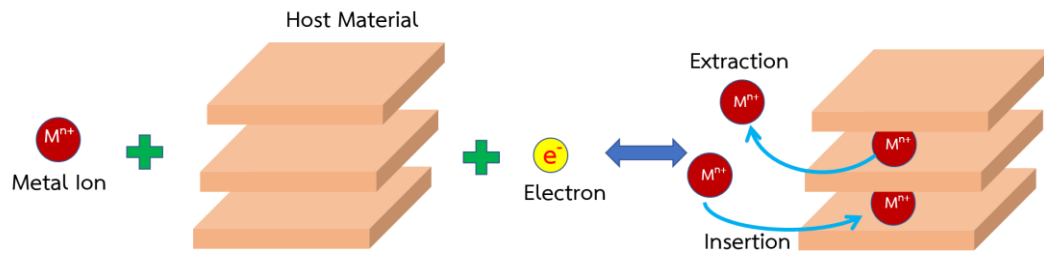
Figure 2.6 Illustration of the charge-storage mechanism of MIBs

The reduction reaction can be illustrated as:

Anode reaction: $x\text{M}^{n+} + (n \cdot x)\text{e}^- \leftrightarrow x\text{M}$ (2.4)

Cathode reaction: $x\text{M}^{n+} + \text{H} + (n \cdot x)\text{e}^- \leftrightarrow \text{M}_x\text{H}$ (2.5)
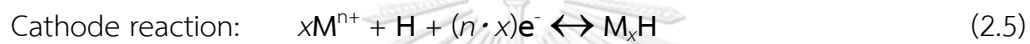
The overall reaction of the cell can be written as:

Overall reaction: $x\text{M} + \text{H} \leftrightarrow \text{M}_x\text{H}$ (2.6)
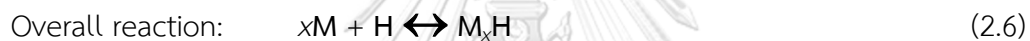
where **M**, n, **H** and x are the metal-ion, the oxidation number of metal-ion, the host material and the state of intercalation, respectively.

One of the noticeable points is that most of the host materials being used for MIBs are the transition-metal oxides which are able to change the oxidation state in order to store both electron and metal-ion in its structure. This charge-storage mechanism proven that they have better reversibility compared to the traditional conversion reaction [47].

2.8 Pseudocapacitive behavior

Traditional supercapacitors are called electric double layer capacitors (EDLCs) where charges are stored electrostatically at the interface of electrodes (a non-Faradaic process). Electrochemical features of pseudocapacitive materials are neither purely capacitive nor bulk Faradaic processes. Hence, the "pseudo" prefix is used to differentiate it from EDLC. The reaction at the cathode of battery when contacts with electrolyte may contribute several reactions, namely, the main reaction (intercalation

of zinc), capacitance (ion adsorption), irreversible conversion and electrolyte decomposition [47]. The capacitive effect is characterized by analyzing the cyclic voltammetry data at different sweep rates. A representative power law relationship between the current (i) and scan rate (v) reveals the charge-storage mechanism in ion battery:

$$i = av^b \tag{2.7}$$

where a and b are constants. The b value can be figured out by profiling the $\ln(i)$–$\ln(v)$ curve. If b = 0.5, the Faradic diffusion is predominant; while b = 1, the pseudo-capacitance assumes the primary contribution. Furthermore, as for a fixed sweep rate, the specific pseudo-capacitance contribution can be given in detail by the following formula:

$$i = k_1 v + k_2 v^{1/2} \tag{2.8}$$

where the parameter $k_1 v$ represents the capacitive process while the $k_2 v^{1/2}$ is in favor of the diffusion process.

The above mentioned pseudocapacitive kinetics are more obvious in battery electrodes of nanomaterials due to the significantly decreased ion diffusion.

2.9 Analytical techniques

2.9.1 Cyclic Voltammetry (CV)

a) Cyclic voltammetry profile

The common technique for investigating the redox reaction characteristic of the electrode is cyclic voltammetry. With this method, the potential of the working electrode, with respect to the reference electrode, added linearly starting from an

initial point to the vertex point, then, is added in the opposite direction to the final

point. The output from this action is the rate of the redox reaction in form of current,

as shown in Fig. 2.7.
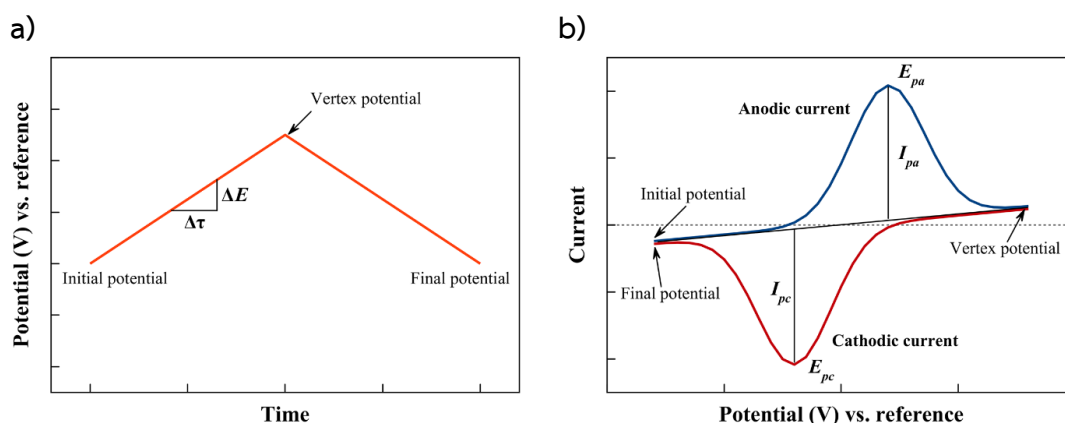
Figure 2.7 a) The input potential profile and b) the typical cyclic voltammogram of

the reversible reaction [48]

The influential parameters for this characterization are the potential range and

the scan rate, which is the rate of the potential ramp with respect to time. According

to the Fig. 2.7 b), the E_{pa}, E_{pc}, I_{pa} and I_{pc} are the anodic peak potential, the cathodic

peak potential, the anodic current and the cathodic current, respectively. The

inclined straight line represents the background current, which is resulted from the

capacitance effect [49].

b) Cyclic voltammetry cell configuration

To perform CV measurement, cell configuration is set up and a brief description

is generally given for the parameter setup used to collect the data. A schematic of a

CV measurement is presented in Figure 2.8.
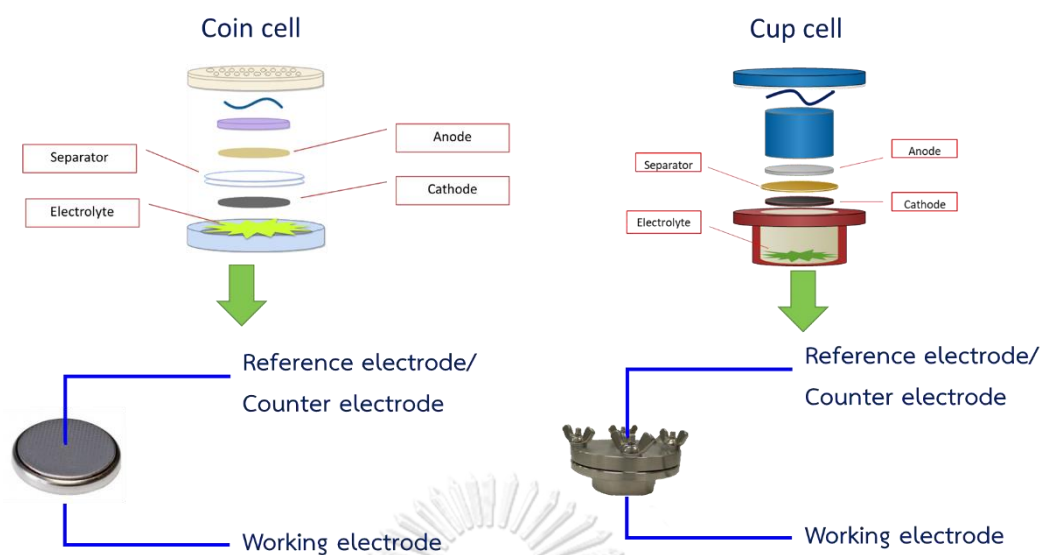
Figure 2.8 Schematic of a CV measurement configuration

The working electrode carries out the electrochemical reaction of interest. A potentiostat is used to control the applied potential of the working electrode as a function of the reference electrode potential. A reference electrode has a well-defined and stable equilibrium potential. The electrical circuit is completely closed by counter electrode [49]. The applied potential is thus typically reported as "versus or vs" with a specific reference as shown in Fig. 2.7. This study used Zn/Zn^{2+} as a specific reference. Zinc anode was used to act as a reference and counter electrode.

2.9.2 Galvanostatic Charge-Discharge

The standard method for determination of the cell performance and cyclability is to apply the discharge and charge currents to the cell repeatedly within the specific voltage, namely upper cut-off current and lower cut-off current. The result is the voltage profile with respect to time [23]. The obtained results can be used to determine the specific capacity, energy density and coulombic efficiency via equation 2.9, 2.10, 2.11 and 2.12, respectively. In general, the testing current is normalized

with the amount of the active host material that the electrode contained, as shown in equation 2.9.

$$\text{Current Density} = \frac{I}{m_{act}} \tag{2.9}$$

where I and m_{act} are testing current and amount of the active host material, respectively.

The capacity of the cathode is determined by measuring the total charge that is delivered from the cathode upon the charging or discharging. This could be obtained via the integration of the current with respect to the time from the initial state to the cut-off state, then normalization of this value by the mass of the active host material, as shown in equation 2.10.

$$\text{Specific capacity} = \frac{1}{m_{act}} \left(\int_{t_0}^{t_f} I \, dt \right) \tag{2.10}$$

where t_0 and t_f are initial time and time at cut-off state, respectively.

The energy for the charging and energy that was obtained from discharging process can be calculated with equation 2.11.

$$\text{Energy density} = \frac{1}{m_{act}} \left(\int_{t_0}^{t_f} IV \, dt \right) \tag{2.11}$$

where V is voltage.

The percentage of discharging capacity compared with the charging capacity, called coulombic efficiency, is one of the most critical factors to consider the reversibility of the battery. This value can be calculated by using equation 2.12.

$$\text{Coulombic efficiency (\%)} = \frac{Discharging\ Capacity}{Charging\ Capacity} \times 100 \qquad (2.12)$$

2.9.3 Electrochemical Impedance Spectroscopy (EIS)

The electrochemical impedance spectroscopy is the technique for analysis of the electroactive compound or the electrochemical cell via the applying of both frequency-varying sinusoidal potential (2-10 mV) and static potential to the testing cell. The result from this technique is the impedance spectra, which comprises of the size of impedance and phase lag between the input and output signal at each frequency [50].
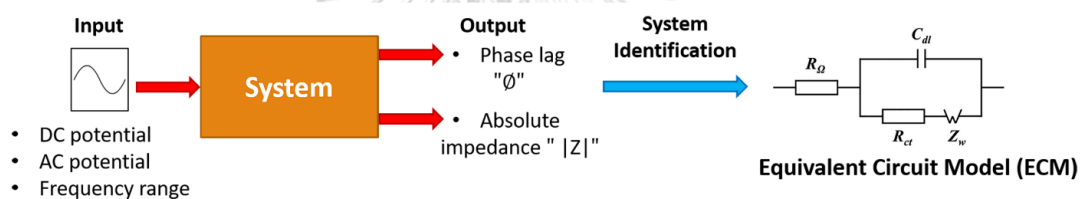
Figure 2.9 Schematic represents the system analysis via EIS technique

In battery application, this technique is a powerful tool to interpret the change in charge transfer characteristic upon the cycling. The impedance spectra is fitted with some proposed model in order to retrieve the internal resistance, the double-layer capacitance, the charge transfer resistance and the other associated parameters to the charge transport in the battery [51].

2.9.4 X-Ray Diffraction (XRD)

X-ray diffraction is a characterization technique used for the analysis of the crystal structure of the material. The benefit of this technique is to identify the phase of new materials. The XRD is based on the applying of X-ray beam to the sample at

various angles, then detecting the scattering reflected beam. The result is the relation between the intensity of reflected beam and the angle, which can indicate the allocation of lattices structure of the tested sample.

2.9.5 Field Emission Scanning Electron Microscopy (FESEM)

Field emission scanning electron microscopy (FESEM) is used to study the surface of a sample on a nanoscale, specifically morphological characteristics, such as shape characteristics and nanostructure pattern or nanosize of components. The working principle of FESEM is that the beam of the electron will penetrate only the outer surface of the object which is visible as a 3D image.

2.9.6 Transmission Electron Microscopy with Energy Dispersive Spectroscopy (TEM-EDS)

Transmission electron microscopy with energy dispersive spectroscopy (TEM-EDS) is an imaging mode of specialized transmission electron microscope (TEM) that allows for direct imaging of the atomic structure and providing chemical composition of the sample. It is a powerful tool to study the properties of materials on an atomic scale, such as semiconductors, metals, nanoparticles. It is also possible to produce an image from electrons deflected by a particular crystal plane.

CHAPTER 3

RERSEARCH ARTICLES

This topic includes 2 research articles:

3.1 **δ**-MnO$_2$ nanoflower/graphite cathode for rechargeable aqueous zinc-ion batteries

3.2 MnO$_2$ heterostructure on carbon nanotubes as cathode material for aqueous zinc-ion batteries

All research articles are partial fulfillment of dissertation for graduation.

3.1 Article I

δ-MnO$_2$ nanoflower/graphite cathode for rechargeable aqueous zinc-ion batteries

Sonti Khamsanga[1], Rojana Pornprasertsuk[2,3,4], Tetsu Yonezawa[5], Ahmad Azmin Mohamad[6] and Soorathep Kheawhom[1,3,*]

[1]*Department of Chemical Engineering, Faculty of Engineering, Chulalongkorn University, Bangkok, 10330, Thailand.*

[2]*Department of Materials Science, Faculty of Science, Chulalongkorn University, Bangkok, 10330, Thailand.*

[3]*Research Unit of Advanced Materials for Energy Storage, Chulalongkorn University, Bangkok, 10330, Thailand.*

[4]*Center of Excellence in Petrochemical and Materials Technology, Chulalongkorn University, Bangkok, 10330, Thailand.*

[5]*Division of Materials Science and Engineering, Faculty of Engineering, Hokkaido University, Kita 13 Nishi 8, Sapporo, Hokkaido, 060-8628, Japan.*

[6]*School of Materials and Mineral Resources Engineering, Universiti of Sains Malaysia, 14300 Nibong Tebal, Pulau Pinang, Malaysia.*

*Correspondence and requests for materials should be addressed to S. Kheawhom

(email: soorathep.k@chula.ac.th)

Article I: δ-MnO$_2$ nanoflower/graphite cathode for rechargeable aqueous zinc-ion batteries

Abstract

Manganese oxide (MnO$_2$) is one of the most promising intercalation cathode materials for zinc-ion batteries (ZIBs). Specifically, a layered type delta manganese oxide (δ-MnO$_2$) allows reversible insertion/extraction of Zn^{2+} ions and exhibits high storage capacity of Zn^{2+} ions. However, a poor conductivity of δ-MnO$_2$, as well as other crystallographic forms, limits its potential applications. This study focused on δ-MnO$_2$ with nanoflower structure supported on graphite flake, namely MNG, for use as an intercalation host material of rechargeable aqueous ZIBs. Pristine δ-MnO$_2$ nanoflowers and MNG were synthesized and examined using X-ray diffraction, electron spectroscopy, and electrochemical techniques. Also, performances of the batteries with the pristine δ-MnO$_2$ nanoflowers and MNG cathodes were studied in CR2032 coin cells. MNG exhibited a fast insertion/extraction of Zn^{2+} ions with diffusion scheme and pseudocapacitive behavior. The battery using MNG cathode exhibited a high initial discharge capacity of 235 mA h/g at 200 mA/g specific current density compared to 130 mA h/g which was displayed by the pristine δ-MnO$_2$ cathode at the same specific current density. MNG demonstrated superior electrical conductivity compared to the pristine δ-MnO$_2$. The results obtained paved the way for improving the electrical conductivity of MnO$_2$ by using graphite flake support. The graphite flake support significantly improved performances of ZIBs and made them attractive for use in a wide variety of energy applications.

3.1.1 Introduction

Manganese dioxide (MnO_2) is widely used as a cathode material in battery technologies because of its several advantageous properties such as low-cost, abundance, low toxicity, and environmental friendliness [5, 52, 53]. MnO_2 were previously studied and applied for a variety of energy storage devices [10, 54-56]. Also, it was applied in different metal-ion batteries including Li-ion battery (LIB) [6], Mg-ion battery (MIB) [7] and Zn-ion battery (ZIB) [8, 57]. MnO_2 cathodes are inexpensive and exhibit a high theoretical capacity. Recently, aqueous Zn/MnO_2 batteries are considered as promising alternative energy devices due to their high safety and the abundance of both Zn, MnO_2 and the electrolyte [9, 29, 58].

However, MnO_2 suffers from its poor conductivity that often occurs in high internal resistance of the electrode resulting in poor performance of the battery [27]. Therefore, to improve the performance of the MnO_2 cathode, it is necessary to increase the specific surface area of MnO_2 as well as the ion diffusion rate [59, 60]. MnO_2 has various crystallographic polymorphs such as α-MnO_2, β-MnO_2, and δ-MnO_2, etc. Among these, δ-MnO_2 was reported to be a potential intercalation host material for aqueous ZIBs [61] due to a substantial interlayer distance for the reversible insertion/extraction of Zn^{2+} ions. δ-MnO_2 can be prepared by a chemical reduction or hydrothermal process [62]. The conventional synthesis method is the direct reduction of $KMnO_4$ aqueous solution by dropwise introduction of concentrated HCl. Previously, δ-MnO_2 nanoflakes were synthesized and used in aqueous ZIBs [61]. It led to a significant increase in the power density of the ZIB. Another approach undertaken was to support MnO_2 nanostructures on a matrix material with a high surface area [10, 63, 64]. It was observed that these nanostructures could accelerate the charge transport during the electrochemical redox process. In this respect, various carbonaceous materials, namely activated carbon, carbon nanotubes (CNTs), carbon nanofibers (CNFs), graphene and graphite, have been integrated with MnO_2.

MnO_2/graphene nanoflowers were synthesized in the form of sandwich-structured nanoflowers which exhibited excellent super capacitive properties effectively making it a very conductive electrode material for high-performance supercapacitors [12]. However, it is significant that MnO_2 supported on graphite has not been reported previously in ZIBs application. The crystal structure of graphite consists of parallel planes of carbon atoms which is conductive primarily along its planes [65, 66]. In this way, graphite is classified as a semimetal due to its high electrical conductivity [67]. Therefore, MnO_2 supported on graphite is considered as the candidate due to an improvement in electronic conductivity and an increase in the stability of the electrode materials for ZIBs.

The present study reports on $δ$-MnO_2 nanoflower/graphite as a cathode host material for rechargeable aqueous ZIBs. The $δ$-MnO_2 nanoflower supported on graphite not only increases the electrical conductivity and discharge capacity of the battery but also improves the insertion/extraction acceleration by increasing the active area of the $δ$-MnO_2 nanoflower. Accordingly, the electrochemical properties and performances of the batteries which use the MNG as host material cathode are examined and discussed.

3.1.2 Experimental

Chemical and materials

Reagent grade chemicals were obtained and used without further purification unless noted otherwise. The graphite powder was purchased from Aldrich Company. Potassium permanganate ($KMnO_4$), manganese sulfate monohydrate ($MnSO_4.H_2O$), zinc sulfate ($ZnSO_4$), sulfuric acid (H_2SO_4), and cellulose acetate were purchased from Ajax Finechem. Nickel foam (0.5 mm thick, 100 PPI) was purchased from Qijing Trading Co., Ltd. Whatman filter paper No. 1 was purchased from Sigma-Aldrich.

Graphite foil was purchased from Shenzhen 3KS Electronic Material Co. Ltd. Zn sheet (99.99%) was purchased from Sirikul Engineering Ltd.

Preparation of δ-MnO₂ nanoflower and δ-MnO₂ nanoflower/graphite (MNG)

The pristine δ-MnO_2 nanoparticles were synthesized by dissolving $KMnO_4$ (1.98 g) in 60 mL of deionized (DI) water. Then, $MnSO_4.H_2O$ (0.336 g) was dissolved in 20 mL of DI water. Next, the $MnSO_4.H_2O$ solution was added dropwise to the $KMnO_4$ solution, and continuous stirring was followed for 30 min. Afterward, the mixture was transferred into a 100 mL Teflon autoclave and kept at 160 °C for 24 hr in an oil bath. The product was collected and washed with DI water several times. Then, it was dried at 80 °C for 12 hr. The MNG synthesis was similar to the method reported by Liu et al. [12] with some modifications. Graphite (1.0 g) was mixed in DI water (500 mL) with $KMnO_4$ (10.0 g). The mixture of graphite and $KMnO_4$ was stirred for 18 hr. Then, 98% of H_2SO_4 (5 mL) was added dropwise into the mixture. The solution was continuously stirred for 1 hr and heated to and maintained at 80 °C for 1 hr. After that, the solution was diluted in 1 L of DI water and allowed to stand at room temperature. The solution was filtered using cellulose filter paper (pore size 11 μm). Then, the MNG precipitates were collected and washed by DI water several times until the violet color disappeared. Subsequently, the precipitates were dried at 80 °C overnight.

Characterization and electrochemical measurement

X-ray Diffraction (XRD, Bruker AXS Model D8 Discover) of the powder samples was carried out with Cu Kα radiation at a scanning range of 5-80°. Field Emission Scanning Electron Microscope (FESEM, JEOL JSM-7610F, Tokyo, Japan) was used to take the morphology image and nanoflower size of MNG.

The cathode using MNG was prepared by mixing together 70% wt. of MNG, 20% wt. of carbon black (CB), and 10% wt. of cellulose acetate binder. Alternatively, the cathode using pristine δ-MnO$_2$ was prepared by mixing together 70% wt. of the pristine δ-MnO$_2$, 20% wt. of carbon black (CB), and 10% wt. of cellulose acetate binder. Acetone was used to adjust the viscosity of the slurries. Each mixed slurry was coated on graphite foil using a lab coating machine (AOT-FCM-250, AOT Electronic Technology Co., LTD) and dried at 70 °C under vacuum. The thickness of the deposited cathode material was 25 μm. The zinc anode was prepared by electrodeposition of zinc from ZnSO$_4$ (0.5 M) aqueous solution onto Ni-foam using zinc sheet as a counter electrode at the current density of 60 mA/cm^2. The amount of zinc deposited was 20 mg/cm^2. Both cathode and anode were punched into a 15 mm diameter disk. The filter paper was punched into a 19 mm disk and used as the separator. Then, 0.3 mL of ZnSO$_4$ (1 M) was added to the cell. The testing cells were fabricated as a coin cell (CR2032).

Electrochemical measurements were carried out by using a CR2032 coin cell. Cyclic Voltammetry (CV) was performed by Potentiostat (VersaStat3, Princeton Applied Research) at a scan rate of 0.5 mV/s in the voltage range 1.0-1.8 V versus Zn^{2+}/Zn. A battery testing system (BTS-5V10mA, Neware, China) was used to investigate the performance of the battery. The charge-transfer resistance, as illustrated by the Nyquist plots for the cathode, was carried out using an Electrochemical Impedance Spectroscopy (EIS) technique using an amplitude of 10 mV in the frequency range of 1-100,000 Hz.

3.1.3 Results and discussion
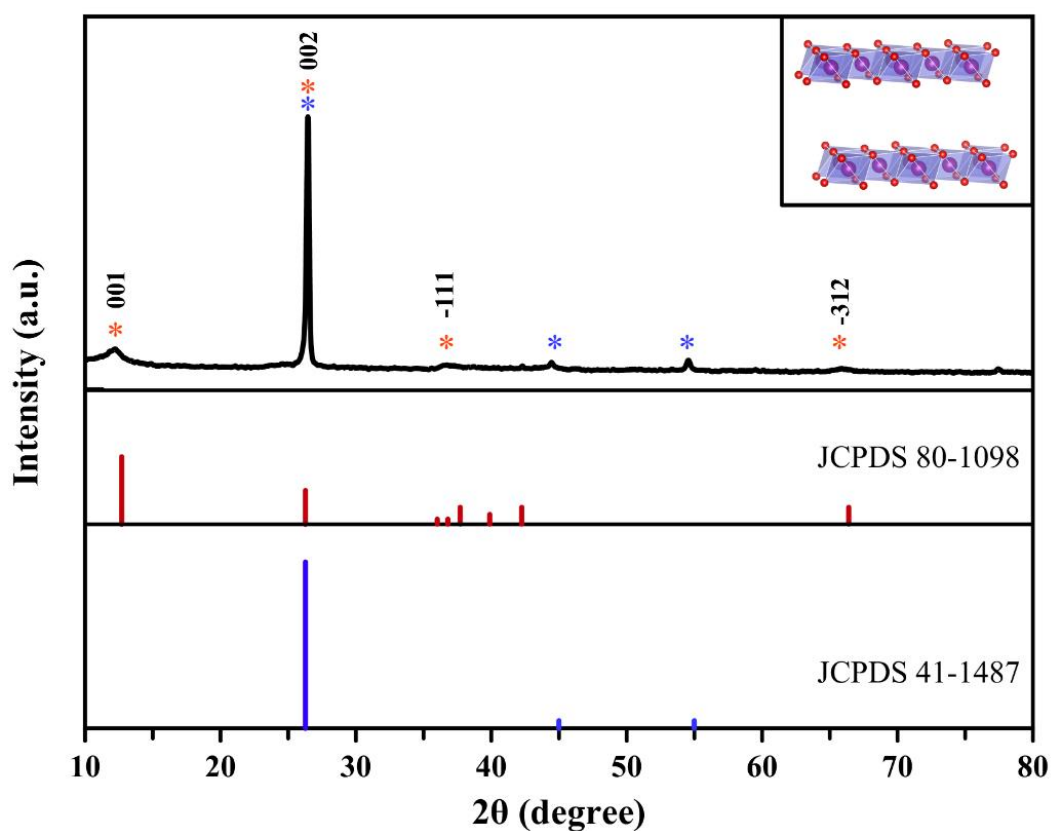
Figure 3.1 XRD pattern of the synthesized δ-MnO$_2$ nanoflower/graphite (MNG) and crystallographic structure of δ-MnO$_2$ (inset)

In this study, δ-MnO$_2$ nanoflower/graphite (MNG) was prepared by a modified method of Liu et al. [12]. In Fig. 3.1, the XRD patterns of MNG, δ-MnO$_2$ and graphite are shown. Thus, it can be seen that both patterns, i.e. δ-MnO$_2$ (JCPDS card no. 80-1098) [68, 69] and graphite (JCPDS card no. 41-1487) [70] match well with the XRD pattern of MNG. The diffraction peaks (2θ) at 12.2°, 26.5°, 36.6°, and 65.6° of MNG correspond to the (001), (002), (-111) and (-312) crystal planes of δ-MnO$_2$, respectively [71]. The high-intensity diffraction peak of MNG at 26.5° indicates the high crystallinity of graphite. δ-MnO$_2$ possesses a planar layered-structure as illustrated by the inset of Fig. 3.1. This structure suggests that the interlayer gap is easy to insert/extract foreign cations and thereby can be useful for energy storage

applications [69]. Further, the XRD analysis confirmed that the delta (δ) phase was presented in the pristine δ-MnO$_2$ sample (see Fig. B1 of Appendix B).
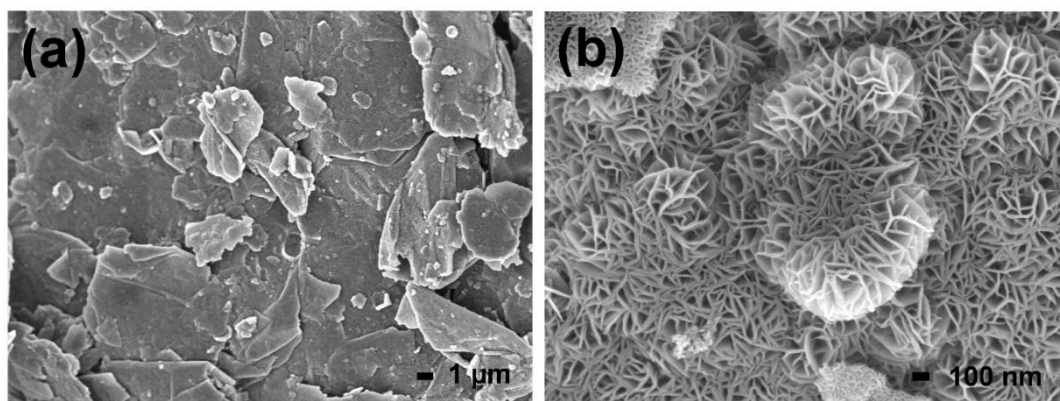
Figure 3.2 FESEM images of the synthesized δ-MnO$_2$ nanoflower/graphite (MNG): (a) low magnification image, and (b) high–magnification image

In Fig. 3.2 (a), the FESEM image of MNG is shown. It is observed that the numerous MnO$_2$ nanoflowers constructed on the graphite surface reveal a flake-like sample. Fig. 3.2 (b) shows the higher magnification image of MNG which indicates that many petals can interconnect forming micropores about 50 nm in diameter size. The MNG having micropores among petals will assist in increasing the contact area between the electrolyte and cathode material as well as ensure fast ion transfer in the charge/discharge process [12].
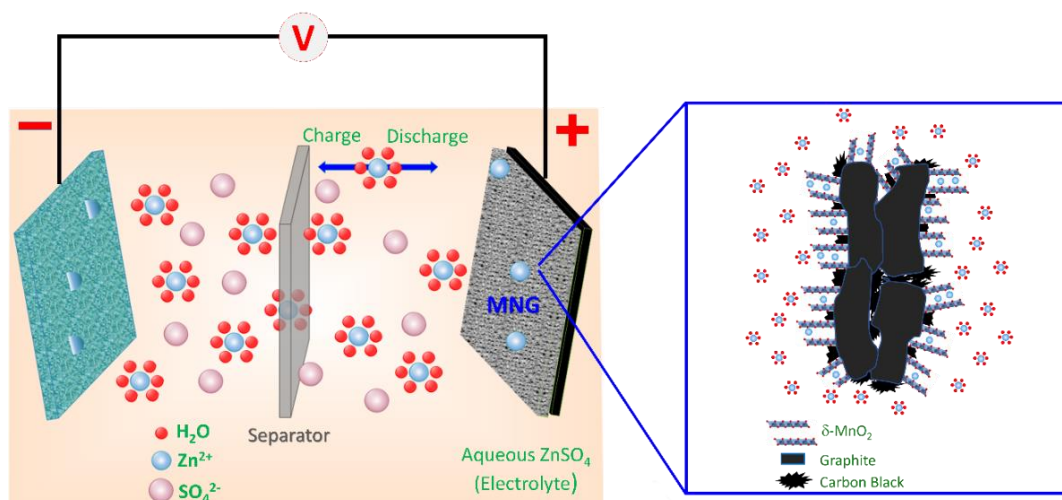
Figure 3.3 Schematics of the chemistry of the zinc-ion battery. Zn^{2+} ions migrate between tunnels of the MNG cathode and Zn anode. The inset on the right shows Zn^{2+} ion insertion and interconnection between δ-MnO_2 and graphite

In Fig. 3.3, the battery configuration in this study which is composed of the MNG cathode, zinc anode, and $ZnSO_4$ aqueous electrolyte is shown. During discharging, anodic zinc is dissolved in the form of Zn^{2+} ions into an aqueous electrolyte, containing Zn^{2+} ions and rapidly solvate in the form of solvated Zn^{2+} ion. Then, they diffuse and pass through the separator to the MNG cathode. The solvated Zn^{2+} ions are de-solvated in the form of Zn^{2+} ions and intercalated into δ-MnO_2 structure [22, 72] as illustrated by the inset of Fig. 3.3. Further, an electron current starts to flow in the electrical loop from the electrical conduction of graphite. These three processes can be reversed by (1) the de-intercalation of Zn^{2+} ions from MNG cathode, then (2) solvated species are formed and lastly (3) Zn^{2+} ions are reduced to Zn and deposited back on the zinc anode, respectively. The electrochemical reaction may be expressed as in Equation (3.1) anode reaction and Equation (3.2) cathode reaction:
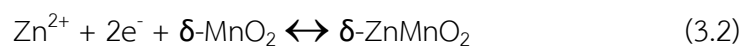
$$Zn \leftrightarrow Zn^{2+} + 2e^- \qquad (3.1)$$

$$Zn^{2+} + 2e^- + \delta\text{-}MnO_2 \leftrightarrow \delta\text{-}ZnMnO_2 \qquad (3.2)$$

During the electrochemical Zn^{2+} ion insertion, the layered type δ-MnO_2 structure can transform to spinel-type $ZnMn_2O_4$ with Mn(III) state and layered type δ-Zn_xMnO_2 with Mn(II) state [9].
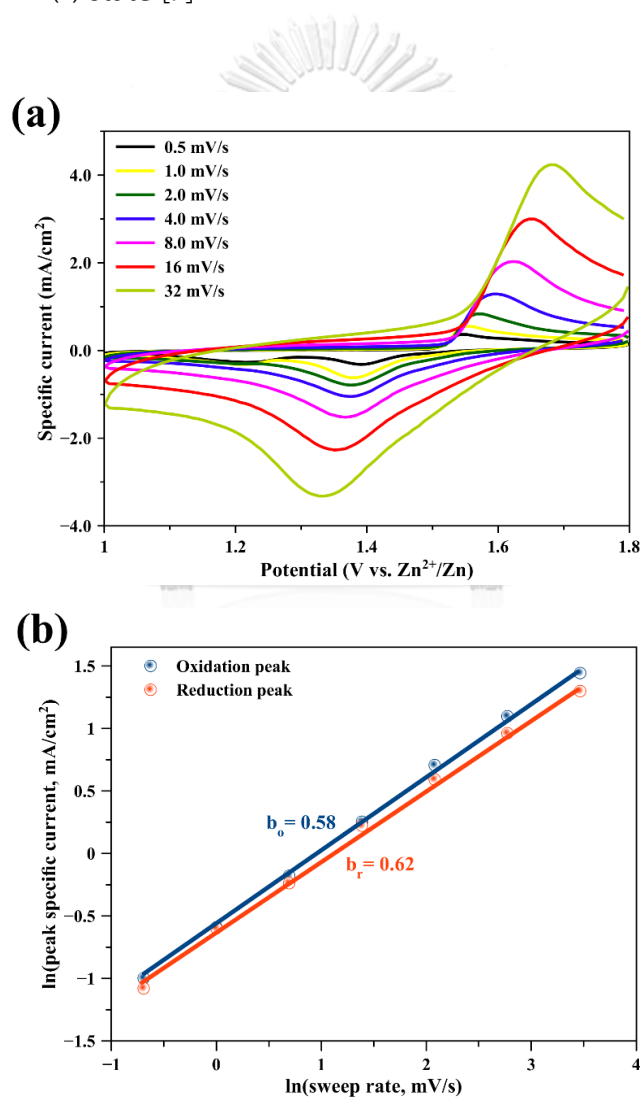
Figure 3.4 (a) Cyclic voltammograms of δ-MnO_2 nanoflower/graphite (MNG) cycling at different sweep rates, and (b) the fitted lines: ln(peak specific current) versus ln(sweep rate)

To investigate the kinetics of the MNG electrode, cyclic voltammograms using sweep rates of 0.5 to 32 mV/s in the voltage range 1.0-1.8 V versus Zn^{2+}/Zn were measured using CR2032 coin cells. As shown in Fig. 3.4 (a), a dominating pair of redox peaks exhibits increasing currents when the sweep rates increase, which do not display rectangular-shape and symmetrical voltammograms even at high scan rates, compared to MnO_2/activated carbon composite for supercapacitors [73]. It is noted that the MNG electrode does not present the capacitive behavior of the electrode [74, 75]. The capacitive effect is characterized by analyzing the cyclic voltammetry data at different sweep rates as in Equation (3.3):

$$i = av^b \qquad (3.3)$$

where i is the peak specific current, v is a potential sweep rate and a , b are adjustable parameters. The redox reaction is limited by the diffusion-controlled behavior; the peak current i varies as $v^{1/2}$. Although the capacitance contribution suggests that the peak current i varies as v [76, 77]. Equation (3.3) can be taken with logarithm and can be expressed according to Equation (3.4):

$$\ln i = b \ln v + \ln a \qquad (3.4)$$

The b value denotes the slope of the plot of $\ln i$ versus $\ln v$. When b value is close to 1, the system is mainly controlled by capacitance; when b value is close to 0.5, the Zn^{2+} ion insertion process dominates. Fig. 3.4 (b) shows the $\ln i$ versus $\ln v$ plots at oxidation and reduction process of the cyclic voltammogram. The b_o (oxidation process) and b_r (reduction process) of the MNG cathode are 0.58 and 0.62, respectively. Since the average b values are close to 0.5, it may imply that the redox reactions on the MNG cathode are controlled by the diffusion process. MnO_2 is a

transition metal oxide that typically displays the pseudocapacitance behavior [78]. The capacitive-controlled process occurs only on the surface. However, in the case of MNG cathode, the characteristic of Zn^{2+} ions insertion/extraction deviates from capacitive-controlled process towards the diffusion-controlled process. That is, the insertion/extraction of Zn^{2+} ions occur not only on the surface but also in the pores. The result shows good agreement of a fast Zn^{2+} ion insertion/extraction or high rate property for the battery [76].

(c)

(d)
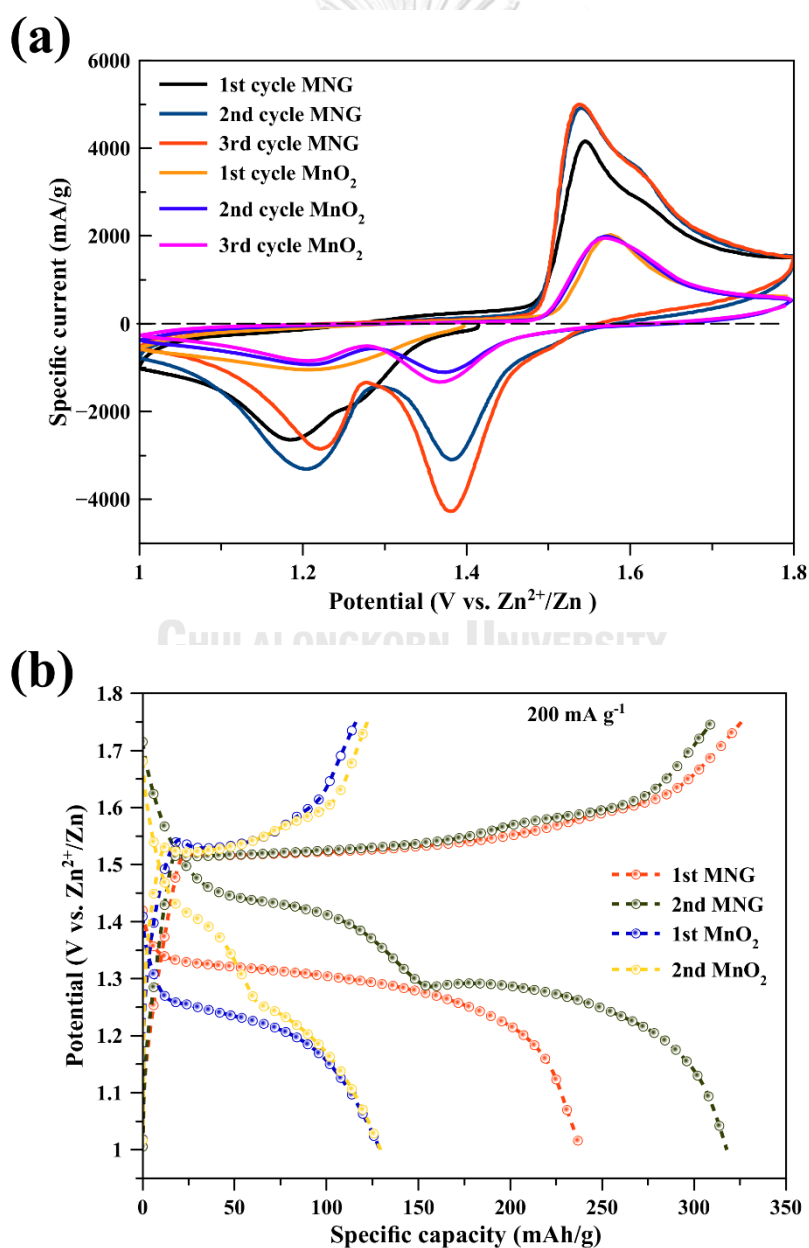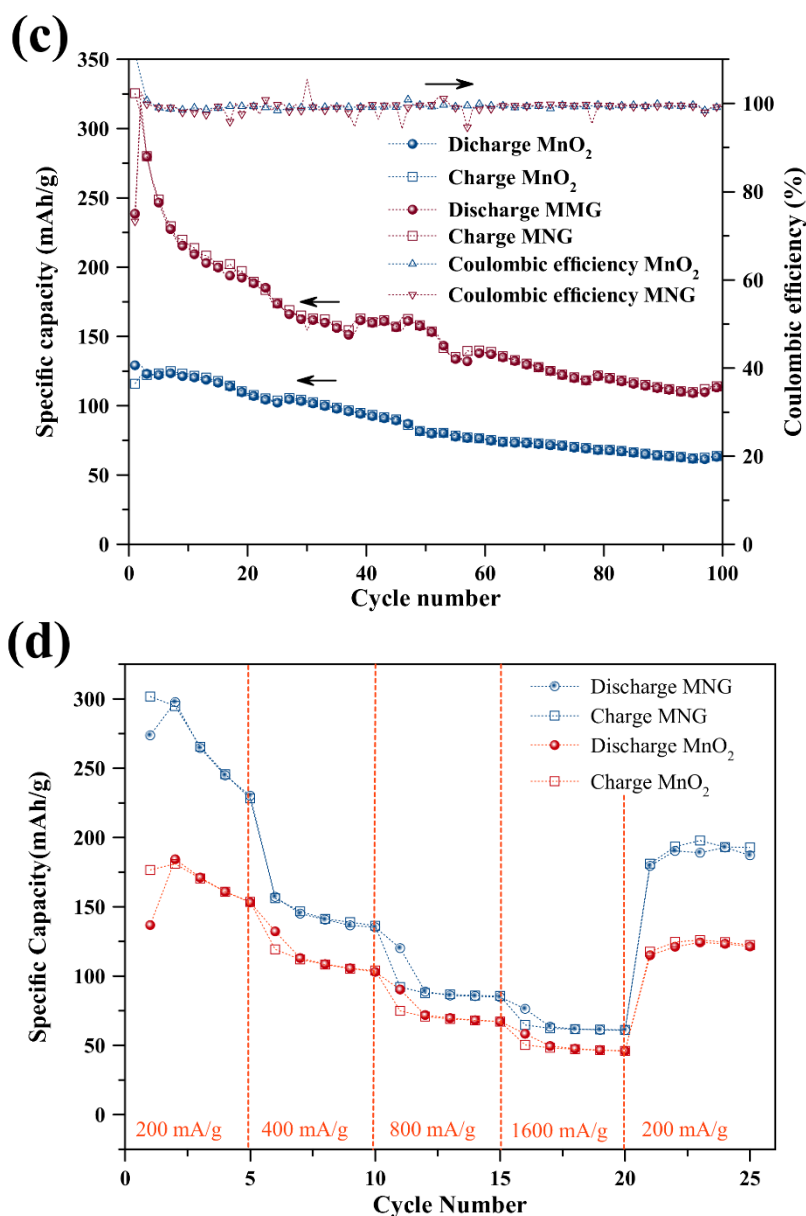
Figure 3.5 Performances of the batteries: (a) cyclic voltammograms of the batteries at a scan rate of 0.5 mV/s, (b) galvanostatic charge-discharge profile of the batteries at 200 mA/g, (c) Cycling performance of the batteries at 400 mA/g, and (d) rate capability of the batteries at different discharge rates

In order to compare the improved electrochemical properties of MNG as the cathode for ZIB, the pristine δ-MnO_2 is used as a comparable cathode. Fig. 3.5 (a) shows the CV profiles of the pristine δ-MnO_2 and MNG electrodes at a scan rate of

0.5 mV/s over the potential range 1.0-1.8 V for the initial three cycles. During the first cycle, two distinct peaks are observed at 1.20 and 1.57 V for the pristine δ-MnO$_2$ electrode and at 1.18 and 1.54 V for MNG. The peaks in the low potential region appear at 1.20 and 1.18 V which can be attributed to Zn^{2+} ion insertion into the δ-MnO$_2$ host structure. In the higher potential region, two oxidation peaks can be seen at 1.57 and 1.54 V for δ-MnO$_2$ and MNG, respectively, which correspond to the extraction of Zn^{2+} ions from the δ-MnO$_2$ host structure. The results suggest that, the oxidation state of Mn is reduced to Mn^{3+} states and is oxidized back to Mn^{4+} states, during Zn^{2+} ion insertion and extraction, respectively [9, 29, 61, 79]. On subsequent cycling, two distinct peaks appear at 1.37 and 1.21 V for Zn^{2+} ion insertion into δ-MnO$_2$ whereas the peaks at 1.38 and 1.20 V were observed for MNG in the low voltage region. In the high voltage region, the peak at 1.57 and shoulder at 1.62 V can be clearly seen for the pristine δ-MnO$_2$. Likewise, the peak at 1.53 V and shoulder at 1.60 V can be clearly seen for the MNG electrodes. The cyclic voltammogram, having two peaks during discharge and having a peak with shoulder during charge, exhibits typical characteristics of the electrochemical insertion/extraction of Zn^{2+} ions in MnO$_2$ structure [9, 28, 58, 80, 81]. These results with two peaks during discharge may be more clearly described by the two-step reaction of Zn^{2+} ion insertion in electrochemical reaction [58, 79] and spinel-type ZnMn$_2$O$_4$ transformation [74]. In the following scan cycles, the peaks at 1.37 V for δ-MnO$_2$ and at 1.38 for MNG increase gradually during discharge indicating an activation process [79]. The CV curve of MNG exhibits a higher peak intensity and a larger enclosed area when compared with the pristine δ-MnO$_2$ indicating improved electrochemical performance and fast Zn^{2+} ion insertion/extraction [11].

Fig. 3.5(b) shows the first and second discharge/charge profiles of the pristine δ-MnO$_2$ and MNG cathode in a coin cell battery when cycled at a specific current density of 200 mA/g in the potential range of 1.0-1.8 V. The battery fabricated with

the pristine δ-MnO$_2$ and MNG host cathode material under open air condition displays an open-circuit voltage (OCV) of about 1.4 V. The first discharge capacity for MNG is 235 mA h/g whereas the pristine δ-MnO$_2$ registers only 130 mA h/g. Compared to todorokite-type MnO$_2$ [29] and δ-MnO$_2$ nanoflake [9], the initial discharge capacity can deliver only 98 mA h/g (at 50 mA/g) and 122 mA h/g (at 83 mA/g), respectively. It is clear that δ-MnO$_2$ supported on graphite samples can accommodate more numbers of Zn^{2+} ions than the unsupported δ-MnO$_2$ (pristine δ-MnO$_2$). It appears that the nanoflower δ-MnO$_2$ in the structure of MNG tends to enhance the electrode/electrolyte contact area, thereby favoring Zn^{2+} ion insertion [28]. In addition, MNG shows a longer horizontal discharge curve than that of pristine δ-MnO$_2$, suggesting a more stable Zn^{2+} ion insertion into the MNG than in the pristine δ-MnO$_2$. On the subsequent cycle, during the continuous discharge, the voltage profiles present two distinct plateaus at 1.45 and 1.25 V for MNG and 1.4 and 1.2 V for pristine δ-MnO$_2$. These characteristics were also observed for MnO$_2$ electrodes in aqueous ZIB systems [21, 29]. It can be implied that Zn^{2+} ions can insert into the layered δ-MnO$_2$ [80] which is in agreement with the two distinct peaks during discharge, as shown in Fig. 3.5(a).

Fig. 3.5(c) displays the cycling behavior and corresponding coulombic efficiency of the pristine δ-MnO$_2$ and MNG electrodes, under the specific current density of 400 mA/g. At the 100th cycle, the discharge and charge capacities registered by pristine δ-MnO$_2$ were 63.3 and 63.8 mA h/g, respectively, while that of MNG were 113.4 and 114.2 mA h/g, respectively. The lower capacity retention of pristine δ-MnO$_2$ may result from low intrinsic electronic conductivity because of the appearance of unstable Mn^{3+} states during zinc-ion insertion [8]. The higher capacity retention of MNG may indicate that the electronic conductivity of MNG is improved. In the initial cycles, gradual capacity fade was observed for the pristine δ-MnO$_2$ electrode, but fast capacity fade was observed for the MNG electrode. The formation

of $ZnMn_2O_4$ with the Jahn-Teller Mn^{3+} ion may contribute to electrode degradation and, hence, lead to the fast capacity fade [9]. However, MNG demonstrates higher capacity than the pristine δ-MnO_2. Over long-term cycling, the coulombic efficiency of both host material electrodes is maintained at around 100%. Thus, this clearly demonstrates that no irreversible capacity losses occurred [28].

In Fig. 3.5(d), the rate performances of the pristine δ-MnO_2 and MNG host material cathodes are shown. Cycling takes place at various specific current densities of 200, 400, 800 and 1600 mA/g, namely 5 times for each rate. The rate performance of MNG is significantly higher than those of the pristine δ-MnO_2. It is indicated that nanoscale morphology of δ-MnO_2 nanoflowers on graphite increases the contact area between the electrode and the electrolyte and provides more electrochemically active sites for ion-insertion [9]. Graphite not only improves the electronic conductivity of the MNG electrode but also tends to disperse the δ-MnO_2 nanoflower sites. The MNG cathode can be charged and discharged at different rates; a high rate of 1600 mA/g leads to a discharge and charge capacity of 76 and 64 mA h/g, respectively. When cycled at a specific current density of 200 mA/g, the MNG cathode can deliver a discharge and charge capacity of 181 and 179 mA h/g, respectively. This behavior indicates that the MNG cathode can well be considered for the Zn^{2+} ion storage material [8]. It is clear therefore that MNG can improve not only the cycling performance but also the rate performance for ZIBs.

(a)

(b)

(c)

(d)
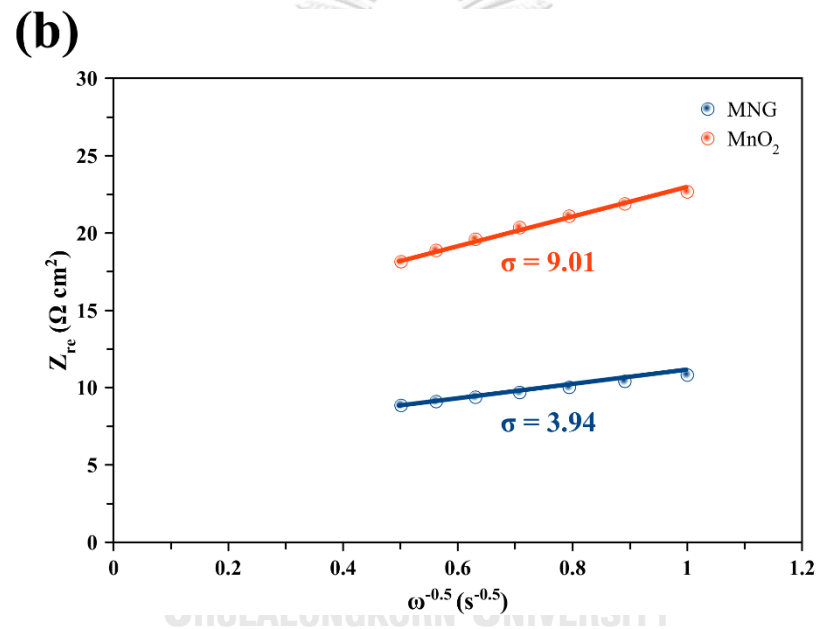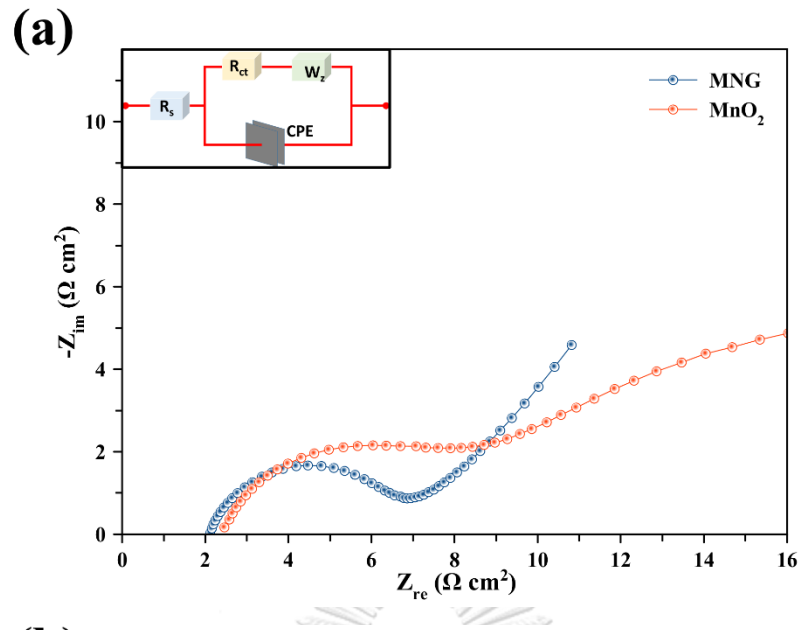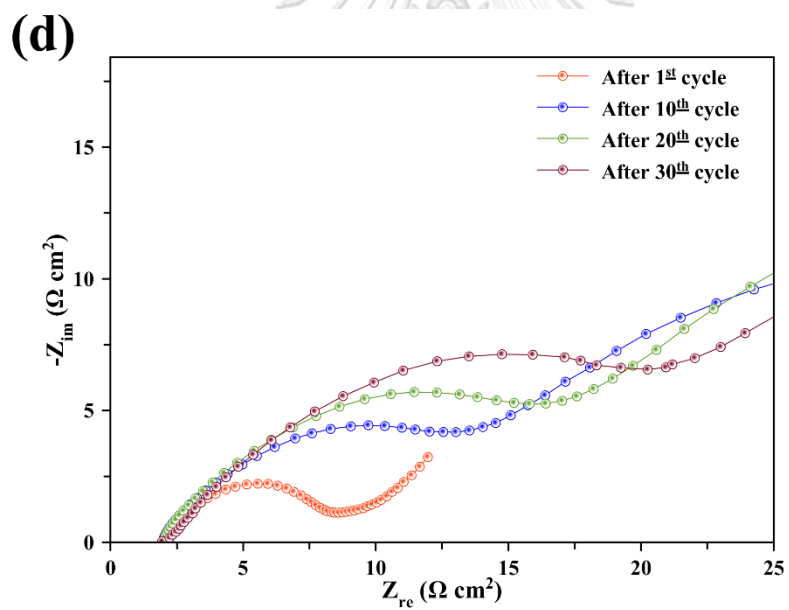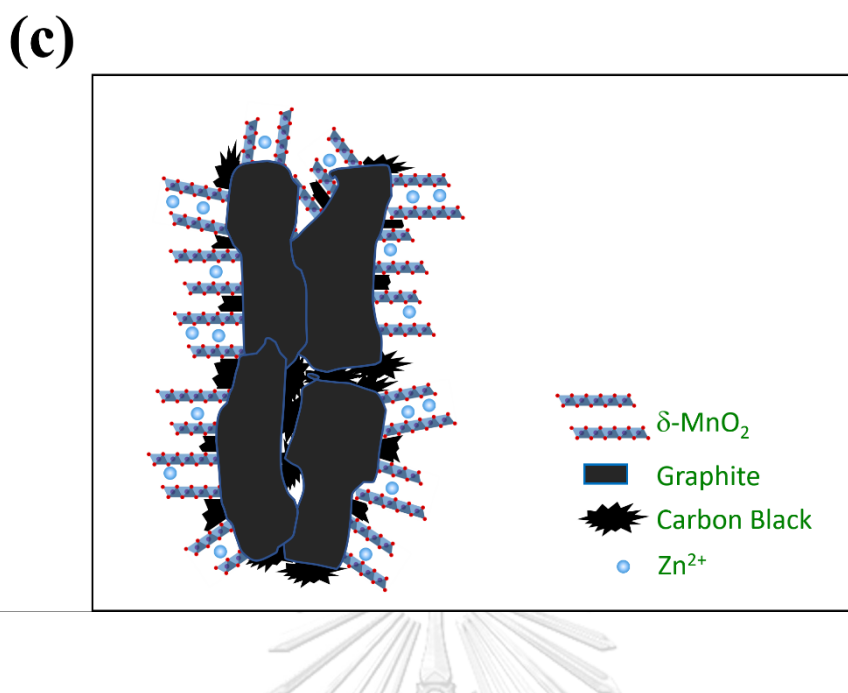
Figure 3.6 EIS results of the batteries: (a) Nyquist plot of EIS spectra, (b) relationship between real part of impedance versus $\omega^{-0.5}$ for the batteries using MNG and the pristine δ-MnO$_2$, (c) schematic illustration for the Zn^{2+} ion insertion into the MNG electrode, and (d) Nyquist plot of EIS spectra of MNG at various charge/discharge cycles

As displayed in Fig. 3.6(a), the difference in electrochemical conductivity before cycling between the pristine δ-MnO$_2$ and MNG host cathodes was examined using EIS. The curves of the pristine δ-MnO$_2$ and MNG host cathodes consist of depressed semicircles and diffusion drift which can be perfectly fitted using Randles equivalent circuit (see Inset Fig. 3.6(a)). Hence, in the equivalent circuit, R_s is the solution resistance, R_{ct} is the charge-transfer resistance at the interfaces and W_z is the Warburg impedance related to the diffusion of Zn^{2+} ions. The R_{ct} value for the pristine δ-MnO$_2$ is 5.9 Ω and the value reduces to 4.8 Ω when supported on graphite (MNG). The result indicates that the electrical conductivity of the MNG sample is improved by constructing a conductive support using the graphite. The relationship between real impedance (Z_{re}) and angular frequency (ω) in the low frequency region can be expressed accordingly by Equation (3.5) [82]:

$$Z_{re} = R_s + R_{ct} + \sigma\omega^{-0.5} \qquad (3.5)$$

where σ is the Warburg factor which is relative to Z_{re}- ω obtained from the slope of the lines in Fig. 3.6(b). The diffusion coefficient of zinc ion can be calculated as in Equation (3.6) [83]:

$$D = \frac{R^2 T^2}{2A^2 n^4 F^4 C^2 \sigma^2} \qquad (3.6)$$

where R is the gas constant, T is the absolute temperature, n is the number of electrons per molecule oxidized, A is the surface area, F is Faraday's constant, C is the concentration and D is the diffusion coefficient.

As shown in Fig. 3.6(b), the slope which is the σ value of MNG (3.94) host electrode is lower than that of the pristine δ-MnO$_2$ (9.01) indicating that the diffusion coefficient of MNG is higher than that of the pristine δ-MnO$_2$, according to Equation

(3.6). It is clear that the MNG host material electrode can enhance the diffusion coefficient of Zn^{2+} ion, highlighting the electrical conductivity improvement [82, 84].

In Fig. 3.6(c), the MNG cathode which is a **δ**-MnO_2 structure supported on graphite is drawn and illustrated. It is highly possible that Zn^{2+} ions can insert into the **δ**-MnO_2 nanoflower structure having short diffusion length. Thereby, electrochemical performance can be improved during cycling at high rate [85].

In Fig. 3.6(d), after charge/discharge cycling, the EIS measurements of MNG are shown. After the 1st, 10th, 20th, and 30th cycles, the MNG host cathode exhibits the R_{ct} values, namely, 6.51, 10.9, 13.7 and 18.2 Ω, respectively. After the first cycle, the charge-transfer resistance increases which indicates that the intercalation of Zn^{2+} ions into the **δ**-MnO_2 structure becomes more difficult. The conduction of ions before intercalation depends not only on the cathode material but also on the electrolyte access into the cathode. The porosity of the cathode material is an important factor which can affect the electrolyte access. The SEM images of MNG and the pristine **δ**-MnO_2 compound are displayed in Fig. B2 of the Appendix B.

3.2 Article II

MnO$_2$ heterostructure on carbon nanotubes as cathode material for aqueous zinc-ion batteries

Sonti Khamsanga[1], Mai Thanh Nguyen[2], Tetsu Yonezawa[2,3], Patchanita Thamyongkit[4], Rojana Pornprasertsuk[5,6,7], Prasit Pattananuwat[5,6,7], Adisorn Tuantranont[8], Siwaruk Siwamogsatham[8] and Soorathep Kheawhom[1,7,*]

[1]Department of Chemical Engineering, Faculty of Engineering, Chulalongkorn University, Bangkok 10330, Thailand; 6071443721@student.chula.ac.th

[2]Division of Materials Science and Engineering, Faculty of Engineering, Hokkaido University, Hokkaido 060-8628, Japan; mai_nt@eng.hokudai.ac.jp (M.T.N.); tetsu@eng.hokudai.ac.jp (T.Y.)

[3]Institute of Business-Regional Collaborations, Hokkaido University, Hokkaido 001-0021, Japan

[4]Department of Chemistry, Faculty of Science, Chulalongkorn University, Bangkok 10330, Thailand; patchanita.v@chula.ac.th

[5]Department of Materials Science, Faculty of Science, Chulalongkorn University, Bangkok 10330, Thailand; rojana.p@chula.ac.th (R.P.); prasit.pat@chula.ac.th (P.P.)

[6]Center of Excellence in Petrochemical and Materials Technology, Chulalongkorn University, Bangkok 10330, Thailand

[7]Research Unit of Advanced Materials for Energy Storage, Chulalongkorn University, Bangkok 10330, Thailand

[8]National Science and Technology Development Agency, Pathumthani 12120, Thailand; adisorn.tua@nstda.or.th (A.T.); siwaruk.siw@nstda.or.th (S.S.)

* Correspondence: soorathep.k@chula.ac.th; Tel.: +66-81-490-5280

Article II: MnO_2 heterostructure on carbon nanotubes as cathode material for aqueous zinc-ion batteries

Abstract

Due to their cost effectiveness, high safety, and eco-friendliness, zinc-ion batteries (ZIBs) are receiving much attention nowadays. In the production of rechargeable ZIBs, the cathode plays an important role. Manganese oxide (MnO_2) is considered the most promising and widely investigated intercalation cathode material. Nonetheless, MnO_2 cathodes are subjected to challenging issues viz. limited capacity, low rate capability and poor cycling stability. It is seen that MnO_2 heterostructure can enable long-term cycling stability in different types of energy devices. Herein, a versatile chemical method for the preparation of MnO_2 heterostructure on multi-walled carbon nanotubes (MNH-CNT) is reported. Besides, the synthesized MNH-CNT is composed of δ-MnO_2 and γ-MnO_2. The ZIB using the MNH-CNT cathode delivers a high initial discharge capacity of 236 mA h/g at 400 mA/g, 108 mA h/g at 1600 mA/g and excellent cycling stability. Pseudocapacitive behavior investigation demonstrates fast zinc ion diffusion via a diffusion-controlled process with low capacitive contribution. Overall, the MNH-CNT cathode is seen to exhibit superior electrochemical performance. This work presents new opportunities for improving the discharge capacity and cycling stability of aqueous ZIBs.

3.2.1 Introduction

Metal-ion batteries (MIBs) are rechargeable batteries that use metal ions as a charge carrier being capable of reversible intercalation and deintercalation into the host material [86-90]. In recent years, on account of their low self-discharge, less memory effect and high efficiency, implementation of MIBs for energy storage has become very popular [91, 92]. Of different types of MIBs, lithium-ion batteries (LIBs) are widely used for various applications due to their high energy density and long cycle life [93, 94]. However, some important factors such as high cost and safety issues tarnish the large-scale application of LIBs [95, 96]. Besides LIBs, various monovalent (Na^+, K^+) and multivalent (Mg^{2+}, Zn^{2+}, Al^{3+}) ions have been considered as charge carriers in MIBs. In view of this, ZIBs have attracted the interest of researchers [22, 57, 80, 97]. It is noted that zinc (Zn) has low redox potential of −0.763 V vs. standard hydrogen electrode (SHE), which is favorable for near neutral or slightly acidic aqueous electrolytes [98]. In addition, Zn has a higher specific volumetric capacity compared to that of lithium viz. 5855 mA h/cm^3 and 2066 mA h/cm^3, respectively [52]. As compared to lithium, Zn is lower in cost and highly abundant [54, 55].

A typical ZIB consists of a cathode (for hosting Zn ions), a Zn metal anode, an electrolyte, and a separator (to separate the cathode and anode) [99, 100]. In general, the development of aqueous ZIBs has been limited by the cathode materials used [32, 79, 101]. In this respect, MnO_2 has been found to be one of the most promising alternatives due to its low cost and good environmental compatibility along with high operating voltage and a theoretical capacity of 308 mA h/g [26, 80, 102, 103]. Various types of MnO_2 have been employed as cathode material for ZIBs such as α-MnO_2 nanorods with onion-like carbon (OLC) (reported capacity of 168 mA h/g at 246 mA/g) [93], δ-MnO_2 nanosheets (reported capacity of

133 mA h/g at 100 mA/g) [24], and MnO_2 nanorods with graphene (reported capacity of 301 mA h/g at 500 mA/g) [104]. In addition, MnO_2 can exist in a variety of crystallographic polymorphs such as α-, β-, γ-, δ- and λ-MnO_2, depending on how MnO_6 octahedral units are connected by different types of network. While α-, β- and γ-MnO_2 have tunnel structures, δ-MnO_2 has a layered structure [69]. Nevertheless, during cycling, MnO_2 suffers poor capacity and inadequate performance because of its poor electronic conductivity and unstable cycling of the electrode [10, 79].

In order to solve these issues, graphite and carbon nanotubes (CNTs) have been introduced to support the MnO_2 nanostructure because of their excellent electrical conductivity and high surface area [105-108]. Among conductive materials, CNTs including single-walled carbon nanotubes (SWCNTs) and multi-walled carbon nanotubes (MWCNTs) have been used as supporting materials to form composites with MnO_2 [10]. Researchers have reported several significant results concerning MnO_2 with CNTs. Chou et al. [109], for example, successfully electrodeposited MnO_2 nanowires onto CNT paper. The composite CNT paper demonstrated good cyclability after 3000 cycles. For this result, it acted as a conductive and active substrate for flexible electrodes of a supercapacitor. Wang et al. [107] synthesized a nanocomposite of MnO_2/CNTs by direct redox reaction. The result indicated that capacitance retained more than 90% of initial capacitance after 2000 cycles because electrical conductivity influenced the specific capacitance.

Besides conductive carbon support, using heterostructure is an attractive concept in that two types of materials and/or nanostructures have been directly grown on supporting material, as binder-free electrodes [110-112]. The birnessite-type δ-MnO_2 exhibited a favorable electrochemical performance due to its relatively large interlayer distance (70 Å) for energy storage applications [9, 79]. Moreover, γ-MnO_2, as the anode material of rechargeable LIBs, provided high initial reversible capacity [113]. It is challenging that the MnO_2 heterostructure could lead to

remarkable electrochemical properties as well as enhanced battery performance. Thus, the MnO_2 heterostructure was synthesized leading to improvement not only of the electrical conductivity of the cathode but also the capacity and cycling stability of ZIBs.

Herein, in-situ reduction of potassium permanganate ($KMnO_4$) using multi-walled carbon nanotubes (MWCNTs) as supporting material has been carried out to produce MnO_2 heterostructure on multi-walled carbon nanotubes (MNH-CNT). The heterostructure was controlled via the ratio of an initial amount of $KMnO_4$ and MWCNTs. The as-prepared composite was examined to determine its physical characteristics. Subsequently, the electrochemical properties and performances of ZIBs which used the MnO_2 on multi-walled carbon nanotubes (MN-CNT), as host material cathode, are investigated and discussed.

3.2.2 Results and discussion

Material Characterization

1. X-ray Diffraction (XRD)

In this study, MN-CNT was synthesized via thermal reaction. Accordingly, the growth process of MnO_2 on MWCNTs is stated as in Eq. (3.7) [27]:

$$4KMnO_4 + 4C + 2H_2SO_4 \rightarrow 4MnO_2 + 3CO_2 + 2K_2SO_4 + 2H_2O \qquad (3.7)$$
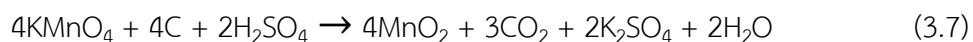
The outer wall of MWCNTs was oxidized by $KMnO_4$ under strong acid condition. Further, MnO_2 was materialized due to redox reaction in which $KMnO_4$ acted as an oxidant. This process led to the homogenous coverage of MnO_2 formed on the MWCNTs surface.
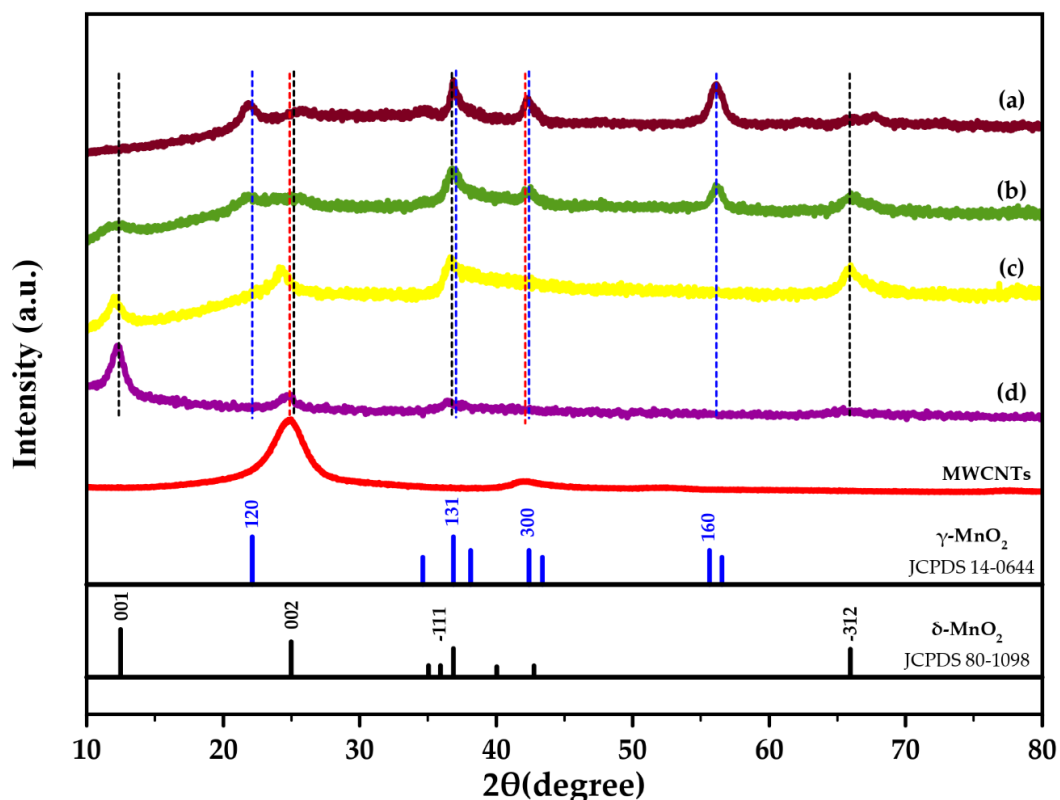
Figure 3.7 XRD patterns of MWCNTs and synthesized MN-CNT with different weight ratios of MnO_2:MWCNTs: (a) 60:40;MN-CNT6040 (b) 75:25;MN-CNT7525 (c) 90:10;MN-CNT9010 and (d) synthesized δ-MnO_2

XRD was conducted to study the crystal structure of the samples. In Fig. 3.7, XRD patterns of pristine δ-MnO_2, MWCNTs and MN-CNTs having different ratios of MnO_2 and MWCNTs are shown. MN-CNT6040, MN-CNT7525 and MN-CNT9010 represent the MN-CNTs having MnO_2 and MWCNT weight ratios of 60:40, 75:25 and 90:10, respectively. It can be seen that the pure MWCNTs show a sharp peak at around 26° and broad weak peaks at around 42°, which are characteristic of MWCNTs [108]. The four broad peaks of the MN-CNT9010 at around 12, 24, 37, and 66° correspond to the crystal planes of (001), (002), (-111), and (-312) in δ-type MnO_2 (JCPDS 80-1098), respectively [69, 71]. They are similar to all the peaks of δ-MnO_2. The broad peaks of the MN-CNT6040 at around 22, 36.5, 42, and 56° correspond to

the crystal planes of (120), (131), (300), and (160) in γ-type MnO_2 (JCPDS 14-0644), respectively [71, 113]. The MN-CNT7525 presents all the peaks of δ-type and γ-type MnO_2, indicating that the heterostructure of MnO_2 is growth with 75:25 weight ratio of MnO_2 and MWCNT. The weak-intensity diffraction peaks of MWCNTs on the XRD pattern of the MN-CNT may result from both the broad and high diffraction peaks of MnO_2 at around 24° and 22° for δ-type and γ-type MnO_2, which defeats the signal of MWCNTs [109]. The calculated crystallite sizes of MN-CNT9010 and MN-CNT6040, obtained via Scherrer equation, are 7 and 12 nm, respectively. The calculated crystallite sizes of γ-MnO_2 and δ-MnO_2 in MN-CNT7525 are 13 and 8 nm, respectively. The crystallite sizes of δ-MnO_2 and γ-MnO_2 are the same when they are in the MnO_2 heterostructure of MN-CNT. δ-MnO_2 and γ-MnO_2 possess a layered-structure and a tunneled-structure, respectively. It is suggested that foreign cations can insert to/extract from both a layered-structure and a tunneled-structure, with the result that electrochemical performance can be enhanced by the MNH-CNT and thereby can be useful for energy storage application.

2. Field Emission Scanning Electron Microscope (FESEM)

In Fig. 3.8a, the structure of MN-CNT, having different weight ratios of MnO_2 and MWCNTs, is depicted and the corresponding morphological changes are shown. To determine the morphology of MN-CNTs, FESEM was carried out and the images are displayed in Figs. 3.8b-d. MnO_2 nanostructures are continuously dispersed on the MWCNTs. Besides, the type of MnO_2 changed from δ-MnO_2 to γ-MnO_2, as the amount of $KMnO_4$ in the solution decreased. To be specific, the flower-like δ-MnO_2 nanostructures, having petals about 100 nm in size in the MN-CNT9010 sample, change to the heterostructure of δ-MnO_2 with petals being the size of 50 nm as well as leaf-like γ-MnO_2 nanostructures having leaves around 150 nm in the MN-CNT7525 sample. It is demonstrated that, by limiting the amount of $KMnO_4$, the δ-MnO_2

cannot be completely generated. On the contrary, γ-MnO_2 can form while the concentration of $KMnO_4$ is still low during redox reaction. By continuing to decrease the amount of $KMnO_4$ to 60 percent by weight, γ-MnO_2 nanostructures can only be observed in the MN-CNT6040 sample. In Fig. B3 of Appendix B, lower magnification FESEM images of MN-CNT9010, MN-CNT7525, and MN-CNT6040 are presented. The MN-CNT, having two nanostructures of δ-MnO_2 and γ-MnO_2, assists in increasing the contact area of the smaller petal size of δ-MnO_2 between the electrolyte and cathode material; ensuring fast ion transfer in the charge/discharge process [5]. Besides, the γ-MnO_2 in MNH-CNT is comprised not only of randomly arranged 1×1 and 1×2 tunnels, which are beneficial for Zn^{2+} ions intercalation/deintercalation but also accommodates the structural transformation from tunneled-type γ-MnO_2 to the layered-type of Zn_yMnO_2. Such a random-arranged structure can improve the stability of capacity during the cycling process.

In Fig. B4 of Appendix B, transmission electron microscope (TEM) images of MN-CNT having different weight ratios of MnO_2 and MWCNTs are shown. In the case of MN-CNT6040 and MN-CNT7525, it is obvious that MnO_2 formed on the MWCNTs. However, in the case of MN-CNT9010, MWCNTs cannot be seen clearly in the TEM image as a high amount of MnO_2 was loaded. Thus, all parts of the MWCNTs were covered by MnO_2. Transmission electron microscope with energy dispersive spectroscopy (TEM-EDS) (Fig. B5 of Appendix B) confirmed that carbon atoms of MWCNTs existed on MN-CNT9010. This proved to be in good agreement with XRD results (Fig. 3.7), where the presence of MWCNTs in MN-CNT9010 was observed.
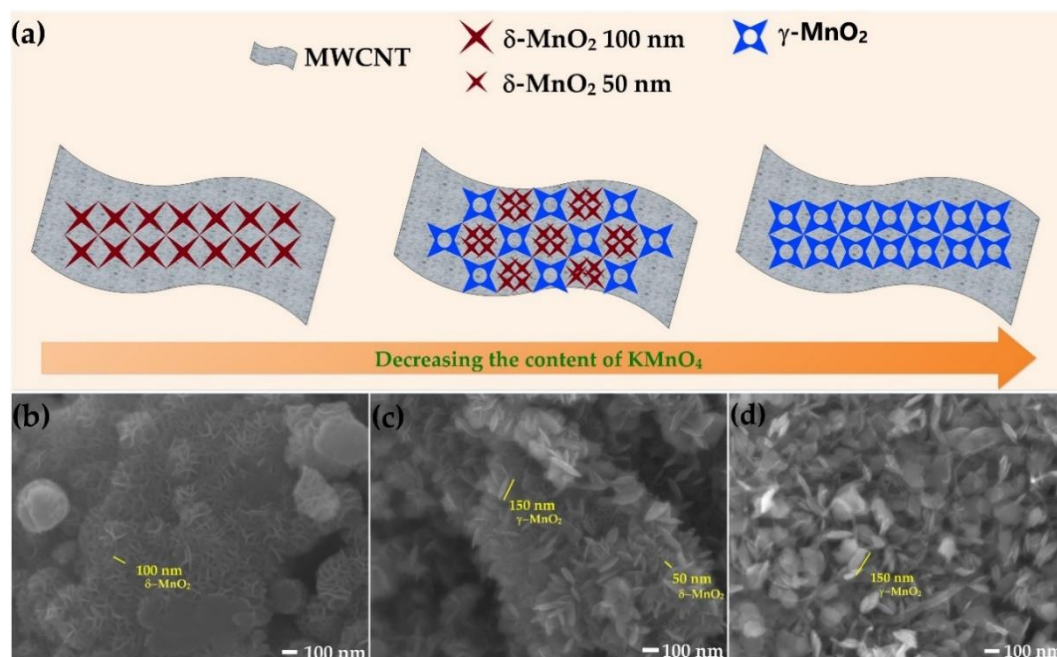
Figure 3.8 (a) Schema of changes in morphology of MN-CNT followed by decreasing the content of $KMnO_4$ (b) FESEM image of MN-CNT9010 (c) FESEM image of MN-CNT7525 and (d) FESEM image of MN-CNT6040.

Electrochemical performances

    1. Battery system
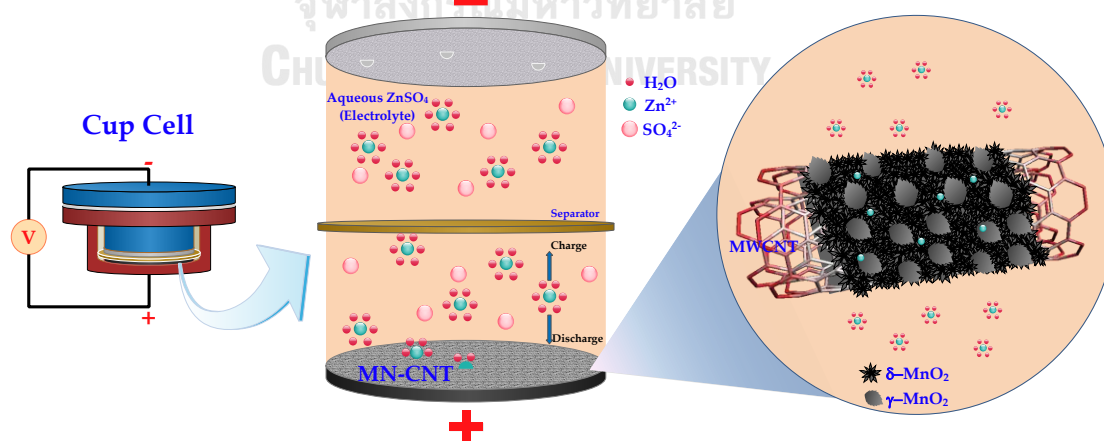
Figure 3.9 Schema of the chemistry of the zinc-ion battery. The inset on the right shows Zn^{2+} ion insertion into MnO_2 heterostructure of MN-CNT

In Fig. 3.9, the battery configuration of cup cell in this study, which is composed of the MNH-CNT electrode, zinc electrode, and $ZnSO_4$ aqueous electrolyte, is shown. Anodic zinc, dissolved in the form of Zn^{2+} ions into an aqueous electrolyte containing Zn^{2+} ions, rapidly solvates in the form of solvated Zn^{2+} ions during the discharge process. Then, the solvated Zn^{2+} ions diffuse and pass through the separator to the MN-CNT electrode (cathode). The solvated Zn^{2+} ions are de-solvated in the form of Zn^{2+} ions [22, 72] and intercalate into MnO_2 heterostructure of MN-CNT, as illustrated by the inset in Fig. 3.9. Further, an electron current starts to flow in the electrical loop from the electrical conduction of MWCNTs. These three processes can be reversed when the charging process occurs. Firstly, Zn^{2+} ions will de-intercalate from the MN-CNT electrode (anode). Then, solvated species are formed. Lastly, Zn^{2+} ions are reduced to Zn and deposited back on the Zn electrode (cathode). The electrochemical reaction may be expressed as in Eq. (3.8) for the Zn electrode and Eq. (3.9) for the MN-CNT electrode:
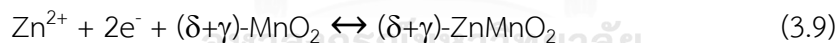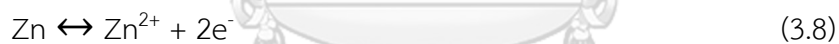
$$Zn \leftrightarrow Zn^{2+} + 2e^- \qquad\qquad (3.8)$$

$$Zn^{2+} + 2e^- + (\delta+\gamma)\text{-}MnO_2 \leftrightarrow (\delta+\gamma)\text{-}ZnMnO_2 \qquad\qquad (3.9)$$

During the electrochemical Zn^{2+} ion insertion, the layered-type δ-MnO_2 structure can transform to spinel-type $ZnMn_2O_4$ with Mn(III) state and layered-type δ-Zn_xMnO_2 with Mn(II) state [80]. Meanwhile, the tunnel-type γ-MnO_2 suffered a structural transformation to spinel-type Mn(III) phase ($ZnMn_2O_4$), tunnel-type γ-Zn_xMnO_2 and layered-type L-Zn_yMnO_2 [9].

2. Electrochemical performances

The electrochemical properties of δ-MnO$_2$ and MN-CNT, having different weight ratios of MnO$_2$ and MWCNTs cathodes, were evaluated by cyclic voltammetry (CV) within the potential range of 1.0-1.8 V vs. Zn/Zn^{2+} at a scan rate of 0.5 mV/s. Fig. 3.10a displays CV plots of their corresponding samples. Two distinct peaks of MN-CNT are observed: the cathodic peak at around 1.3 and 1.1 V and the anodic peak at 1.54 and 1.65 V. CV having two peaks, during discharge and charge, exhibits typical characteristics of the electrochemical insertion/extraction of Zn^{2+} ions in MnO$_2$ structure [114-116]. According to previous studies, these peaks mainly suggest that the insertion/extraction of Zn^{2+} ions into/out of the interlayers of δ-MnO$_2$ are associated with the reduction of Mn (IV) to Mn (III) and oxidation of Mn (III) to Mn (IV), respectively [9, 29, 61, 79]. It is noted that the cathodic peak of MN-CNT7525 ∼1.1 V shifts to lower potential ∼1.05 V and the anodic peak of MN-CNT7525 ∼1.65 V shifts to higher potential ∼1.7 V. This may be affected by the insertion/extraction of zinc ions into/out of the γ-MnO$_2$ of the MnO$_2$ heterostructure of MN-CNT cathode.

In contrast, the cathodic peak of δ-MnO$_2$ shifts to higher potential and the anodic peak shifts to lower potential. The CV curve of MN-CNT exhibits higher peak intensity and a larger enclosed area when compared with the δ-MnO$_2$, indicating improved electrochemical performance and fast Zn^{2+} ion insertion/extraction in the cathode [11]. These results are consistent with the galvanostatic charge/discharge curves in Fig. 3.10b which have two discharge plateaus at about 1.3 and 1.1 V. The discharge capacity for MN-CNT7525 is 245 mA h/g whereas the δ-MnO$_2$, MN-CNT6040, and MN-CNT9010 register only 184, 193 and 202 mA h/g, respectively. In addition, MN-CNT7525 shows a larger discharge plateau than that of δ-MnO$_2$, MN-CNT6040, and MN-CNT9010, suggesting a higher capacity for Zn^{2+} ion insertion into the MnO$_2$ heterostructure of MN-CNT than in the δ-MnO$_2$ and single structure MnO$_2$ of MN-CNT.

(a)

(b)
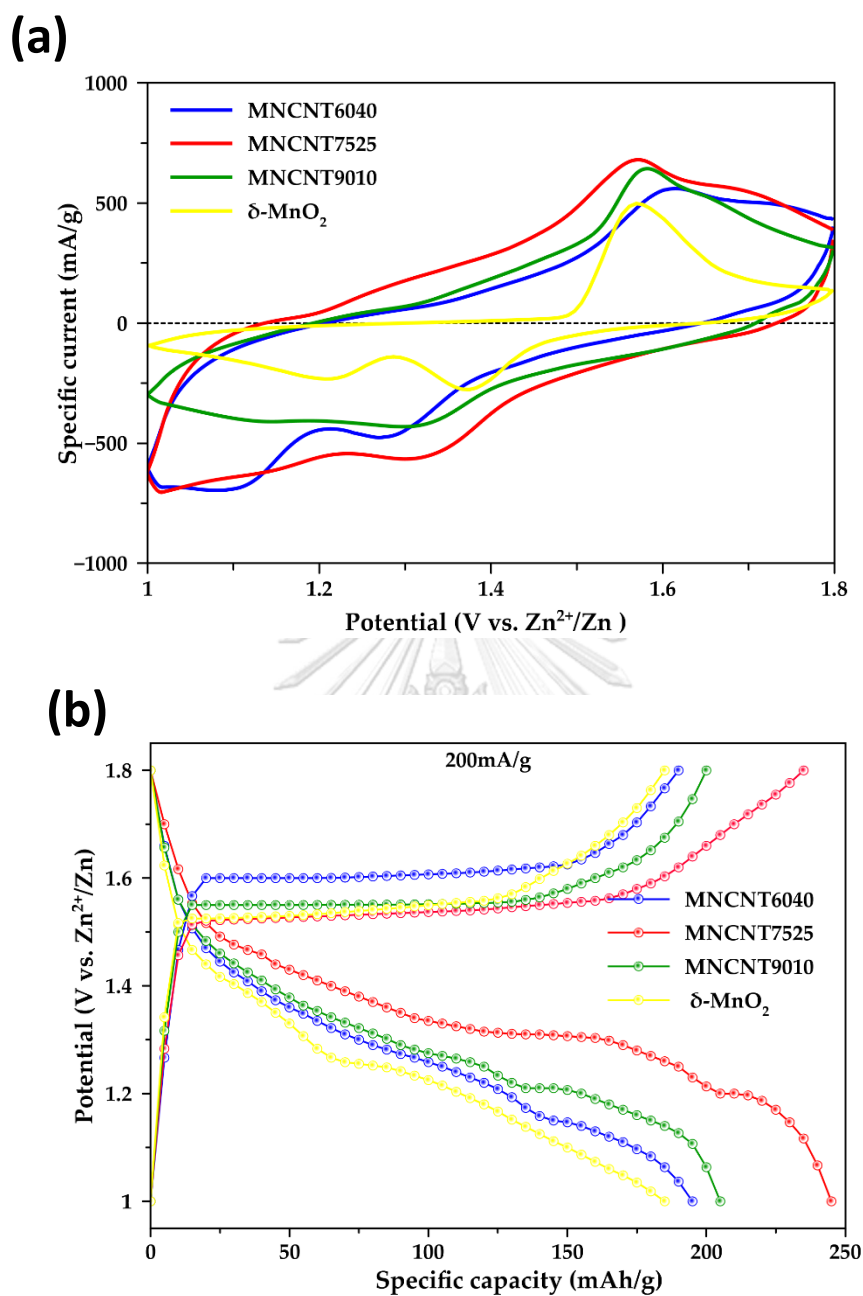
Figure 3.10 Electrochemical properties: (a) Cyclic voltammograms at a scan rate of 0.5 mV/s (b) Galvanostatic charge-discharge profile at 200 mA/g of the MN-CNT and δ-MnO$_2$ cathode

In order to compare the battery performance of MN-CNT, having different weight ratios of MnO$_2$ and MWCNTs, as the cathode for ZIBs, δ-MnO$_2$ is used as a comparable cathode. Fig. 3.11a displays the cycling behavior of the δ-MnO$_2$ and MN-

CNT electrodes along with the corresponding coulombic efficiency (CE) of MN-CNT7525, under the specific current density of 400 mA/g in the potential range of 1.0-1.8 V. The initial discharge capacities of MN-CNT6040, MN-CNT7525, MN-CNT9010 and δ-MnO$_2$ are 177, 236, 135, and 129 mA h/g, respectively.

The lower initial capacity of δ-MnO$_2$ may result from its low intrinsic electronic conductivity because of the unstable state of Mn^{3+} during Zn-ion insertion [8]. This low capacity of the unsupported δ-MnO$_2$ (pristine δ-MnO$_2$) indicates that MWCNTs can enhance electrical conductivity of the cathode active material. It is noted that the MN-CNT7525 exhibited the highest initial capacity. This high initial capacity may be attributed to the heterostructure of MnO$_2$ on MWCNTs for Zn^{2+} insertion/extraction during the cycling process. The Zn^{2+} ions can insert into both δ-MnO$_2$, being smaller nanoflower-like with layered-structure, and γ-MnO$_2$ which is nanoleaf-like with tunnel-structure. Such a high initial capacity is superior to that of the δ-MnO$_2$ cathode and most reported Zn-ion batteries, including onion-like carbon (OLC) integrated α-MnO$_2$ nanorods (168 mA h/g at 246 mA/g) [93], δ-MnO$_2$ nanosheets (133 mA h/g at 100 mA/g) [24], and ZnMn$_2$O$_4$/Mn$_2$O$_3$ (82.6 mA h/g at 500 mA/g) [117].

In the initial cycles, gradual capacity fading was observed for the batteries having δ-MnO$_2$, MN-CNT6040, and MN-CNT9010 electrodes. However, the battery using MN-CNT7525 electrode showed a higher rate of capacity fading. This capacity fading may be attributed to the dissolution of MnO$_2$ into the electrolyte during cycling. Moreover, in the case of MN-CNT7525, higher dissolution was observed. After the initial 30 cycles, capacity fading was seen to slow down. This is probably because the equilibrium of Mn dissolution takes place from gradual Mn^{2+} ions dissolution in the electrolyte [20]. Interestingly, around the 20th cycle, the capacity of the MN-CNT7525 electrode starts to decrease gradually. Subsequently, after the 30th cycle, stable capacity is observed. The capacity of the δ-MnO$_2$, MN-CNT6040, and MN-

CNT9010 electrodes, however, continuously decrease until the 100th cycle. The better performance can be due to the structural transformation between δ-MnO$_2$ and γ-MnO$_2$ of MNH-CNT [80]. After 100 cycles, the MN-CNT7525 electrode delivers a capacity of 140 mA h/g; Coulombic efficiency being around 100%, indicating its good reversibility during the charging/discharging process. In contrast, the δ-MnO$_2$, MN-CNT6040, and MN-CNT9010 cathodes deliver capacities of 63, 81, and 96 mA h/g, respectively.

In Fig. 3.11b, rate performances of the δ-MnO$_2$ and MN-CNTs host material cathodes are displayed. Cycling takes place at various specific current densities of 200, 400, 800 and 1600 mA/g having 5 cycles for each rate. The rate performance of MN-CNT7525 was significantly higher than those of δ-MnO$_2$, MN-CNT6040, and MN-CNT9010. The MN-CNT7525 cathode can be charged and discharged at a high rate of 1600 mA/g, leading to a discharge and charge capacity of 108 and 95 mA h/g, respectively. It is indicated that the MnO$_2$ heterostructure of MN-CNT with its small nanoscale morphology of δ-MnO$_2$ nanoflower-like and short length crystal structure of γ-MnO$_2$ provides faster ion diffusion rate at high current density. When the current turns back to 200 mA/g, the MN-CNT7525 cathode can deliver both discharge and charge capacity of 226 and 212 mA h/g, respectively. It is clear therefore that the MnO$_2$ heterostructure of MN-CNT can improve not only cycling stability but also the rate performance for ZIBs. This behavior indicates that the MNH-CNT cathode can well be considered as Zn^{2+} ion storage material.
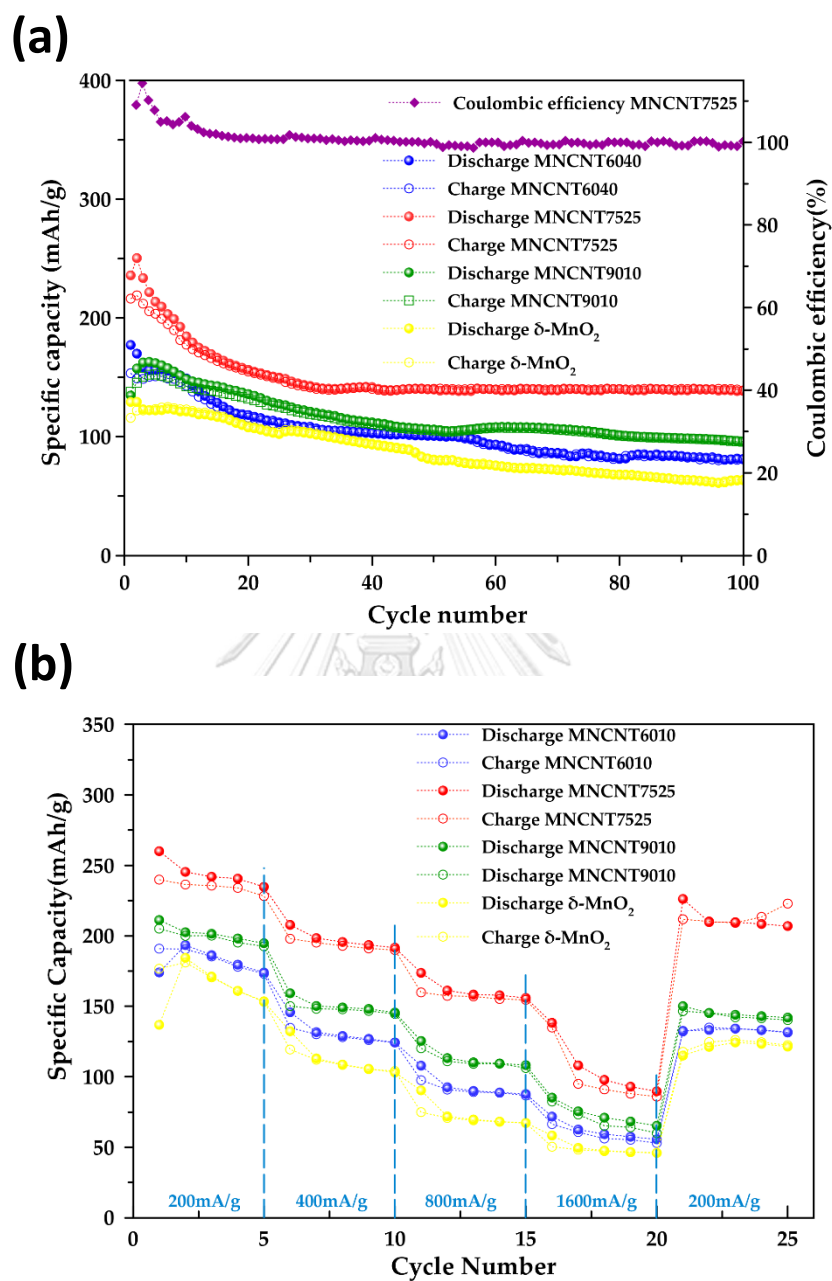
Figure 3.11 Performances of the batteries: (a) Cycling performance of the batteries at 400 mA/g and (b) Rate capability of the batteries at different discharge/charge rates

3. Pseudocapacitive behavior

To further investigate the electrochemical storage mechanism of the MN-CNT7525 electrode, CV curves at different scan rates between 0.25 and 4.0 mV/s in the voltage range 1.0-1.8 V were recorded and shown, as in Fig. 3.12a. It is seen that one maximum reduction peak and oxidation peak distinctly exist in each cycle, with an increase in specific current exhibited, as scan rates are raised. At much higher scan rates, redox peaks are still maintained at an increased specific current. According to previous studies, the peak current (i) of the CV curves allows a power-law relationship with the scan rate (v) and can be used to analyze the charge storage mechanism, as in Eq. (3.10):

$$i = av^b \tag{3.10}$$

where i and v are the peak specific current and scan rate, respectively, and a, b are adjustable parameters. Eq. (3.10) can be converted to logarithmic form, as in Eq. (3.11):

$$\ln i = b \ln v + \ln a \tag{3.11}$$

In Fig. 3.12b, the plots of $\ln i$ vs $\ln v$ for both oxidation and reduction peaks are shown. The b-value denotes the slope of the plots. If b-value is approximately equal to 1, the electrochemical system shows pseudocapacitive behavior controlled by a surface faradic reaction, whereas if b-value is approximately equal to 0.5, typical ionic diffusion dominates the charge/discharge process by cation intercalation [118]. With scan rates ranging from 0.25 to 4 mV/s, the peak specific current increases linearly with the increase in scan rate. The b-values for the peaks of b_o (oxidation process) and b_r (reduction process) are 0.75 and 0.77, respectively. It is indicated

that the redox processes of MN-CNT7525 dominated both pseudocapacitive and diffusion kinetics. That is, the insertion/extraction of Zn^{2+} ions occurred not only on the surface but also took place at the pores inside. These results confirm the pseudocapacitive behavior of MN-CNT7525, leading to fast Zn^{2+} intercalation/extraction and excellent long-term cycling stability. Such an outcome may occur with the heterostructure of MnO_2 on MWCNTs, demonstrating the material's suitability as cathode material for ZIBs.

To quantitatively distinguish the capacitive contribution from the current response, the equation can be rewritten as in Eq. (3.12):

$$i = k_1 v + k_2 v^{1/2} \qquad (3.12)$$

where k_1 and k_2 are constants. Thus, the redox reaction is limited by the diffusion-controlled behavior; the current i at a fixed potential varies as $k_2 v^{1/2}$. The capacitive contribution suggests that the peak current i varies as $k_1 v$ [119-121]. By plotting $i/v^{1/2}$ vs $v^{1/2}$, k_1 and k_2 are calculated from the slope and the y-axis intercept at the point of a straight line, respectively.

In Fig. 3.12c, the ratio of the pseudocapacitive contribution at various scan rates can be quantitatively determined, and the results are displayed. The capacitive contributions of MN-CNT7525 are 40%, 43%, 46%, 57%, and 74% at scan rates of 0.25, 0.5, 1.0, 2.0, and 4.0 mV/s, respectively. It can be seen that as scan rates increase, the capacitive contribution further increases. These results are consistent with the b-values obtained which are around 0.7 for MN-CNT7525.

In Fig. 3.12d, the detail of the pseudocapacitive fraction at a scan rate of 0.5 mV/s is presented; 43% of the total charge, denoted by the blue shaded region, comes from capacitive processes. The low capacitive contribution is attributed to the

fast ion diffusion of the MN-CNT7525 electrode, which leads to high capacity and good cycling stability of the battery.

(a)

(b)
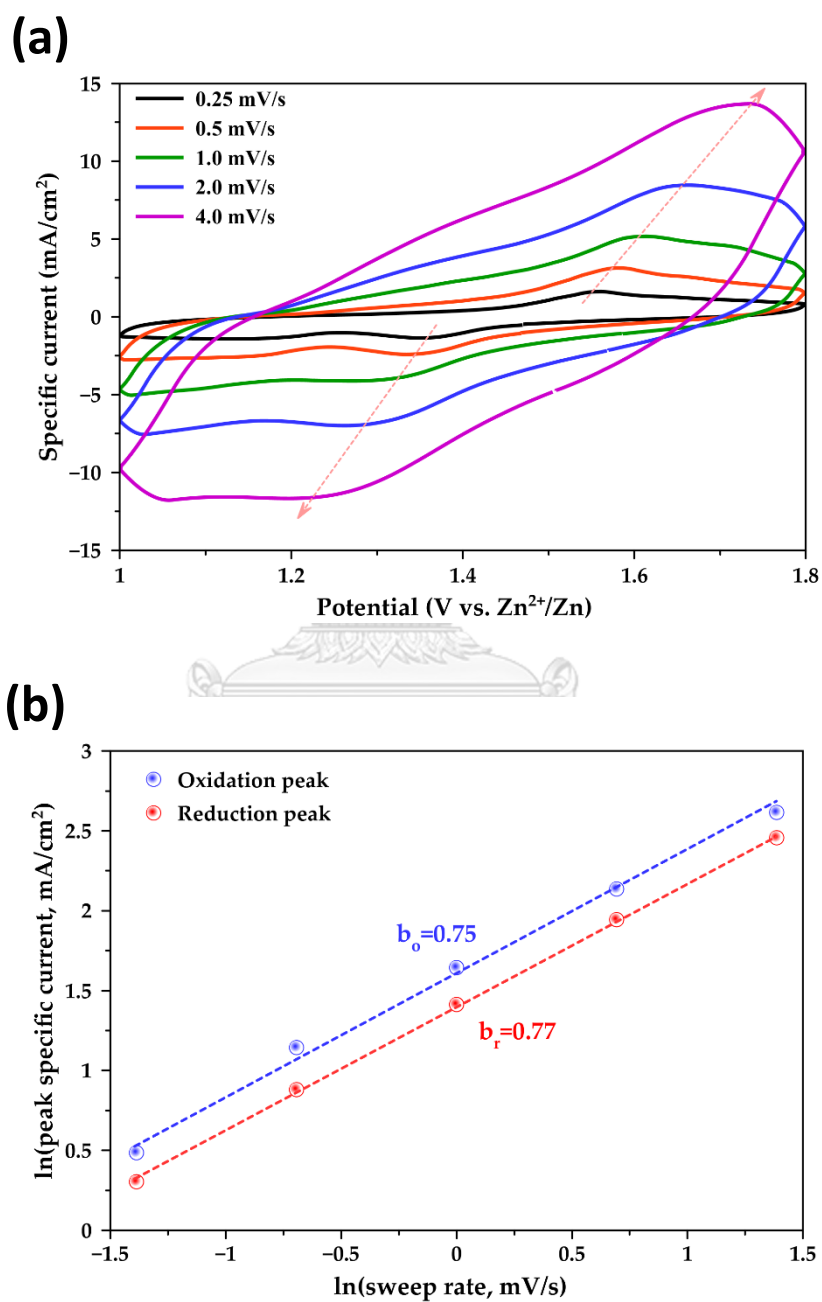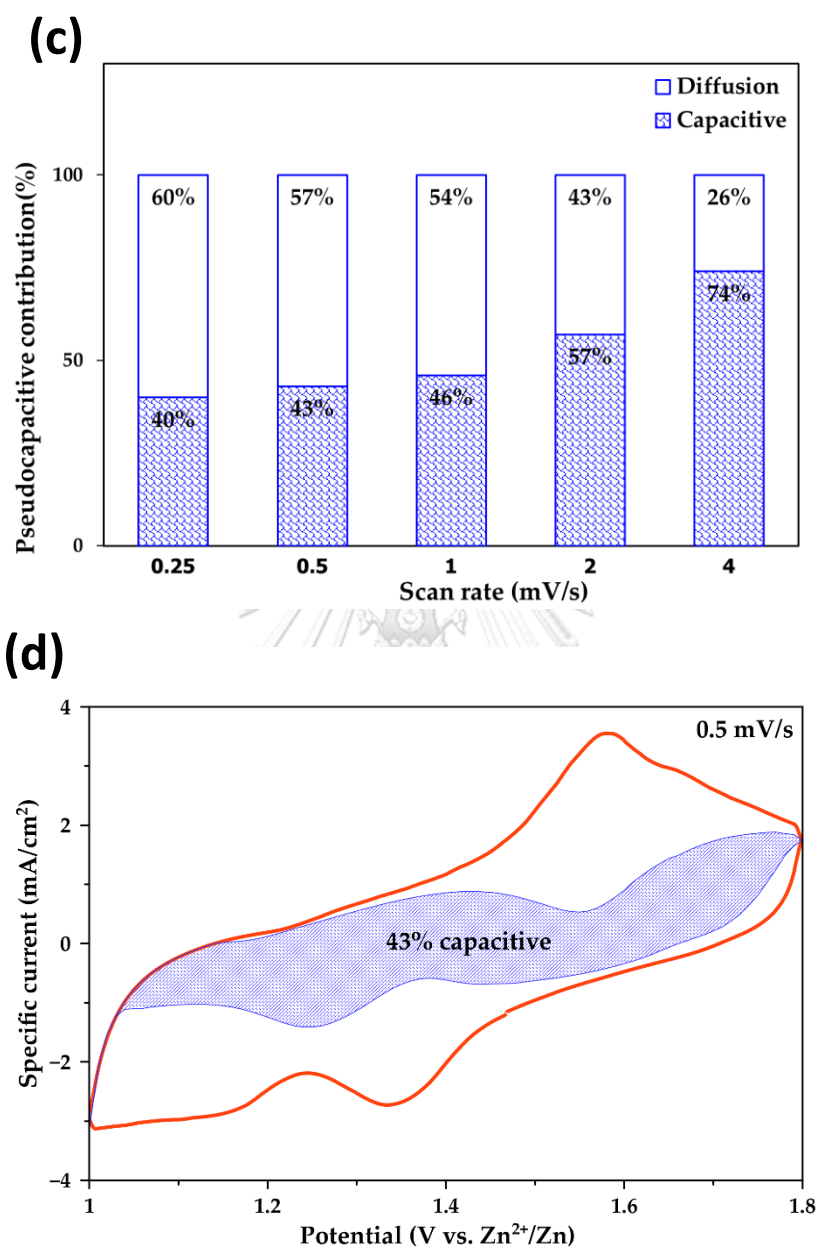
Figure 3.12 (a) Cyclic voltammograms of MN-CNT7525 cycling at different scan rates (b) Analysis of b-value for oxidation and reduction peaks (c) Capacitive contribution ratio of MN-CNT7525 electrode at different scan rates and (d) Capacitive contribution at a scan rate of 0.5 mV/s

3.2.3 Materials and methods

Material

Sulfuric acid (H_2SO_4, 95%), zinc sulfate heptahydrate ($ZnSO_4 \cdot 7H_2O$, 95 %), carboxymethylcellulose sodium salt (CMC, 93%) and Pottasium permanganese ($KMnO_4$, 99.3%) were supplied by Fujifilm Wako Pure Chemical Corporation (Osaka, Japan). MWCNTs (cocoon type with outer diameter 40-60 nm, 90 %) were purchased from Suzhou Tanfeng Graphene Technology Co., Ltd. (Jiangsu, China). Manganese sulfate monohydrate ($MnSO_4 \cdot H_2O$, 99%) was purchased from Ajax Finechem Pty. Ltd. (Sydney, Australia). Nickel (Ni) foam (0.5 mm thick, 100 PPI) was purchased from Qijing Trading Co., Ltd. (Wenzhou, China). Double ring qualitative, Fast101 filter paper was purchased from GE Healthcare (Chicago, IL, USA). Carbon black (Vulcan® XC-72, 99.99%) was supplied by Cabot Corporation (Boston, MA, USA). Graphite foil was purchased from Shenzhen 3KS Electronic Material Co. Ltd. (Shenzhen, China). Zinc sheet (99.99%) was purchased from Sirikul Engineering Ltd., Part. (Samutprakan, Thailand).

Preparation of δ-MnO_2 and MnO_2 heterostructure/MWCNTs (MNH-CNT)

The compared δ-MnO_2 nanoparticles were synthesized by dissolving 1.98 g of $KMnO_4$ in 60 mL of deionized (DI) water. Next, 0.336 g of $MnSO_4 \cdot H_2O$ was dissolved in 20 mL of DI water. Then, $MnSO_4 \cdot H_2O$ solution was added dropwise to $KMnO_4$ solution, and continuous stirring was followed for 30 min. Afterwards, the mixture was transferred into a 100 mL Teflon autoclave and kept at 160 °C for 24 h. in an oil bath. The product was dried at 80 °C for 12 h. It was duly collected and washed with DI water several times. MN-CNT was synthesized via thermal reaction. 300 mg of MWCNTs were ground together in a mortar with $KMnO_4$. The amount of $KMnO_4$ was varied (1.35, 1.95, and 2.85 g) to provide different weight ratios of MnO_2 and MWCNTs

by 60:40 (MN-CNT6040), 75:25 (MN-CNT7525), and 90:10 (MN-CNT9010), respectively. Next, the mixed powder was dispersed in 300 mL of water stirring for 10 min. 0.5 mL of concentrated H_2SO_4 was added to the above mixture with an additional 30 min of stirring. After that, the mixed solution was heated in an oil bath at 80 °C with continuous magnetic stirring for 1 h. The precipitate was washed and collected by centrifuging repeatedly with deionized water after the mixture was cooled to room temperature. Then, the solid product was dried in a vacuum at 50 °C for 24 h to obtain MN-CNT composite.

Electrodes and cup cell preparation

The cathode using MN-CNT was prepared by mixing together 70% wt. of MN-CNT, 20% wt. of carbon black, and 10% wt. of carboxymethylcellulose sodium salt binder. For comparison, the cathode of δ-MnO_2 was fabricated the same way using pristine δ-MnO_2 instead of MN-CNT. DI water was used to adjust the viscosity of the slurries. Each mixed slurry was stirred for 24 h at room temperature. Then, it was coated on a graphite foil current collector using a doctor blade and dried at 50 °C under vacuum before it was pressed by hydraulic press at 5 kPa for 1 min. The cathode contained about 5 mg of MN-CNT. Zinc anode was prepared by electrodeposition of zinc from $ZnSO_4$ (0.5 M) aqueous solution onto Ni foam using zinc sheet as a counter electrode at current density of 60 mA/cm^2. The amount of Zn deposited was 20 mg/cm^2. Both cathode and anode were punched into a 16 mm diameter disk. The filter paper was punched into a 20 mm disk and used as the separator. Then, the cathode, anode and separator were fabricated in a cup cell by using 0.3 mL of aqueous $ZnSO_4$ (1 M) as electrolyte.

Materials Characterization

The phase states of MN-CNT were analyzed using X-Ray Diffraction (XRD, Rigaku Model Miniflex II, Tokyo, Japan) of the powder samples with Cu Kα radiation, λ = 1.5418 Å at a scanning range of 5-90°. Field emission-scanning electron microscope (FESEM, JEOL JSM-6701F, Tokyo, Japan) was used to observe the morphological image of MN-CNT. Transmission electron microscope with energy dispersive spectroscopy (TEM-EDS, JEOL JEM-2000FX, Tokyo, Japan) was used to prove the presence of MWCNTs in MN-CNTs.

Electrochemical performances

Electrochemical measurements were carried out using a cup cell. CV was performed by electrochemical measurement system (HZ-5000, Hokuto Denko, Tokyo, Japan) at a scan rate of 0.5 mV/s in the voltage range 1.0 - 1.8 V versus Zn^{2+}/Zn. A battery testing system (EF-7100P, Electrofield, Osaka, Japan) was used to investigate the performance of the battery. The CVs for investigating capacitive behavior were tested at scanning rates from 0.25 to 4.0 mV/s between 1.0 and 1.8 V.

CHAPTER 4

CONCLUSION AND RECOMMENDATIONS

4.1 Conclusion

It was clear that the electrical conductivity of cathode material using the MnO_2/carbon material was improved. MnO_2 supported on different allotropes of carbon as a cathode host material improved the electrochemical properties and performances of the rechargeable aqueous electrolyte-based ZIB. Stability of ZIB which used cathode of MnO_2 supported on MWCNTs was better than that which used cathode of MnO_2 supported on graphite.

Part I: δ-MnO_2 nanoflower/graphite cathode for rechargeable aqueous zinc-ion batteries

δ-MnO_2 nanoflower supported on graphite flake was synthesized and used as an intercalation host material for a rechargeable ZIB. While the XRD studies confirmed the crystallographic structure, the FESEM studies revealed that the sample showed a nanoflower-like morphology having micropores about 50 nm in diameter. This study demonstrated that a diffusion process controlled the electrochemical reactions of the MNG cathode. When tested in ZIB, the MNG sample registered a prominent discharge capacity of 235 mA h/g, which was higher than the discharge capacity of pristine δ-MnO_2 (130 mA h/g). After the 100th cycle, the discharge capacity registered by the δ-MnO_2 was only 63.3 mA h/g whereas the MNG delivered a discharge capacity of 113.4 mA h/g. Moreover, the conductivity of the supporting graphite improved the conductivity by reducing the charge transfer resistance of the cathode materials. The present results concluded that the supporting graphite not only improved the electrical conductivity but also enhanced the specific capacity

and the cycling performance of the pristine δ-MnO_2. Thus, MNG is one of promising candidate cathode materials for ZIBs.

Part II: MnO_2 heterostructure on carbon nanotubes as cathode material for aqueous zinc-Ion batteries

It was evident that the MnO_2 heterostructure on MWCNTs proved to be a high-performance cathode for aqueous ZIBs. The incorporation of MWCNTs was found to improve the conductivity of MnO_2. The formation of the δ-MnO_2/γ-MnO_2 heterostructure on MWCNTs not only enhanced specific capacity but also improved cycling stability of the MnO_2 cathode. Consequently, the battery utilizing the MNH-CNT cathode demonstrated high discharge capacity, high-rate capability, as well as impressive cycling stability; exhibiting its superiority to the pristine δ-MnO_2 electrode. Additionally, the capacitive contribution ratio of 43% at scan rate 0.5 mV/s, reflecting the diffusion-controlled process, played a dominant role in the pseudocapacitive behavior of the MNH-CNT cathode. This work highlighted the design of MnO_2 heterostructure on CNTs for high-performance aqueous ZIBs.

4.2 Research Limitations

1. Pressed force in coin cell of Part I may be different from that in cup cell of Part II. The different force may affect the distance between the electrodes.

2. Battery testing temperatures of Part I and Part II was different due to different location of experiment. The viscosity of electrolytes, which were varying with the temperature, were different. This affected the diffusion rate of zinc-ion in the electrolyte.

4.3 Recommendations

        1. The different weight ratio of MnO_2 and graphite in Part I should be studied. This study only investigated with weight ratio of MnO_2 and graphite at 20:80. Different weight ratio of MnO_2 and graphite may improve more performance of the battery.

        2. Binder should be developed for good adhesion as well as good electrical conductivity. The resistance of binder is a parameter which affects the electron conduction of cathode.

        3. Anode should be improved to avoid the hydrogen evolution reaction. Hydrogen gas from hydrogen evolution reaction, which is a side reaction at anode, may damage of the battery.
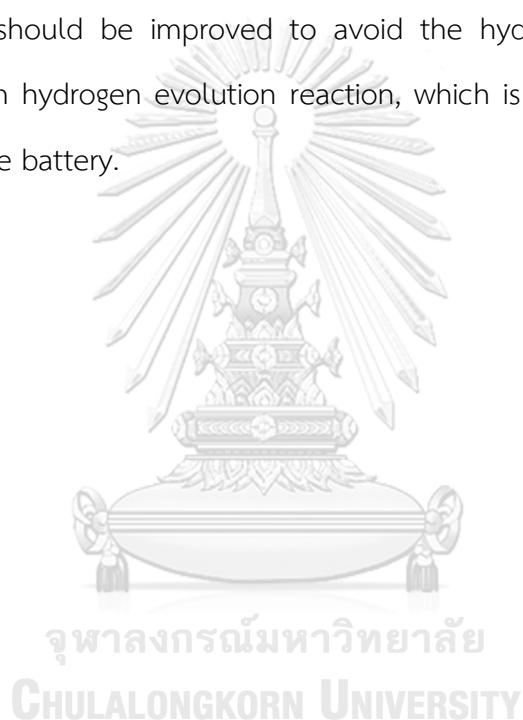
APPENDIX A

LIST OF ABBREVIATIONS

ZIB	Zinc-ion battery
MNG	MnO_2 on graphite
MNH-CNT	MnO_2 heterostructure on multi-walled carbon nanotubes
MN-CNT	MnO_2 on multi-walled carbon nanotubes
MN-CNT6040	MN-CNT having MnO_2 and MWCNT weight ratio of 60:40
MN-CNT7525	MN-CNT having MnO_2 and MWCNT weight ratio of 75:25
MN-CNT9010	MN-CNT having MnO_2 and MWCNT weight ratio of 90:10
MIB	Metal-ion battery
LIB	Lithium-ion battery
SHE	Standard hydrogen potential
CNT	Carbon nanotube
SWCNT	Single-walled carbon nanotube
MWCNT	Multi-walled carbon nanotube
CNF	Carbon nanofiber
XRD	X-ray diffraction
FESEM	Field emission scanning electron microscope
TEM-EDS	Transmission electron microscope with energy dispersive spectroscopy
EIS	Electrochemical Impedance Spectroscopy
CV	Cyclic voltammetry
CE	Coulombic efficiency
OLC	Onion-like carbon
DI water	Deionized water

APPENDIX B

SUPPLEMENTARY FIGURES
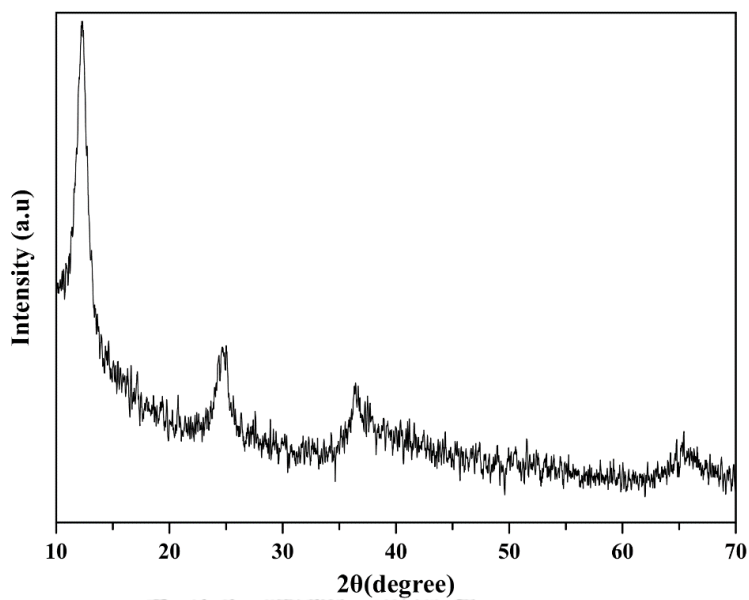
Figure B1 XRD pattern and crystallographic structure of the pristine δ-MnO$_2$.
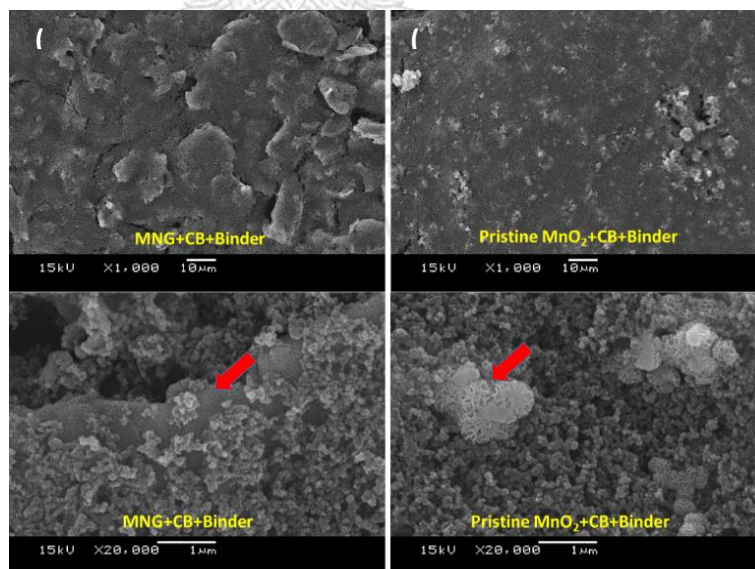
Figure B2 SEM images of (a) MNG, and (b) the pristine MnO$_2$ compound at different magnification.
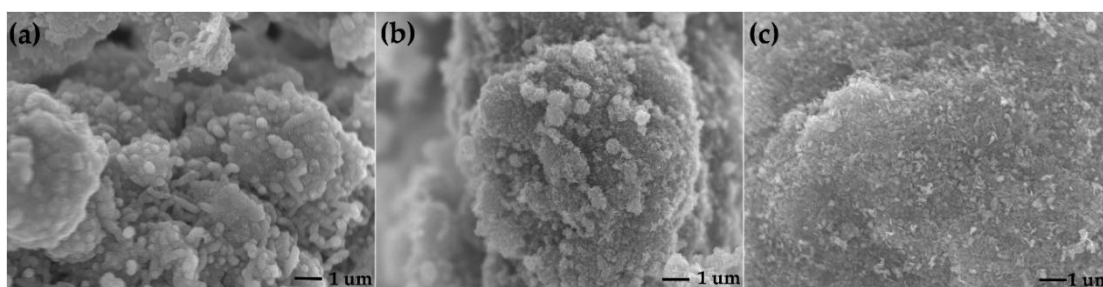
Figure B3 FESEM images at low magnification of (a) MN-CNT9010 (b) MN-CNT7525 and (c) MN-CNT6040
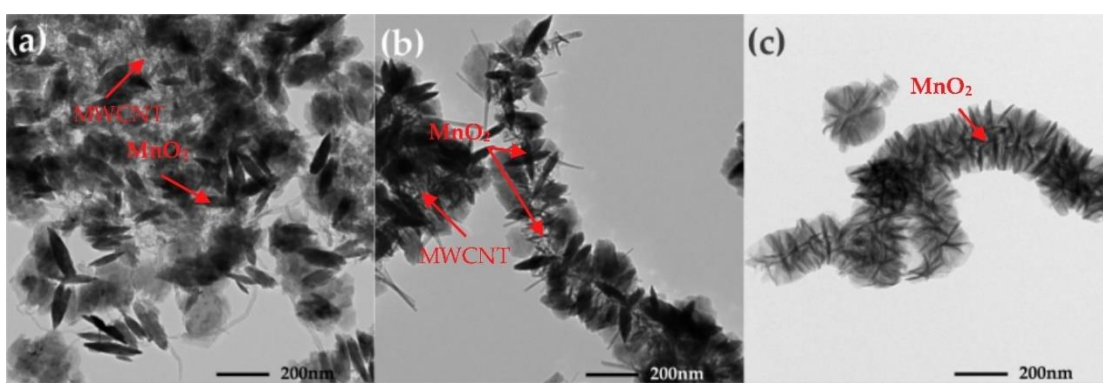
Figure B4 TEM images of (a) MN-CNT9010 (b) MN-CNT7525 and (c) MN-CNT6040

Position	C	O	Mn
C	41.54	43.43	15.40

Position	C	O	Mn
B	28.65	55.58	15.77

Position	C	O	Mn
A	41.22	45.44	13.34
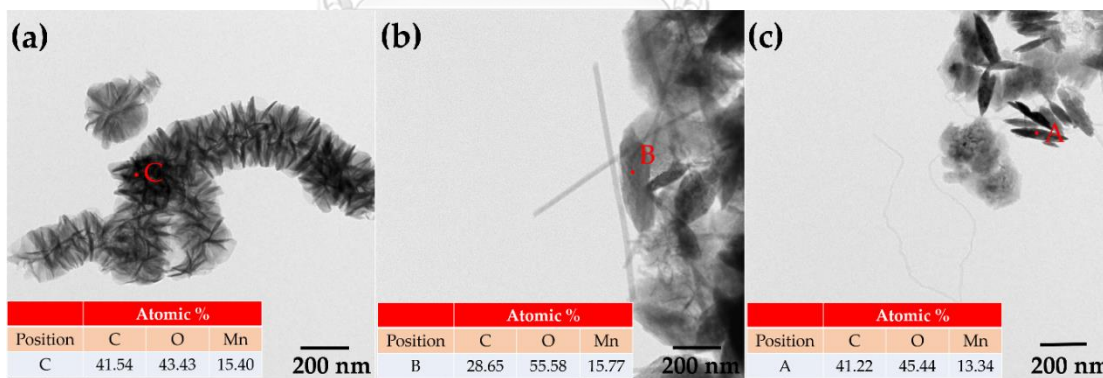
Figure B5 TEM-EDS of (a) MN-CNT9010 (b) MN-CNT7525 and (c) MN-CNT6040

APPENDIX C

LIST OF PUBLICATIONS

1. S. Khamsanga, R. Pornprasertsuk, T. Yonezawa, A. A. Mohamad and S. Kheawhom, "δ-MnO$_2$ nanoflower/graphite cathode for rechargeable aqueous zinc ion batteries", *SCIENTIFIC REPORTS* (2019) 9, 8441.

2. S. Khamsanga, M. Th. Nguyen, T. Yonezawa, P. Thamyongkit, R. Pornprasertsuk, P. Pattananuwat, A. Tuantranont, S. Siwamogsatham and S. Kheawhom, "MnO$_2$ heterostructure on carbon nanotubes as cathode material for aqueous zinc-Ion batteries", *INTERNATIONAL JOURNAL OF MOLECULAR SCIENCES* (2020) 21, 4689.

จุฬาลงกรณ์มหาวิทยาลัย
CHULALONGKORN UNIVERSITY

REFERENCES

[1] G. Wu, P. Li, C. Zhu, Y. Lei, H. Zhao, T. Li, H. Yue, B. Dou, Y. Gao, X. Yang, Amorphous titanium oxide passivated lithium titanium phosphate electrode for high stable aqueous lithium ion batteries with oxygen tolerance, Electrochimica Acta 246 (2017) 720-729.

[2] W.L. Wang, J. Jang, V.H. Nguyen, F.M. Auxilia, H. Song, K. Jang, E.M. Jin, G.-Y. Lee, H.-B. Gu, M.-H. Ham, Cerium vanadate and reduced graphene oxide composites for lithium-ion batteries, Journal of Alloys and Compounds 724 (2017) 1075-1082.

[3] A.S. Childress, P. Parajuli, J. Zhu, R. Podila, A.M. Rao, A Raman spectroscopic study of graphene cathodes in high-performance aluminum ion batteries, Nano Energy 39 (2017) 69-76.

[4] A. Bani Hashemi, G. Kasiri, F. La Mantia, The effect of polyethyleneimine as an electrolyte additive on zinc electrodeposition mechanism in aqueous zinc-ion batteries, Electrochimica Acta 258 (2017) 703-708.

[5] I.I. Misnon, R.A. Aziz, N.K.M. Zain, B. Vidhyadharan, S.G. Krishnan, R. Jose, High performance MnO_2 nanoflower electrode and the relationship between solvated ion size and specific capacitance in highly conductive electrolytes, Materials Research Bulletin 57 (2014) 221-230.

[6] J. Chen, Y. Wang, X. He, S. Xu, M. Fang, X. Zhao, Y. Shang, Electrochemical properties of MnO_2 nanorods as anode materials for lithium ion batteries, Electrochimica Acta 142 (2014) 152-156.

[7] J.-S. Kim, W.-S. Chang, R.-H. Kim, D.-Y. Kim, D.-W. Han, K.-H. Lee, S.-S. Lee, S.-G. Doo, High-capacity nanostructured manganese dioxide cathode for rechargeable magnesium ion batteries, Journal of Power Sources 273 (2015) 210-215.

[8] M.H. Alfaruqi, S. Islam, J. Gim, J. Song, S. Kim, D.T. Pham, J. Jo, Z. Xiu, V. Mathew, J. Kim, A high surface area tunnel-type α-MnO_2 nanorod cathode by a simple solvent-free synthesis for rechargeable aqueous zinc-ion batteries, Chemical Physics Letters 650 (2016) 64-68.

[9] M.H. Alfaruqi, J. Gim, S. Kim, J. Song, D.T. Pham, J. Jo, Z. Xiu, V. Mathew, J. Kim, A layered δ-MnO_2 nanoflake cathode with high zinc-storage capacities for eco-friendly

battery applications, Electrochem commun. 60 (2015) 121-125.

[10] J.-W. Wang, Y. Chen, B.-Z. Chen, Synthesis and control of high-performance MnO_2 /carbon nanotubes nanocomposites for supercapacitors, Journal of Alloys and Compounds 688 (2016) 184-197.

[11] S. Islam, M.H. Alfaruqi, J. Song, S. Kim, D.T. Pham, J. Jo, S. Kim, V. Mathew, J.P. Baboo, Z. Xiu, J. Kim, Carbon-coated manganese dioxide nanoparticles and their enhanced electrochemical properties for zinc-ion battery applications, Journal of Energy Chemistry 26(4) (2017) 815-819.

[12] J. Liu, Y. Zhang, Y. Li, J. Li, Z. Chen, H. Feng, J. Li, J. Jiang, D. Qian, In situ chemical synthesis of sandwich-structured MnO_2 /graphene nanoflowers and their supercapacitive behavior, Electrochimica Acta 173 (2015) 148-155.

[13] U.S.E.I. Administration, What is energy?, 2020. https://www.eia.gov/energyexplained/what-is-energy/. (Accessed 1 Dec 2020.

[14] M. Mofijur, T. Mahlia, A. Silitonga, H. Ong, M. Silakhori, M. Hasan, N. Putra, S.M. Rahman, Phase Change Materials (PCM) for Solar Energy Usages and Storage: An Overview, Energies 12(16) (2019).

[15] M. Cultu, Batteries and Their Chemistry, ENERGY STORAGE SYSTEMS 2 (1988) 1-9.

[16] N. Kakimoto, K. Goto, Capacity-Fading Model of Lithium-Ion Battery Applicable to Multicell Storage Systems, IEEE Transactions on Sustainable Energy 7(1) (2016) 108-117.

[17] K. Huang, J. Li, Z. Xu, Characterization and recycling of cadmium from waste nickel-cadmium batteries, Waste Manag 30(11) (2010) 2292-8.

[18] C.C. Wang, Y.T. Zhou, C.C. Yang, Q. Jiang, Clarifying the capacity deterioration mechanism sheds light on the design of ultra-long-life hydrogen storage alloys, Chemical Engineering Journal 352 (2018) 325-332.

[19] L.T. Lam, N.P. Haigh, C.G. Phyland, A.J. Urban, Failure mode of valve-regulated lead-acid batteries under high-rate partial-state-of-charge operation, Journal of Power Sources 133(1) (2004) 126-134.

[20] H. Pan, Y. Shao, P. Yan, Y. Cheng, K.S. Han, Z. Nie, C. Wang, J. Yang, X. Li, P. Bhattacharya, K.T. Mueller, J. Liu, Reversible aqueous zinc/manganese oxide energy storage from conversion reactions, Nature Energy 1(5) (2016).

[21] C. Xu, B. Li, H. Du, F. Kang, Energetic zinc ion chemistry: the rechargeable zinc ion

battery, Angew Chem Int Ed Engl 51(4) (2012) 933-5.

[22] D. Kundu, S. Hosseini Vajargah, L. Wan, B. Adams, D. Prendergast, L.F. Nazar, Aqueous vs. nonaqueous Zn-ion batteries: consequences of the desolvation penalty at the interface, Energy Environ. Sci. 11(4) (2018) 881-892.

[23] G. Fang, J. Zhou, A. Pan, S. Liang, Recent Advances in Aqueous Zinc-Ion Batteries, ACS Energy Letters 3(10) (2018) 2480-2501.

[24] C. Guo, H. Liu, J. Li, Z. Hou, J. Liang, J. Zhou, Y. Zhu, Y. Qian, Ultrathin δ-MnO$_2$ nanosheets as cathode for aqueous rechargeable zinc ion battery, Electrochimica Acta 304 (2019) 370-377.

[25] C. Xia, J. Guo, Y. Lei, H. Liang, C. Zhao, H.N. Alshareef, Rechargeable Aqueous Zinc-Ion Battery Based on Porous Framework Zinc Pyrovanadate Intercalation Cathode, Advanced Materials 32(9) (2020).

[26] J. Ming, J. Guo, C. Xia, W. Wang, H.N. Alshareef, Zinc-ion batteries: Materials, mechanisms, and applications, Materials Science and Engineering: R: Reports 135 (2019) 58-84.

[27] M. Toupin, T. Brousse, D. Bélanger, Charge storage mechanism of MnO$_2$ electrode used in aqueous electrochemical capacitor, Chem. Mater. 16(16) (2004) 3184-3190.

[28] M.H. Alfaruqi, V. Mathew, J. Gim, S. Kim, J. Song, J.P. Baboo, S.H. Choi, J. Kim, Electrochemically Induced Structural Transformation in a γ-MnO$_2$ Cathode of a High Capacity Zinc-Ion Battery System, Chemistry of Materials 27(10) (2015) 3609-3620.

[29] J. Lee, J.B. Ju, W.I. Cho, B.W. Cho, S.H. Oh, Todorokite-type MnO$_2$ as a zinc-ion intercalating material, Electrochimica Acta 112 (2013) 138-143.

[30] B. Lee, H.R. Lee, H. Kim, K.Y. Chung, B.W. Cho, S.H. Oh, Elucidating the intercalation mechanism of zinc ions into alpha-MnO$_2$ for rechargeable zinc batteries, Chem Commun (Camb) 51(45) (2015) 9265-8.

[31] Z. Jia, B. Wang, Y. Wang, Copper hexacyanoferrate with a well-defined open framework as a positive electrode for aqueous zinc ion batteries, Materials Chemistry and Physics 149-150 (2015) 601-606.

[32] B. Jiang, C. Xu, C. Wu, L. Dong, J. Li, F. Kang, Manganese Sesquioxide as Cathode Material for Multivalent Zinc Ion Battery with High Capacity and Long Cycle Life,

Electrochimica Acta 229 (2017) 422-428.

[33] M.S. Chae, J.W. Heo, H.H. Kwak, H. Lee, S.-T. Hong, Organic electrolyte-based rechargeable zinc-ion batteries using potassium nickel hexacyanoferrate as a cathode material, Journal of Power Sources 337(John Wiley & Sons) (2017) 204-211.

[34] Y. Xia, D. Zhu, S. Si, D. Li, S. Wu, Nickel foam-supported polyaniline cathode prepared with electrophoresis for improvement of rechargeable Zn battery performance, Journal of Power Sources 283 (2015) 125-131.

[35] G. Zhao, D. Zhang, L. Zhang, K. Sun, Ti@δ-MnO2 core-shell nanowire arrays as self-supported electrodes of supercapacitors and Li ion batteries, Electrochimica Acta 202 (2016) 8-13.

[36] J.-K. Chang, M.-T. Lee, W.-T. Tsai, In situ Mn K-edge X-ray absorption spectroscopic studies of anodically deposited manganese oxide with relevance to supercapacitor applications, Journal of Power Sources 166(2) (2007) 590-594.

[37] V. Mathew, J. Lim, J. Kang, J. Gim, A.K. Rai, J. Kim, Self-assembled mesoporous manganese oxide with high surface area by ambient temperature synthesis and its enhanced electrochemical properties, Electrochemistry Communications 13(7) (2011) 730-733.

[38] D.A. Kitchaev, S.T. Dacek, W. Sun, G. Ceder, Thermodynamics of Phase Selection in MnO_2 Framework Structures through Alkali Intercalation and Hydration, J Am Chem Soc 139(7) (2017) 2672-2681.

[39] C.M. Julien, A. Mauger, Nanostructured MnO_2 as Electrode Materials for Energy Storage, Nanomaterials (Basel) 7(11) (2017).

[40] G.A.M. Ali, L.L. Tan, R. Jose, M.M. Yusoff, K.F. Chong, Electrochemical performance studies of MnO_2 nanoflowers recovered from spent battery, Materials Research Bulletin 60 (2014) 5-9.

[41] D. Xu, B. Li, C. Wei, Y.-B. He, H. Du, X. Chu, X. Qin, Q.-H. Yang, F. Kang, Preparation and Characterization of MnO_2/acid-treated CNT Nanocomposites for Energy Storage with Zinc Ions, Electrochimica Acta 133 (2014) 254-261.

[42] L. Wang, W. Ma, Y. Li, H. Cui, Synthesis of δ-MnO_2 with nanoflower-like architecture by a microwave-assisted hydrothermal method, Journal of Sol-Gel Science and

Technology 82(1) (2016) 85-91.

[43] T. Jayaraman, A.P. Murthy, V. Elakkiya, S. Chandrasekaran, P. Nithyadharseni, Z. Khan, R.A. Senthil, R. Shanker, M. Raghavender, P. Kuppusami, M. Jagannathan, M. Ashokkumar, Recent development on carbon based heterostructures for their applications in energy and environment: A review, Journal of Industrial and Engineering Chemistry 64 (2018) 16-59.

[44] L. David R., Handbook of Chemistry and Physics, 87 ed., CRC Press2004.

[45] M.A. González, R. Trócoli, I. Pavlovic, C. Barriga, F. La Mantia, Layered double hydroxides as a suitable substrate to improve the efficiency of Zn anode in neutral pH Zn-ion batteries, Electrochemistry Communications 68 (2016) 1-4.

[46] R.K. Guduru, J.C. Icaza, A Brief Review on Multivalent Intercalation Batteries with Aqueous Electrolytes, Nanomaterials (Basel) 6(3) (2016).

[47] V. Augustyn, Tuning the interlayer of transition metal oxides for electrochemical energy storage, Journal of Materials Research 32(1) (2016) 2-15.

[48] A.J. Bard, L.R. Faulkner, ELECTROCHEMICAL METHODS: Fundamentals and Applications, 2 ed., JOHN WILEY & SONS, INC.1980.

[49] N. Elgrishi, K.J. Rountree, B.D. McCarthy, E.S. Rountree, T.T. Eisenhart, J.L. Dempsey, A Practical Beginner's Guide to Cyclic Voltammetry, Journal of Chemical Education 95(2) (2017) 197-206.

[50] M.E. Orazem, B. Tribollet, Electrochemical Impedance Spectroscopy, 2 ed., Wiley-Interscience, New York, 2008.

[51] P. Agarwal, M.E. Orazem, L.H. Garcia-Rubio, Measurement Models for Electrochemical Impedance Spectroscopy: I . Demonstration of Applicability, Journal of The Electrochemical Society 139(7) (1992) 1917-1927.

[52] W. Lao-atiman, T. Julaphatachote, P. Boonmongkolras, S. Kheawhom, Printed transparent thin film Zn-MnO$_2$ battery, J. Electrochem. Soc. 164(4) (2017) A859-A863.

[53] S. Suren, S. Kheawhom, Development of a high energy density flexible zinc-air battery, J. Electrochem. Soc. 163(6) (2016) A846-A850.

[54] S. Hosseini, W. Lao-atiman, S.J. Han, A. Arpornwichanop, T. Yonezawa, S. Kheawhom, Discharge Performance of Zinc-Air Flow Batteries Under the Effects of

Sodium Dodecyl Sulfate and Pluronic F-127, Sci. Rep. 8(1) (2018) 14909.

[55] S. Hosseini, S.J. Han, A. Arponwichanop, T. Yonezawa, S. Kheawhom, Ethanol as an electrolyte additive for alkaline zinc-air flow batteries, Scientific Reports 8(1) (2018) 11273.

[56] W. Lao-atiman, K. Bumroongsil, A. Arpornwichanop, P. Bumroongsakulsawat, S. Olaru, S. Kheawhom, Model-Based Analysis of an Integrated Zinc-Air Flow Battery/Zinc Electrolyzer System, Frontiers in Energy Research 7 (2019).

[57] W. Kao-ian, R. Pornprasertsuk, P. Thamyongkit, T. Maiyalagan, S. Kheawhom, Rechargeable Zinc-Ion Battery Based on Choline Chloride-Urea Deep Eutectic Solvent, Journal of The Electrochemical Society 166(6) (2019) A1063-A1069.

[58] M.H. Alfaruqi, J. Gim, S. Kim, J. Song, J. Jo, S. Kim, V. Mathew, J. Kim, Enhanced reversible divalent zinc storage in a structurally stable α-MnO_2 nanorod electrode, Journal of Power Sources 288 (2015) 320-327.

[59] M. Feng, Q. Du, L. Su, G. Zhang, G. Wang, Z. Ma, W. Gao, X. Qin, G. Shao, Manganese oxide electrode with excellent electrochemical performance for sodium ion batteries by pre-intercalation of K and Na ions, Sci. Rep. 7(1) (2017) 2219.

[60] J. Song, J. Kim, T. Kang, D. Kim, Design of a porous cathode for ultrahigh performance of a Li-ion battery: An overlooked pore distribution, Sci. Rep. 7 (2017) 42521.

[61] C. Wei, C. Xu, B. Li, H. Du, F. Kang, Preparation and characterization of manganese dioxides with nano-sized tunnel structures for zinc ion storage, J. Phys. Chem. Solids 73(12) (2012) 1487-1491.

[62] R. Renuka, S. Ramamurthy, An investigation on layered birnessite type manganese oxides for battery applications., J. Power Sources 87 (2000) 144–152.

[63] C. Zhu, S. Guo, Y. Fang, L. Han, E. Wang, S. Dong, One-step electrochemical approach to the synthesis of Graphene/MnO_2 nanowall hybrids, Nano Res. 4(7) (2011) 648-657.

[64] J. Zhou, L. Yu, M. Sun, S. Yang, F. Ye, J. He, Z. Hao, Novel synthesis of birnessite-type MnO_2 nanostructure for water treatment and electrochemical capacitor, Ind. Eng. Chem. Res. 52(28) (2013) 9586-9593.

[65] C. Phillips, A. Al-Ahmadi, S.-J. Potts, T. Claypole, D. Deganello, The effect of graphite and carbon black ratios on conductive ink performance, J. Mater. Sci. 52(16) (2017) 9520-9530.

[66] K. Wongrujipairoj, L. Poolnapol, A. Arpornwichanop, S. Suren, S. Kheawhom, Suppression of zinc anode corrosion for printed flexible zinc-air battery, Phys. Status Solidi B 254(2) (2017).

[67] L.A. Chernozatonskii, P.B. Sorokin, E.É. Belova, J. Brüning, A.S. Fedorov, Metal-semiconductor (semimetal) superlattices on a graphite sheet with vacancies, JETP Lett. 84(3) (2006) 115-118.

[68] F. Li, Y. Xing, M. Huang, K.L. Li, T.T. Yu, Y.X. Zhang, D. Losic, MnO_2 nanostructures with three-dimensional (3D) morphology replicated from diatoms for high-performance supercapacitors, J. Mater. Chem. A 3(15) (2015) 7855-7861.

[69] A.K. Thapa, B. Pandit, R. Thapa, T. Luitel, H.S. Paudel, G. Sumanasekera, M.K. Sunkara, N. Gunawardhana, T. Ishihara, M. Yoshio, Synthesis of mesoporous birnessite-MnO_2 composite as a cathode electrode for lithium battery, Electrochim. Acta 116 (2014) 188-193.

[70] R. Rajarao, B.R. Bhat, Large scale synthesis of carbon nanofibres on sodium chloride support, Nanomater. Nanotechno. 2 (2012) 5.

[71] J. Zhang, Y. Li, L. Wang, C. Zhang, H. He, Catalytic oxidation of formaldehyde over manganese oxides with different crystal structures, Catal. Sci. Technol. 5(4) (2015) 2305-2313.

[72] A.C. Hayes, P. Kruus, W.A. Adams, Raman spectroscopic study of aqueous $(NH_4)_2SO_4$ and $ZnSO_4$ solutions, J. Solution Chem. 13(1) (1984) 61-75.

[73] J.-W. Wang, Y. Chen, B.-Z. Chen, A synthesis method of MnO_2/activated carbon composite for electrochemical supercapacitors, J. Electrochem. Soc. 162(8) (2015) A1654-A1661.

[74] C. Ji, H. Ren, S. Yang, Control of manganese dioxide crystallographic structure in the redox reaction between graphene and permanganate ions and their electrochemical performance, RSC Adv. 5(28) (2015) 21978-21987.

[75] Y.-j. Yang, E.-H. Liu, L.-m. Li, Z.-z. Huang, H.-j. Shen, X.-x. Xiang, Nanostructured MnO_2/exfoliated graphite composite electrode as supercapacitors, J. Alloy Compd.

487(1-2) (2009) 564-567.

[76] J. Li, J. Huang, J. Li, L. Cao, H. Qi, Y. Cheng, Q. Xi, H. Dang, Improved Li-ion diffusion process in TiO_2/rGO anode for lithium-ion battery, J. Alloy Compd. 727 (2017) 998-1005.

[77] P. Simon, Y. Gogotsi, B. Dunn, Where do batteries end and supercapacitors begin, Science 343 (2014) 1210-1211.

[78] D. Chen, D. Ding, X. Li, G.H. Waller, X. Xiong, M.A. El-Sayed, M. Liu, Probing the charge storage mechanism of a pseudocapacitive MnO_2 electrode using in operando raman spectroscopy, Chem. Mater. 27(19) (2015) 6608-6619.

[79] X. Guo, J. Li, X. Jin, Y. Han, Y. Lin, Z. Lei, S. Wang, L. Qin, S. Jiao, R. Cao, A hollow-structured manganese oxide cathode for stable Zn-MnO_2 batteries, Nanomaterials 8(5) (2018).

[80] M.H. Alfaruqi, S. Islam, D.Y. Putro, V. Mathew, S. Kim, J. Jo, S. Kim, Y.-K. Sun, K. Kim, J. Kim, Structural transformation and electrochemical study of layered MnO_2 in rechargeable aqueous zinc-ion battery, Electrochim. Acta 276 (2018) 1-11.

[81] W. Qiu, Y. Li, A. You, Z. Zhang, G. Li, X. Lu, Y. Tong, High-performance flexible quasi-solid-state Zn–MnO_2 battery based on MnO_2 nanorod arrays coated 3D porous nitrogen-doped carbon cloth, J. Mater. Chem. A 5(28) (2017) 14838-14846.

[82] H. Liu, C. Li, H.P. Zhang, L.J. Fu, Y.P. Wu, H.Q. Wu, Kinetic study on $LiFePO_4$/C nanocomposites synthesized by solid state technique, J. Power Sources 159(1) (2006) 717-720.

[83] A.J. Bard, L.R. Faulkner, Electrochemical Methods, 2 ed., JOHN WILEY & SONS, INC., New York, 2001.

[84] H. Li, B. Zhang, Q. Zhou, J. Zhang, W. Yu, Z. Ding, M.A. Tsiamtsouri, J. Zheng, H. Tong, Dual-carbon confined SnO_2 as ultralong-life anode for Li-ion batteries, Ceram. Int. 45(6) (2019) 7830-7838.

[85] Q. Cao, H.P. Zhang, G.J. Wang, Q. Xia, Y.P. Wu, H.Q. Wu, A novel carbon-coated $LiCoO_2$ as cathode material for lithium ion battery, Electrochem commun. 9(5) (2007) 1228-1232.

[86] R.D. Corpuz, L.M.Z. De Juan, S. Praserthdam, R. Pornprasertsuk, T. Yonezawa, M.T. Nguyen, S. Kheawhom, Annealing induced a well-ordered single crystal δ-MnO_2 and its

electrochemical performance in zinc-ion battery, Scientific Reports 9(1) (2019) 15107.

[87] L.M. De Juan-Corpuz, R.D. Corpuz, A. Somwangthanaroj, M.T. Nguyen, T. Yonezawa, J. Ma, S. Kheawhom, Binder-Free Centimeter-Long V_2O_5 Nanofibers on Carbon Cloth as Cathode Material for Zinc-Ion Batteries, Energies 13(1) (2019) 31.

[88] Y. Huang, J. Mou, W. Liu, X. Wang, L. Dong, F. Kang, C. Xu, Novel Insights into Energy Storage Mechanism of Aqueous Rechargeable Zn/MnO_2 Batteries with Participation of Mn^{2+}, Nano-Micro Letters 11(1) (2019) 49.

[89] T. Leisegang, F. Meutzner, M. Zschornak, W. Münchgesang, R. Schmid, T. Nestler, R.A. Eremin, A.A. Kabanov, V.A. Blatov, D.C. Meyer, The Aluminum-Ion Battery: A Sustainable and Seminal Concept?, Frontiers in Chemistry 7(268) (2019).

[90] B. Su, J. Zhang, M. Fujita, W. Zhou, P.H.-L. Sit, D.Y.W. Yu, Na_2SeO_3: A Na-Ion Battery Positive Electrode Material with High Capacity, Journal of The Electrochemical Society 166(3) (2019) A5075-A5080.

[91] L.H. Saw, Y. Ye, A.A.O. Tay, Integration issues of lithium-ion battery into electric vehicles battery pack, Journal of Cleaner Production 113 (2016) 1032-1045.

[92] Z. Rao, S. Wang, G. Zhang, Simulation and experiment of thermal energy management with phase change material for ageing $LiFePO_4$ power battery, Energy Conversion and Management 52(12) (2011) 3408-3414.

[93] N. Palaniyandy, M.A. Kebede, K. Raju, K.I. Ozoemena, L. le Roux, M.K. Mathe, R. Jayaprakasam, α-MnO_2 nanorod/onion-like carbon composite cathode material for aqueous zinc-ion battery, Materials Chemistry and Physics 230 (2019) 258-266.

[94] M. Qin, W. Liu, L. Shan, G. Fang, X. Cao, S. Liang, J. Zhou, Construction of V_2O_5/NaV_6O_{15} biphase composites as aqueous zinc-ion battery cathode, Journal of Electroanalytical Chemistry 847 (2019) 113246.

[95] T. Ould Ely, D. Kamzabek, D. Chakraborty, Batteries Safety: Recent Progress and Current Challenges, Frontiers in Energy Research 7(71) (2019).

[96] X. Wu, K. Song, X. Zhang, N. Hu, L. Li, W. Li, L. Zhang, H. Zhang, Safety Issues in Lithium Ion Batteries: Materials and Cell Design, Frontiers in Energy Research 7(65) (2019).

[97] R.D. Corpuz, L.M. De Juan-Corpuz, M.T. Nguyen, T. Yonezawa, H.-L. Wu, A.

Somwangthanaroj, S. Kheawhom, Binder-Free α-MnO$_2$ Nanowires on Carbon Cloth as Cathode Material for Zinc-Ion Batteries, International Journal of Molecular Sciences 21(9) (2020) 3113.

[98] H. Li, L. Ma, C. Han, Z. Wang, Z. Liu, Z. Tang, C. Zhi, Advanced rechargeable zinc-based batteries: Recent progress and future perspectives, Nano Energy 62 (2019) 550-587.

[99] N. Ma, P. Wu, Y. Wu, D. Jiang, G. Lei, Progress and perspective of aqueous zinc-ion battery, Functional Materials Letters 12(5) (2019) 1930003.

[100] W. Xu, Y. Wang, Recent Progress on Zinc-Ion Rechargeable Batteries, Nano-Micro Letters 11(1) (2019) 90.

[101] B. Lan, Z. Peng, L. Chen, C. Tang, S. Dong, C. Chen, M. Zhou, C. Chen, Q. An, P. Luo, Metallic silver doped vanadium pentoxide cathode for aqueous rechargeable zinc ion batteries, Journal of Alloys and Compounds 787 (2019) 9-16.

[102] D. Yang, H. Tan, X. Rui, Y. Yu, Electrode Materials for Rechargeable Zinc-Ion and Zinc-Air Batteries: Current Status and Future Perspectives, Electrochemical Energy Reviews 2(3) (2019) 395-427.

[103] B. Tang, L. Shan, S. Liang, J. Zhou, Issues and opportunities facing aqueous zinc-ion batteries, Energy & Environmental Science 12(11) (2019) 3288-3304

[104] C. Wang, Y. Zeng, X. Xiao, S. Wu, G. Zhong, K. Xu, Z. Wei, W. Su, X. Lu, γ-MnO$_2$ nanorods/graphene composite as efficient cathode for advanced rechargeable aqueous zinc-ion battery, Journal of Energy Chemistry 43 (2020) 182-187.

[105] S. Khamsanga, R. Pornprasertsuk, T. Yonezawa, A.A. Mohamad, S. Kheawhom, δ-MnO2 nanoflower/graphite cathode for rechargeable aqueous zinc ion batteries, Scientific Reports 9(1) (2019) 8441.

[106] L. Li, Z.A. Hu, N. An, Y.Y. Yang, Z.M. Li, H.Y. Wu, Facile Synthesis of MnO$_2$/CNTs Composite for Supercapacitor Electrodes with Long Cycle Stability, The Journal of Physical Chemistry C 118(40) (2014) 22865-22872.

[107] H. Wang, C. Peng, F. Peng, H. Yu, J. Yang, Facile synthesis of MnO$_2$/CNT nanocomposite and its electrochemical performance for supercapacitors, Materials Science and Engineering: B 176(14) (2011) 1073-1078.

[108] Y. Zhang, Y. Hu, S. Li, J. Sun, B. Hou, Manganese dioxide-coated carbon nanotubes as an improved cathodic catalyst for oxygen reduction in a microbial fuel cell, Journal of Power Sources 196(22) (2011) 9284-9289.

[109] S.-L. Chou, J.-Z. Wang, S.-Y. Chew, H.-K. Liu, S.-X. Dou, Electrodeposition of MnO_2 nanowires on carbon nanotube paper as free-standing, flexible electrode for supercapacitors, Electrochemistry Communications 10(11) (2008) 1724-1727.

[110] J. Yang, M. Ma, C. Sun, Y. Zhang, W. Huang, X. Dong, Hybrid $NiCo_2S_4$@MnO_2 heterostructures for high-performance supercapacitor electrodes, Journal of Materials Chemistry A 3(3) (2015) 1258-1264.

[111] L. Liu, L. Fang, F. Wu, J. Hu, S. Zhang, H. Luo, B. Hu, M. Zhou, Self-supported core-shell heterostructure MnO_2/NiCo-LDH composite for flexible high-performance supercapacitor, Journal of Alloys and Compounds 824 (2020) 153929.

[112] R. Peng, H. Zhang, L. Gui, Y. Zheng, Z. Wu, Y. Luo, P. Yu, Construction of 0D CeO2/2D MnO_2 heterostructure with high electrochemical performance, Electrochimica Acta 319 (2019) 95-100.

[113] J. Zhao, Z. Tao, J. Liang, J. Chen, Facile Synthesis of Nanoporous γ-MnO_2 Structures and Their Application in Rechargeable Li-Ion Batteries, Crystal Growth & Design 8(8) (2008) 2799-2805.

[114] J. Zhao, H. Ren, Q. Liang, D. Yuan, S. Xi, C. Wu, W. Manalastas, J. Ma, W. Fang, Y. Zheng, C.-F. Du, M. Srinivasan, Q. Yan, High-performance flexible quasi-solid-state zinc-ion batteries with layer-expanded vanadium oxide cathode and zinc/stainless steel mesh composite anode, Nano Energy 62 (2019) 94-102.

[115] D.A. Kitchaev, H. Peng, Y. Liu, J. Sun, J.P. Perdew, G. Ceder, Energetics of MnO_2 polymorphs in density functional theory, Physical Review B 93(4) (2016) 045132.

[116] R.Y. Wang, C.D. Wessells, R.A. Huggins, Y. Cui, Highly Reversible Open Framework Nanoscale Electrodes for Divalent Ion Batteries, Nano Letters 13(11) (2013) 5748-5752.

[117] S. Yang, M. Zhang, X. Wu, X. Wu, F. Zeng, Y. Li, S. Duan, D. Fan, Y. Yang, X. Wu, The excellent electrochemical performances of $ZnMn_2O_4$/Mn_2O_3: The composite cathode material for potential aqueous zinc ion batteries, Journal of Electroanalytical Chemistry 832 (2019) 69-74.

[118] J. Wang, J. Polleux, J. Lim, B. Dunn, Pseudocapacitive Contributions to Electrochemical Energy Storage in TiO_2 (Anatase) Nanoparticles, The Journal of Physical Chemistry C 111(40) (2007) 14925-14931.

[119] F. Wan, L. Zhang, X. Dai, X. Wang, Z. Niu, J. Chen, Aqueous rechargeable zinc/sodium vanadate batteries with enhanced performance from simultaneous insertion of dual carriers, Nature Communications 9(1) (2018) 1656.

[120] G. Sun, X. Jin, H. Yang, J. Gao, L. Qu, An aqueous $Zn–MnO_2$ rechargeable microbattery, Journal of Materials Chemistry A 6(23) (2018) 10926-10931.

[121] C. Xia, J. Guo, Y. Lei, H. Liang, C. Zhao, H.N. Alshareef, Rechargeable Aqueous Zinc-Ion Battery Based on Porous Framework Zinc Pyrovanadate Intercalation Cathode, Advanced Materials 30(5) (2018) 1705580.

จุฬาลงกรณ์มหาวิทยาลัย

CHULALONGKORN UNIVERSITY

[1] G. Wu, P. Li, C. Zhu, Y. Lei, H. Zhao, T. Li, H. Yue, B. Dou, Y. Gao, X. Yang, Amorphous titanium oxide passivated lithium titanium phosphate electrode for high stable aqueous lithium ion batteries with oxygen tolerance, Electrochimica Acta 246 (2017) 720-729.

[2] W.L. Wang, J. Jang, V.H. Nguyen, F.M. Auxilia, H. Song, K. Jang, E.M. Jin, G.-Y. Lee, H.-B. Gu, M.-H. Ham, Cerium vanadate and reduced graphene oxide composites for lithium-ion batteries, Journal of Alloys and Compounds 724 (2017) 1075-1082.

[3] A.S. Childress, P. Parajuli, J. Zhu, R. Podila, A.M. Rao, A Raman spectroscopic study of graphene cathodes in high-performance aluminum ion batteries, Nano Energy 39 (2017) 69-76.

[4] A. Bani Hashemi, G. Kasiri, F. La Mantia, The effect of polyethyleneimine as an electrolyte additive on zinc electrodeposition mechanism in aqueous zinc-ion batteries, Electrochimica Acta 258 (2017) 703-708.

[5] I.I. Misnon, R.A. Aziz, N.K.M. Zain, B. Vidhyadharan, S.G. Krishnan, R. Jose, High performance MnO_2 nanoflower electrode and the relationship between solvated ion size and specific capacitance in highly conductive electrolytes, Materials Research Bulletin 57 (2014) 221-230.

[6] J. Chen, Y. Wang, X. He, S. Xu, M. Fang, X. Zhao, Y. Shang, Electrochemical properties of MnO_2 nanorods as anode materials for lithium ion batteries, Electrochimica Acta 142 (2014) 152-156.

[7] J.-S. Kim, W.-S. Chang, R.-H. Kim, D.-Y. Kim, D.-W. Han, K.-H. Lee, S.-S. Lee, S.-G. Doo, High-capacity nanostructured manganese dioxide cathode for rechargeable magnesium ion batteries, Journal of Power Sources 273 (2015) 210-215.

[8] M.H. Alfaruqi, S. Islam, J. Gim, J. Song, S. Kim, D.T. Pham, J. Jo, Z. Xiu, V. Mathew, J. Kim, A high surface area tunnel-type α-MnO_2 nanorod cathode by a simple solvent-free synthesis for rechargeable aqueous zinc-ion batteries, Chemical Physics Letters 650 (2016) 64-68.

[9] J.-W. Wang, Y. Chen, B.-Z. Chen, Synthesis and control of high-performance MnO_2 /carbon nanotubes nanocomposites for supercapacitors, Journal of Alloys and Compounds 688 (2016) 184-197.

[10] S. Islam, M.H. Alfaruqi, J. Song, S. Kim, D.T. Pham, J. Jo, S. Kim, V. Mathew, J.P. Baboo, Z. Xiu, J. Kim, Carbon-coated manganese dioxide nanoparticles and their enhanced electrochemical properties for zinc-ion battery applications, Journal of Energy Chemistry 26(4) (2017) 815-819.

[11] J. Liu, Y. Zhang, Y. Li, J. Li, Z. Chen, H. Feng, J. Li, J. Jiang, D. Qian, In situ chemical synthesis of sandwich-structured MnO_2/graphene nanoflowers and their supercapacitive behavior, Electrochimica Acta 173 (2015) 148-155.

[12] U.S.E.I. Administration, What is energy?, (online) 2020. https://www.eia.gov/energyexplained/what-is-energy/. (Accessed 1 Dec 2020.

[13] M. Mofijur, T. Mahlia, A. Silitonga, H. Ong, M. Silakhori, M. Hasan, N. Putra, S.M. Rahman, Phase Change Materials (PCM) for Solar Energy Usages and Storage: An Overview, Energies 12(16) (2019).

[14] M. Cultu, Batteries and Their Chemistry, ENERGY STORAGE SYSTEMS 2 (1988) 1-9.

[15] N. Kakimoto, K. Goto, Capacity-Fading Model of Lithium-Ion Battery Applicable to Multicell Storage Systems, IEEE Transactions on Sustainable Energy 7(1) (2016) 108-117.

[16] K. Huang, J. Li, Z. Xu, Characterization and recycling of cadmium from waste nickel-cadmium batteries, Waste Manag 30(11) (2010) 2292-8.

[17] C.C. Wang, Y.T. Zhou, C.C. Yang, Q. Jiang, Clarifying the capacity deterioration mechanism sheds light on the design of ultra-long-life hydrogen storage alloys, Chemical Engineering Journal 352 (2018) 325-332.

[18] L.T. Lam, N.P. Haigh, C.G. Phyland, A.J. Urban, Failure mode of valve-regulated lead-acid batteries under high-rate partial-state-of-charge operation, Journal of Power Sources 133(1) (2004) 126-134.

[19] H. Pan, Y. Shao, P. Yan, Y. Cheng, K.S. Han, Z. Nie, C. Wang, J. Yang, X. Li, P. Bhattacharya, K.T. Mueller, J. Liu, Reversible aqueous zinc/manganese oxide energy storage from conversion reactions, Nature Energy 1(5) (2016).

[20] C. Xu, B. Li, H. Du, F. Kang, Energetic zinc ion chemistry: the rechargeable zinc ion battery, Angew Chem Int Ed Engl 51(4) (2012) 933-5.

[21] D. Kundu, S. Hosseini Vajargah, L. Wan, B. Adams, D. Prendergast, L.F. Nazar, Aqueous vs. nonaqueous Zn-ion batteries: consequences of the desolvation penalty at the interface, Energy Environ. Sci. 11(4) (2018) 881-892.

[22] G. Fang, J. Zhou, A. Pan, S. Liang, Recent Advances in Aqueous Zinc-Ion Batteries, ACS Energy Letters 3(10) (2018) 2480-2501.

[23] C. Xia, J. Guo, Y. Lei, H. Liang, C. Zhao, H.N. Alshareef, Rechargeable Aqueous Zinc‐Ion Battery Based on Porous Framework Zinc Pyrovanadate Intercalation Cathode, Advanced Materials 32(9) (2020).

[24] J. Ming, J. Guo, C. Xia, W. Wang, H.N. Alshareef, Zinc-ion batteries: Materials, mechanisms, and applications, Materials Science and Engineering: R: Reports 135 (2019) 58-84.

[25] M. Toupin, T. Brousse, D. Bélanger, Charge storage mechanism of MnO_2 electrode used in aqueous electrochemical capacitor, Chem. Mater. 16(16) (2004) 3184-3190.

[26] M.H. Alfaruqi, V. Mathew, J. Gim, S. Kim, J. Song, J.P. Baboo, S.H. Choi, J. Kim, Electrochemically Induced Structural Transformation in a γ-MnO_2 Cathode of a High Capacity Zinc-Ion Battery System, Chemistry of Materials 27(10) (2015) 3609-3620.

[27] J. Lee, J.B. Ju, W.I. Cho, B.W. Cho, S.H. Oh, Todorokite-type MnO_2 as a zinc-ion intercalating material, Electrochimica Acta 112 (2013) 138-143.

[28] B. Lee, H.R. Lee, H. Kim, K.Y. Chung, B.W. Cho, S.H. Oh, Elucidating the intercalation mechanism of zinc ions into alpha-MnO_2 for rechargeable zinc batteries, Chem Commun (Camb) 51(45) (2015) 9265-8.

[29] Z. Jia, B. Wang, Y. Wang, Copper hexacyanoferrate with a well-defined open framework as a positive electrode for aqueous zinc ion batteries, Materials Chemistry and Physics 149-150 (2015) 601-606.

[30] B. Jiang, C. Xu, C. Wu, L. Dong, J. Li, F. Kang, Manganese Sesquioxide as Cathode Material for Multivalent Zinc Ion Battery with High Capacity and Long Cycle Life, Electrochimica Acta 229 (2017) 422-428.

[31] M.S. Chae, J.W. Heo, H.H. Kwak, H. Lee, S.-T. Hong, Organic electrolyte-based rechargeable zinc-ion batteries using potassium nickel hexacyanoferrate as a cathode material, Journal of Power Sources 337(John Wiley & Sons) (2017) 204-211.

[32] Y. Xia, D. Zhu, S. Si, D. Li, S. Wu, Nickel foam-supported polyaniline cathode prepared with electrophoresis for improvement of rechargeable Zn battery performance, Journal of Power Sources 283 (2015) 125-131.

[33] G. Zhao, D. Zhang, L. Zhang, K. Sun, Ti@δ-MnO$_2$ core-shell nanowire arrays as self-supported electrodes of supercapacitors and Li ion batteries, Electrochimica Acta 202 (2016) 8-13.

[34] J.-K. Chang, M.-T. Lee, W.-T. Tsai, In situ Mn K-edge X-ray absorption spectroscopic studies of anodically deposited manganese oxide with relevance to supercapacitor applications, Journal of Power Sources 166(2) (2007) 590-594.

[35] V. Mathew, J. Lim, J. Kang, J. Gim, A.K. Rai, J. Kim, Self-assembled mesoporous manganese oxide with high surface area by ambient temperature synthesis and its enhanced electrochemical properties, Electrochemistry Communications 13(7) (2011) 730-733.

[36] D.A. Kitchaev, S.T. Dacek, W. Sun, G. Ceder, Thermodynamics of Phase Selection in MnO$_2$ Framework Structures through Alkali Intercalation and Hydration, J Am Chem Soc 139(7) (2017) 2672-2681.

[37] C.M. Julien, A. Mauger, Nanostructured MnO$_2$ as Electrode Materials for Energy Storage, Nanomaterials (Basel) 7(11) (2017).

[38] G.A.M. Ali, L.L. Tan, R. Jose, M.M. Yusoff, K.F. Chong, Electrochemical performance studies of MnO$_2$ nanoflowers recovered from spent battery, Materials Research Bulletin 60 (2014) 5-9.

[39] D. Xu, B. Li, C. Wei, Y.-B. He, H. Du, X. Chu, X. Qin, Q.-H. Yang, F. Kang, Preparation and Characterization of MnO$_2$/acid-treated CNT Nanocomposites for Energy Storage with Zinc Ions, Electrochimica Acta 133 (2014) 254-261.

[40] L. Wang, W. Ma, Y. Li, H. Cui, Synthesis of δ-MnO$_2$ with nanoflower-like architecture by a microwave-assisted hydrothermal method, Journal of Sol-Gel Science and Technology 82(1) (2016) 85-91.

[41] T. Jayaraman, A.P. Murthy, V. Elakkiya, S. Chandrasekaran, P. Nithyadharseni, Z. Khan, R.A. Senthil, R. Shanker, M. Raghavender, P. Kuppusami, M. Jagannathan, M. Ashokkumar, Recent development on carbon based heterostructures for their

applications in energy and environment: A review, Journal of Industrial and Engineering Chemistry 64 (2018) 16-59.

[42] L. David R., Handbook of Chemistry and Physics, 87 ed., CRC Press2004.

[43] M.A. González, R. Trócoli, I. Pavlovic, C. Barriga, F. La Mantia, Layered double hydroxides as a suitable substrate to improve the efficiency of Zn anode in neutral pH Zn-ion batteries, Electrochemistry Communications 68 (2016) 1-4.

[44] R.K. Guduru, J.C. Icaza, A Brief Review on Multivalent Intercalation Batteries with Aqueous Electrolytes, Nanomaterials (Basel) 6(3) (2016).

[45] V. Augustyn, Tuning the interlayer of transition metal oxides for electrochemical energy storage, Journal of Materials Research 32(1) (2016) 2-15.

[46] A.J. Bard, L.R. Faulkner, ELECTROCHEMICAL METHODS: Fundamentals and Applications, 2 ed., JOHN WILEY & SONS, INC.1980.

[47] N. Elgrishi, K.J. Rountree, B.D. McCarthy, E.S. Rountree, T.T. Eisenhart, J.L. Dempsey, A Practical Beginner's Guide to Cyclic Voltammetry, Journal of Chemical Education 95(2) (2017) 197-206.

[48] M.E. Orazem, B. Tribollet, Electrochemical Impedance Spectroscopy, 2 ed., Wiley-Interscience, New York, 2008.

[49] P. Agarwal, M.E. Orazem, L.H. Garcia-Rubio, Measurement Models for Electrochemical Impedance Spectroscopy: I. Demonstration of Applicability, Journal of The Electrochemical Society 139(7) (1992) 1917-1927.

[50] W. Lao-atiman, T. Julaphatachote, P. Boonmongkolras, S. Kheawhom, Printed transparent thin film $Zn-MnO_2$ battery, J. Electrochem. Soc. 164(4) (2017) A859-A863.

[51] S. Suren, S. Kheawhom, Development of a high energy density flexible zinc-air battery, J. Electrochem. Soc. 163(6) (2016) A846-A850.

[52] S. Hosseini, W. Lao-atiman, S.J. Han, A. Arpornwichanop, T. Yonezawa, S. Kheawhom, Discharge Performance of Zinc-Air Flow Batteries Under the Effects of Sodium Dodecyl Sulfate and Pluronic F-127, Sci. Rep. 8(1) (2018) 14909.

[53] S. Hosseini, S.J. Han, A. Arponwichanop, T. Yonezawa, S. Kheawhom, Ethanol as an electrolyte additive for alkaline zinc-air flow batteries, Scientific Reports 8(1) (2018) 11273.

[54] W. Lao-atiman, K. Bumroongsil, A. Arpornwichanop, P. Bumroongsakulsawat, S. Olaru, S. Kheawhom, Model-Based Analysis of an Integrated Zinc-Air Flow Battery/Zinc Electrolyzer System, Frontiers in Energy Research 7 (2019).

[55] W. Kao-ian, R. Pornprasertsuk, P. Thamyongkit, T. Maiyalagan, S. Kheawhom, Rechargeable Zinc-Ion Battery Based on Choline Chloride-Urea Deep Eutectic Solvent, Journal of The Electrochemical Society 166(6) (2019) A1063-A1069.

[56] M.H. Alfaruqi, J. Gim, S. Kim, J. Song, J. Jo, S. Kim, V. Mathew, J. Kim, Enhanced reversible divalent zinc storage in a structurally stable α-MnO$_2$ nanorod electrode, Journal of Power Sources 288 (2015) 320-327.

[57] M.H. Alfaruqi, J. Gim, S. Kim, J. Song, D.T. Pham, J. Jo, Z. Xiu, V. Mathew, J. Kim, A layered δ-MnO$_2$ nanoflake cathode with high zinc-storage capacities for eco-friendly battery applications, Electrochem commun. 60 (2015) 121-125.

[58] M. Feng, Q. Du, L. Su, G. Zhang, G. Wang, Z. Ma, W. Gao, X. Qin, G. Shao, Manganese oxide electrode with excellent electrochemical performance for sodium ion batteries by pre-intercalation of K and Na ions, Sci. Rep. 7(1) (2017) 2219.

[59] J. Song, J. Kim, T. Kang, D. Kim, Design of a porous cathode for ultrahigh performance of a Li-ion battery: An overlooked pore distribution, Sci. Rep. 7 (2017) 42521.

[60] C. Wei, C. Xu, B. Li, H. Du, F. Kang, Preparation and characterization of manganese dioxides with nano-sized tunnel structures for zinc ion storage, J. Phys. Chem. Solids 73(12) (2012) 1487-1491.

[61] R. Renuka, S. Ramamurthy, An investigation on layered birnessite type manganese oxides for battery applications., J. Power Sources 87 (2000) 144–152.

[62] C. Zhu, S. Guo, Y. Fang, L. Han, E. Wang, S. Dong, One-step electrochemical approach to the synthesis of Graphene/MnO$_2$ nanowall hybrids, Nano Res. 4(7) (2011) 648-657.

[63] J. Zhou, L. Yu, M. Sun, S. Yang, F. Ye, J. He, Z. Hao, Novel synthesis of birnessite-type MnO$_2$ nanostructure for water treatment and electrochemical capacitor, Ind. Eng. Chem. Res. 52(28) (2013) 9586-9593.

[64] C. Phillips, A. Al-Ahmadi, S.-J. Potts, T. Claypole, D. Deganello, The effect of graphite and carbon black ratios on conductive ink performance, J. Mater. Sci. 52(16) (2017) 9520-9530.

[65] K. Wongrujipairoj, L. Poolnapol, A. Arpornwichanop, S. Suren, S. Kheawhom, Suppression of zinc anode corrosion for printed flexible zinc-air battery, Phys. Status Solidi B 254(2) (2017).

[66] L.A. Chernozatonskii, P.B. Sorokin, E.É. Belova, J. Brüning, A.S. Fedorov, Metal-semiconductor (semimetal) superlattices on a graphite sheet with vacancies, JETP Lett. 84(3) (2006) 115-118.

[67] F. Li, Y. Xing, M. Huang, K.L. Li, T.T. Yu, Y.X. Zhang, D. Losic, MnO_2 nanostructures with three-dimensional (3D) morphology replicated from diatoms for high-performance supercapacitors, J. Mater. Chem. A 3(15) (2015) 7855-7861.

[68] A.K. Thapa, B. Pandit, R. Thapa, T. Luitel, H.S. Paudel, G. Sumanasekera, M.K. Sunkara, N. Gunawardhana, T. Ishihara, M. Yoshio, Synthesis of mesoporous birnessite-MnO_2 composite as a cathode electrode for lithium battery, Electrochim. Acta 116 (2014) 188-193.

[69] R. Rajarao, B.R. Bhat, Large scale synthesis of carbon nanofibres on sodium chloride support, Nanomater. Nanotechno. 2 (2012) 5.

[70] J. Zhang, Y. Li, L. Wang, C. Zhang, H. He, Catalytic oxidation of formaldehyde over manganese oxides with different crystal structures, Catal. Sci. Technol. 5(4) (2015) 2305-2313.

[71] A.C. Hayes, P. Kruus, W.A. Adams, Raman spectroscopic study of aqueous $(NH_4)_2SO_4$ and $ZnSO_4$ solutions, J. Solution Chem. 13(1) (1984) 61-75.

[72] J.-W. Wang, Y. Chen, B.-Z. Chen, A synthesis method of MnO_2/activated carbon composite for electrochemical supercapacitors, J. Electrochem. Soc. 162(8) (2015) A1654-A1661.

[73] C. Ji, H. Ren, S. Yang, Control of manganese dioxide crystallographic structure in the redox reaction between graphene and permanganate ions and their electrochemical performance, RSC Adv. 5(28) (2015) 21978-21987.

[74] Y.-j. Yang, E.-H. Liu, L.-m. Li, Z.-z. Huang, H.-j. Shen, X.-x. Xiang, Nanostructured MnO_2/exfoliated graphite composite electrode as supercapacitors, J. Alloy Compd. 487(1-2) (2009) 564-567.

[75] J. Li, J. Huang, J. Li, L. Cao, H. Qi, Y. Cheng, Q. Xi, H. Dang, Improved Li-ion diffusion process in TiO_2/rGO anode for lithium-ion battery, J. Alloy Compd. 727 (2017) 998-1005.

[76] P. Simon, Y. Gogotsi, B. Dunn, Where do batteries end and supercapacitors begin, Science 343 (2014) 1210-1211.

[77] D. Chen, D. Ding, X. Li, G.H. Waller, X. Xiong, M.A. El-Sayed, M. Liu, Probing the charge storage mechanism of a pseudocapacitive MnO_2 electrode using in operando raman spectroscopy, Chem. Mater. 27(19) (2015) 6608-6619.

[78] X. Guo, J. Li, X. Jin, Y. Han, Y. Lin, Z. Lei, S. Wang, L. Qin, S. Jiao, R. Cao, A hollow-structured manganese oxide cathode for stable Zn-MnO_2 batteries, Nanomaterials 8(5) (2018).

[79] M.H. Alfaruqi, S. Islam, D.Y. Putro, V. Mathew, S. Kim, J. Jo, S. Kim, Y.-K. Sun, K. Kim, J. Kim, Structural transformation and electrochemical study of layered MnO_2 in rechargeable aqueous zinc-ion battery, Electrochim. Acta 276 (2018) 1-11.

[80] W. Qiu, Y. Li, A. You, Z. Zhang, G. Li, X. Lu, Y. Tong, High-performance flexible quasi-solid-state Zn–MnO_2 battery based on MnO_2 nanorod arrays coated 3D porous nitrogen-doped carbon cloth, J. Mater. Chem. A 5(28) (2017) 14838-14846.

[81] H. Liu, C. Li, H.P. Zhang, L.J. Fu, Y.P. Wu, H.Q. Wu, Kinetic study on $LiFePO_4$/C nanocomposites synthesized by solid state technique, J. Power Sources 159(1) (2006) 717-720.

[82] A.J. Bard, L.R. Faulkner, Electrochemical Methods, 2 ed., JOHN WILEY & SONS, INC., New York, 2001.

[83] H. Li, B. Zhang, Q. Zhou, J. Zhang, W. Yu, Z. Ding, M.A. Tsiamtsouri, J. Zheng, H. Tong, Dual-carbon confined SnO_2 as ultralong-life anode for Li-ion batteries, Ceram. Int. 45(6) (2019) 7830-7838.

[84] Q. Cao, H.P. Zhang, G.J. Wang, Q. Xia, Y.P. Wu, H.Q. Wu, A novel carbon-coated $LiCoO_2$ as cathode material for lithium ion battery, Electrochem commun. 9(5) (2007) 1228-1232.

[85] R.D. Corpuz, L.M.Z. De Juan, S. Praserthdam, R. Pornprasertsuk, T. Yonezawa, M.T. Nguyen, S. Kheawhom, Annealing induced a well-ordered single crystal δ-MnO_2 and its electrochemical performance in zinc-ion battery, Scientific Reports 9(1) (2019) 15107.

[86] L.M. De Juan-Corpuz, R.D. Corpuz, A. Somwangthanaroj, M.T. Nguyen, T. Yonezawa, J. Ma, S. Kheawhom, Binder-Free Centimeter-Long V_2O_5 Nanofibers on Carbon Cloth as Cathode Material for Zinc-Ion Batteries, Energies 13(1) (2019) 31.

[87] Y. Huang, J. Mou, W. Liu, X. Wang, L. Dong, F. Kang, C. Xu, Novel Insights into Energy Storage Mechanism of Aqueous Rechargeable Zn/MnO_2 Batteries with Participation of Mn^{2+}, Nano-Micro Letters 11(1) (2019) 49.

[88] T. Leisegang, F. Meutzner, M. Zschornak, W. Münchgesang, R. Schmid, T. Nestler, R.A. Eremin, A.A. Kabanov, V.A. Blatov, D.C. Meyer, The Aluminum-Ion Battery: A Sustainable and Seminal Concept?, Frontiers in Chemistry 7(268) (2019).

[89] B. Su, J. Zhang, M. Fujita, W. Zhou, P.H.-L. Sit, D.Y.W. Yu, Na_2SeO_3: A Na-Ion Battery Positive Electrode Material with High Capacity, Journal of The Electrochemical Society 166(3) (2019) A5075-A5080.

[90] L.H. Saw, Y. Ye, A.A.O. Tay, Integration issues of lithium-ion battery into electric vehicles battery pack, Journal of Cleaner Production 113 (2016) 1032-1045.

[91] Z. Rao, S. Wang, G. Zhang, Simulation and experiment of thermal energy management with phase change material for ageing $LiFePO_4$ power battery, Energy Conversion and Management 52(12) (2011) 3408-3414.

[92] N. Palaniyandy, M.A. Kebede, K. Raju, K.I. Ozoemena, L. le Roux, M.K. Mathe, R. Jayaprakasam, α-MnO_2 nanorod/onion-like carbon composite cathode material for aqueous zinc-ion battery, Materials Chemistry and Physics 230 (2019) 258-266.

[93] M. Qin, W. Liu, L. Shan, G. Fang, X. Cao, S. Liang, J. Zhou, Construction of V_2O_5/NaV_6O_{15} biphase composites as aqueous zinc-ion battery cathode, Journal of Electroanalytical Chemistry 847 (2019) 113246.

[94] T. Ould Ely, D. Kamzabek, D. Chakraborty, Batteries Safety: Recent Progress and Current Challenges, Frontiers in Energy Research 7(71) (2019).

[95] X. Wu, K. Song, X. Zhang, N. Hu, L. Li, W. Li, L. Zhang, H. Zhang, Safety Issues in Lithium Ion Batteries: Materials and Cell Design, Frontiers in Energy Research 7(65) (2019).

[96] R.D. Corpuz, L.M. De Juan-Corpuz, M.T. Nguyen, T. Yonezawa, H.-L. Wu, A. Somwangthanaroj, S. Kheawhom, Binder-Free α-MnO_2 Nanowires on Carbon Cloth as Cathode Material for Zinc-Ion Batteries, International Journal of Molecular Sciences 21(9) (2020) 3113.

[97] H. Li, L. Ma, C. Han, Z. Wang, Z. Liu, Z. Tang, C. Zhi, Advanced rechargeable zinc-based batteries: Recent progress and future perspectives, Nano Energy 62 (2019) 550-587.

[98] N. Ma, P. Wu, Y. Wu, D. Jiang, G. Lei, Progress and perspective of aqueous zinc-ion battery, Functional Materials Letters 12(5) (2019) 1930003.

[99] W. Xu, Y. Wang, Recent Progress on Zinc-Ion Rechargeable Batteries, Nano-Micro Letters 11(1) (2019) 90.

[100] B. Lan, Z. Peng, L. Chen, C. Tang, S. Dong, C. Chen, M. Zhou, C. Chen, Q. An, P. Luo, Metallic silver doped vanadium pentoxide cathode for aqueous rechargeable zinc ion batteries, Journal of Alloys and Compounds 787 (2019) 9-16.

[101] D. Yang, H. Tan, X. Rui, Y. Yu, Electrode Materials for Rechargeable Zinc-Ion and Zinc-Air Batteries: Current Status and Future Perspectives, Electrochemical Energy Reviews 2(3) (2019) 395-427.

[102] B. Tang, L. Shan, S. Liang, J. Zhou, Issues and opportunities facing aqueous zinc-ion batteries, Energy & Environmental Science 12(11) (2019) 3288-3304

[103] C. Guo, H. Liu, J. Li, Z. Hou, J. Liang, J. Zhou, Y. Zhu, Y. Qian, Ultrathin δ-MnO_2 nanosheets as cathode for aqueous rechargeable zinc ion battery, Electrochimica Acta 304 (2019) 370-377.

[104] C. Wang, Y. Zeng, X. Xiao, S. Wu, G. Zhong, K. Xu, Z. Wei, W. Su, X. Lu, γ-MnO_2 nanorods/graphene composite as efficient cathode for advanced rechargeable aqueous zinc-ion battery, Journal of Energy Chemistry 43 (2020) 182-187.

[105] S. Khamsanga, R. Pornprasertsuk, T. Yonezawa, A.A. Mohamad, S. Kheawhom, δ-MnO2 nanoflower/graphite cathode for rechargeable aqueous zinc ion batteries, Scientific Reports 9(1) (2019) 8441.

[106] L. Li, Z.A. Hu, N. An, Y.Y. Yang, Z.M. Li, H.Y. Wu, Facile Synthesis of MnO_2/CNTs Composite for Supercapacitor Electrodes with Long Cycle Stability, The Journal of Physical Chemistry C 118(40) (2014) 22865-22872.

[107] H. Wang, C. Peng, F. Peng, H. Yu, J. Yang, Facile synthesis of MnO_2/CNT nanocomposite and its electrochemical performance for supercapacitors, Materials Science and Engineering: B 176(14) (2011) 1073-1078.

[108] Y. Zhang, Y. Hu, S. Li, J. Sun, B. Hou, Manganese dioxide-coated carbon nanotubes as an improved cathodic catalyst for oxygen reduction in a microbial fuel cell, Journal of Power Sources 196(22) (2011) 9284-9289.

[109] S.-L. Chou, J.-Z. Wang, S.-Y. Chew, H.-K. Liu, S.-X. Dou, Electrodeposition of MnO_2 nanowires on carbon nanotube paper as free-standing, flexible electrode for supercapacitors, Electrochemistry Communications 10(11) (2008) 1724-1727.

[110] J. Yang, M. Ma, C. Sun, Y. Zhang, W. Huang, X. Dong, Hybrid $NiCo_2S_4$@MnO_2 heterostructures for high-performance supercapacitor electrodes, Journal of Materials Chemistry A 3(3) (2015) 1258-1264.

[111] L. Liu, L. Fang, F. Wu, J. Hu, S. Zhang, H. Luo, B. Hu, M. Zhou, Self-supported core-shell heterostructure MnO_2/NiCo-LDH composite for flexible high-performance supercapacitor, Journal of Alloys and Compounds 824 (2020) 153929.

[112] R. Peng, H. Zhang, L. Gui, Y. Zheng, Z. Wu, Y. Luo, P. Yu, Construction of 0D CeO2/2D MnO_2 heterostructure with high electrochemical performance, Electrochimica Acta 319 (2019) 95-100.

[113] J. Zhao, Z. Tao, J. Liang, J. Chen, Facile Synthesis of Nanoporous γ-MnO_2 Structures and Their Application in Rechargeable Li-Ion Batteries, Crystal Growth & Design 8(8) (2008) 2799-2805.

[114] J. Zhao, H. Ren, Q. Liang, D. Yuan, S. Xi, C. Wu, W. Manalastas, J. Ma, W. Fang, Y. Zheng, C.-F. Du, M. Srinivasan, Q. Yan, High-performance flexible quasi-solid-state zinc-ion batteries with layer-expanded vanadium oxide cathode and zinc/stainless steel mesh composite anode, Nano Energy 62 (2019) 94-102.

[115] D.A. Kitchaev, H. Peng, Y. Liu, J. Sun, J.P. Perdew, G. Ceder, Energetics of MnO_2 polymorphs in density functional theory, Physical Review B 93(4) (2016) 045132.

[116] R.Y. Wang, C.D. Wessells, R.A. Huggins, Y. Cui, Highly Reversible Open Framework Nanoscale Electrodes for Divalent Ion Batteries, Nano Letters 13(11) (2013) 5748-5752.

[117] S. Yang, M. Zhang, X. Wu, X. Wu, F. Zeng, Y. Li, S. Duan, D. Fan, Y. Yang, X. Wu, The excellent electrochemical performances of $ZnMn_2O_4/Mn_2O_3$: The composite cathode material for potential aqueous zinc ion batteries, Journal of Electroanalytical Chemistry 832 (2019) 69-74.

[118] J. Wang, J. Polleux, J. Lim, B. Dunn, Pseudocapacitive Contributions to Electrochemical Energy Storage in TiO_2 (Anatase) Nanoparticles, The Journal of Physical Chemistry C 111(40) (2007) 14925-14931.

[119] F. Wan, L. Zhang, X. Dai, X. Wang, Z. Niu, J. Chen, Aqueous rechargeable zinc/sodium vanadate batteries with enhanced performance from simultaneous insertion of dual carriers, Nature Communications 9(1) (2018) 1656.

[120] G. Sun, X. Jin, H. Yang, J. Gao, L. Qu, An aqueous $Zn–MnO_2$ rechargeable microbattery, Journal of Materials Chemistry A 6(23) (2018) 10926-10931.

[121] C. Xia, J. Guo, Y. Lei, H. Liang, C. Zhao, H.N. Alshareef, Rechargeable Aqueous Zinc-Ion Battery Based on Porous Framework Zinc Pyrovanadate Intercalation Cathode, Advanced Materials 30(5) (2018) 1705580.

จุฬาลงกรณ์มหาวิทยาลัย

CHULALONGKORN UNIVERSITY

VITA

NAME	SONTI KHAMSANGA
DATE OF BIRTH	5 June 1981
PLACE OF BIRTH	Pathum Thani
INSTITUTIONS ATTENDED	B.Eng. (Chemical Engineering), Suranaree University of Technology, 2003
	M.Eng. (Chemical Engineering), Chulalongkorn University, 2005
	D.Eng. (Chemical Engineering), Chulalongkorn University, 2020
HOME ADDRESS	42/1 Moo. 9, Lamlukka, Lamlukka, Pathum Thani 12150
PUBLICATION	1. S. Khamsanga, R. Pornprasertsuk, T. Yonezawa, A. A. Mohamad and S. Kheawhom, "δ-MnO2 nanoflower/graphite cathode for rechargeable aqueous zinc ion batteries", SCIENTIFIC REPORTS (2019) 9, 8441.
	2. S. Khamsanga, M. Th. Nguyen, T. Yonezawa, P. Thamyongkit, R. Pornprasertsuk, P. Pattananuwat, A. Tuantranont, S. Siwamogsatham and S. Kheawhom, "MnO2 heterostructure on carbon nanotubes as cathode material for aqueous zinc-Ion batteries", INTERNATIONAL JOURNAL OF MOLECULAR SCIENCES (2020) 21, 4689.